

Suspended Sediment Transport in the Colorado River

by

Trine Christiansen

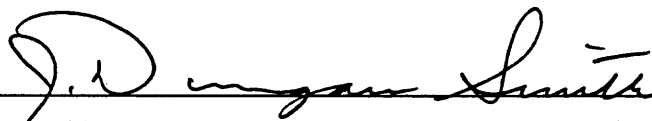
A thesis submitted in partial fulfillment of
the requirements for the degree of

Master of Science in Civil Engineering

University of Washington

1993

Approved by


(Chairperson of Supervisory Committee)

Program Authorized

to Offer Degree

Department of Civil Engineering

Date

Aug 18, 1993

00.03

PR 5-10.00

27 5

(21.12)

2074844

8.

In presenting this thesis in partial fulfillment of the requirements for a Master's degree at the University of Washington, I agree that extensive copying of this thesis is allowable for scholarly purposes, consistent with "fair use" as prescribed in the U.S. Copyright Law. Any other reproduction for any purposes or by any means shall not be allowed without my written permission.

Signature Tine Christia

Date Aug 18, 1993

Table of Contents

List of Tables	iii
List of Figures	iv
List of Symbols	viii
Chapter 1: Introduction	1
Chapter 2: The National Canyon Field Study	7
2.1 The Research Flows	7
2.2 Measurements Made During the Study Period in July, 1991	9
2.3 Velocity Measurements	10
2.4 Suspended Sediment Measurements and Analysis of Samples	12
2.5 National Canyon Bathymetry	15
Chapter 3: Velocity Profile Analysis	44
3.1 The Velocity Profile Model	44
3.2 Statistical Analysis of Velocity Profiles	45
3.3 Error bars on roughness parameter	62
3.4 Roughness at National Canyon	65
3.5 Determining the model parameters	70
3.6 Summary of Results	72
3.7 Discussion of Results	73
Chapter 4: Concentration Profile Analysis	83
4.1 The concentration Profile Model	83
4.2 Matching Concentration Profiles to Measurements	86
4.3 Application of Concentration profile Analysis.	94

Chapter 5: Conclusions

108

Bibliography

111

List of Tables

2.1	Research flow schedule from December 1990 to July 1991.	9
3.1	Characteristics of best fit velocity profile.	48
3.2	Variance of measured velocity profiles around two imposed velocity profiles.	50
3.3	Testing the null-hypothesis, high discharge	51
3.4	Testing the null-hypothesis, low discharge	51
3.5	Results of error analysis	63
3.6	Mean values of bedform height and wavelength.	71
3.7	Summary of results, high discharge	72
3.8	Summary of results, low discharge	72
3.9	Bulk flow properties	73
3.10	Calculation of non-dimensional form drag	76
3.11	Bedform migration rates at high and low discharge	78
3.12	Discharge in wake region relative to total discharge	79
3.13	Comparison between two different values of Mannings n	80
3.14	Comparison between different values of roughness	82
4.1	Characteristics of best fit concentration profiles	87
4.2	F-test of concentration measurements.	88
4.3	Results of concentration profile analysis.	94
4.4	Calculation of the coefficient, γ	94
4.5	Settling velocities	96
4.6	Estimate of thickness of reworked sediment	98
4.7	Effect of limiting the thickness of the reworked sediment layer	100
4.8	Comparison between sediment profile calculated using a single grain sizes versus a distribution of sediment	101
4.9	Suspended sediment transport parameters	101

List of Figures

1.1	Map of the Colorado River in the Grand Canyon National Park	2
2.1	The National Canyon Study Reach.	8
2.2	Suspended sediment sampling from the cableway	11
2.3	Variation in stage during trip G	17
2.4	Location of cross-sections in the National Canyon mapreach	18
2.5	Location of stations of the cableway	19
2.6	Velocity measurements at station 60	20
2.7	Velocity measurements at station 75	21
2.8	Velocity measurements at station 95	21
2.9	Velocity measurements at station 110	22
2.10	Velocity measurements at station 130	22
2.11	Velocity measurements at station 145	23
2.12	Velocity measurements at station 160	23
2.13	Velocity measurements at station 175	24
2.14	Velocity measurements at station 190	24
2.15	Velocity measurements at station 210	25
2.16	Velocity measurements at station 225	25
2.17	P-61 suspended sediment sampler	26
2.18	Example of chart generated during VA-tube analysis.	27
2.19	Distribution of sediment 15 <i>cm</i> above the bed	28
2.20	Distribution of sediment 180 <i>cm</i> above the bed	28
2.21	Distribution of sediment 60 <i>cm</i> below the water surface	29
2.22	Suspended sediment concentration measurements at station 75. . . .	30
2.23	Suspended sediment concentration measurements at station 95. . . .	30
2.24	Suspended sediment concentration measurements at station 110. . . .	31
2.25	Suspended sediment concentration measurements at station 130. . . .	31

2.26	Suspended sediment concentration measurements at station 145. . . .	32
2.27	Suspended sediment concentration measurements at station 160. . . .	32
2.28	Suspended sediment concentration measurements at station 175. . . .	33
2.29	Suspended sediment concentration measurements at station 190. . . .	33
2.30	Suspended sediment concentration measurements at station 210. . . .	34
2.31	Suspended sediment concentration measurements at station 225. . . .	34
2.32	Example of echo-sounding chart	35
2.33	Cross-section 0	36
2.34	Cross-section 200	36
2.35	Cross-section 400	37
2.36	Cross-section 600	37
2.37	Map of the National Canyon Reach.	38
2.38	Location of longitudinal passes	39
2.39	Example of a longitudinal echo-sounding	40
2.40	Longitudinal Pass 1	41
2.41	Longitudinal Pass 2	41
2.42	Longitudinal Pass 3	42
2.43	Longitudinal Pass 4	42
2.44	Longitudinal Pass 5	43
3.1	Velocity profile measured at station 75	52
3.2	High discharge velocity profile measured at station 95	52
3.3	High discharge velocity profile measured at station 110	53
3.4	High discharge velocity profile measured at station 130	53
3.5	High discharge velocity profile measured at station 145	54
3.6	High discharge velocity profile measured at station 160	54
3.7	High discharge velocity profile measured at station 175	55
3.8	High discharge velocity profile measured at station 190	55
3.9	High discharge velocity profile measured at station 210	56
3.10	High discharge velocity profile measured at station 225	56
3.11	Low discharge velocity profile measured at station 75	57
3.12	Low discharge velocity profile measured at station 95	57

3.13	Low discharge velocity profile measured at station 110	58
3.14	Low discharge velocity profile measured at station 130	58
3.15	Low discharge velocity profile measured at station 145	59
3.16	Low discharge velocity profile measured at station 160	59
3.17	Low discharge velocity profile measured at station 175	60
3.18	Low discharge velocity profile measured at station 190	60
3.19	Low discharge velocity profile measured at station 210	61
3.20	Low discharge velocity profile measured at station 225	61
3.21	Results of error analysis	64
3.22	Schematic velocity Profile	69
3.23	Comparison between best fit and calculated velocity profile at high discharge.	74
4.1	Schematic concentration profile	85
4.2	Fits to concentration measurements made at station 75	89
4.3	Fits to concentration measurements made at station 95	89
4.4	Fits to concentration measurements made at station 110	90
4.5	Fits to concentration measurements made at station 130	90
4.6	Fits to concentration measurements made at station 145	91
4.7	Fits to concentration measurements made at station 160	91
4.8	Fits to concentration measurements made at station 175	92
4.9	Fits to concentration measurements made at station 190	92
4.10	Fits to concentration measurements made at station 210	93
4.11	Fits to concentration measurements made at station 225	93
4.12	Comparison between measured and calculated concentration profile .	95
4.13	Concentration profile calculated using a log-normal sediment distribu- tion with $D_{50} = -2.5\phi, \sigma = 0.6\phi$	102
4.14	Relative volume of sediment for unlimited and limited availability of sediment	103
4.15	Concentration profile calculated using a sediment distribution with $D_{50} = -2.7\phi, \sigma = 0.6\phi$	104

4.16	Relative volume of sediment for unlimited and limited availability of sediment	105
4.17	Concentration profile calculated using a sediment distribution with $D_{50} = -2.9\phi, \sigma = 0.6\phi$	106
4.18	Relative volume of sediment for unlimited and limited availability of sediment	107

LIST OF SYMBOLS

- A : cross-sectional area
- A_1 : a coefficient related to sediment saltation height (=0.68)
- A_2 : a coefficient related to grain size moving in the bedload layer
- C : sediment concentration
- C_a : sediment concentration at a level a
- C_b : maximum concentration in the bed (=0.65)
- C_D : drag coefficient
- g : gravitational acceleration
- h : flow depth
- H : bedform height
- i_m : fraction of distribution represented by sediment size component m
- K : turbulent eddy viscosity
- k_s : bed roughness parameter
- m : slope of profile obtained using linear regression
- n : Mannings roughness parameter
- N : number of measurements made below $0.2h$
- M : number of sediment size classes
- p_m : Rouse number
- P : wetted perimeter
- q : unit discharge of water
- Q : discharge of water

q_s : unit sediment flux
 R : hydraulic radius
 S : water surface slope
 S_m : excess shear stress of sediment size component m
 T_s : transport stage
 u : velocity in the direction of flow
 \bar{u} : mean velocity
 u_{sF} : shear velocity associated with the interior flow
 u_{sT} : shear velocity associated with the exterior flow
 U_B : bedform migration rate
 V : unit volume of sediment in suspension
 w : settling velocity
 w_m : settling velocity of sediment size component m
 X_{rms} : root mean square of $\ln(z_0)$
 z : elevation above boundary vertical coordinate direction
 z_0 : general roughness parameter
 z_{0F} : boundary roughness parameter associated with the interior flow
 z_{0T} : boundary roughness parameter associated with the exterior flow
 z_a : level at which sediment reference concentration is specified
 z_m : matching height between interior and exterior flow
 α : angle between water surface and horizontal
 β : a coefficient associated with the turbulent eddy viscosity in the upper 80 % of the flow (=6.24)
 δ_b : thickness of saltation layer

Δ : difference from mean value

γ : coefficient related to the upward suspension of sediment from the bed

κ : von Karmans constant (=0.41)

λ : bedform length

ξ : non-dimensional depth coordinate (z/h)

ξ_{OT} : non-dimensional depth coordinate associated with the bedform roughness (z_{OT}/h)

ξ_b : non-dimensional depth coordinate at 20 % of the flow depth (=0.2)

σ_a : standard deviation of measurements made at one station around a specified curve

σ_b : standard deviation of measurements made at one station around the best fit curve to velocity measurements made at several stations

ρ : density of water

ρ_s : density of sediment

τ_b : boundary shear stress

τ_* : non-dimensional boundary shear stress

τ_{cr} : critical boundary shear stress

τ_{*cr} : non-dimensional critical boundary shear stress

τ_D : stress due to form drag

τ_F : skin friction boundary shear stress

τ_T : total boundary shear stress

Φ_s : non-dimensional bedload transport flux

Acknowledgments

The site of this thesis was chosen due to a wonderful opportunity to collaborate with the US Geological Survey on the Colorado River project provided by my advisor, J. Dungan Smith. I thank him for his guidance and his high expectations to my research, that I feel has taught me a very useful philosophy towards scientific questions.

This thesis was completed because my current advisor at the University of Virginia, Patricia Wiberg, believed that the effort was worth while. I thank her for her support, her critical editing and helpful suggestions.

I thank Ronald E. Nece for his thorough editing of the final draft and for taking the responsibility of allowing me to pursue a research interest that led me not only to conduct my research outside the Civil Engineering Department, but also outside the state of Washington. I also thank Stephen Burges and Catherine Petros for their interesting comments at my defence.

While working for the U.S. Geological Survey in Colorado, I had many interesting discussions with Stephen Wiele which created a fun work environment. I thank him for his help with solving many scientific and practical problems along the way.

I thank my good friends, Henrik Hulgaard for helping me through many of the countless computer problems I came across during this study, Michael Schwar for making me feel a little less foreign by introducing me to the concepts of football and baseball and other specialties of American culture, Elizabeth Boyer, alias Tiny Trucker, for leading the way to Virginia, and Karl Hollebeck for his editing of the final draft and for making the last months of thesis writing an enjoyable experience.

Throughout this study my family has provided immense support on many different levels. I could not have completed this thesis if Claus had not taught me to program in Fortran or if Gunna had not taught me that most things worth while require stamina. I thank Mikkel for his help with field work in the summer of 1992, and Lise

for her financial support.

While working on this project, the author was funded in part by the Valle Scandinavian Exchange Program and a grant from the Fulbright Commission.

Chapter 1

INTRODUCTION

In a non-uniform flow system, such as the Colorado River, it is important to understand the natural variability of the bottom roughness. Knowledge of the scale of roughness and how it changes from one location to another is extremely important when determining the distribution of velocity and suspended sediment. Accurate specification of the roughness parameter is critical in mathematical modeling studies because inaccuracy in this parameter causes error in both water and suspended sediment discharge calculations. The current study was motivated by the need to produce accurate boundary conditions for velocity and suspended sediment concentration under a wide range of flow conditions as input for sophisticated mathematical flow models.

The annual sediment load in the Grand Canyon Reach of the Colorado River has been reduced by 80 % since closure of the Glen Canyon Dam (*Andrews*, 1990 [1]), which is located downstream from the historically most important sediment contributing tributaries to the Colorado River. Concern has arisen that the mode of operation of the Glen Canyon Dam is adversely affecting sand deposits along the river. These deposits provide an important natural habitat for plants and animals and are used extensively as campsites by river-rafters. A map of the region is shown in Figure 1.1. To assess the relationship between discharge at the Glen Canyon Dam and downstream sediment deposits, flow and sediment transport in the Colorado River are currently being studied, and an important part of the study is development of accurate flow and sediment transport models (*Smith and Wiele*, 1992 [21]).

Previous studies of the Colorado River in the Grand Canyon Reach have dealt primarily with the general geomorphology of the fluvial system (*Howard and Dolan*, 1981 [7], *Schmidt and Graf*, 1990 [18] and *Leopold*, 1969 [8]), whereas very few detailed quantitative investigations have been made of flow and sediment transport in the river. For the purpose of producing accurate boundary conditions for mathematical

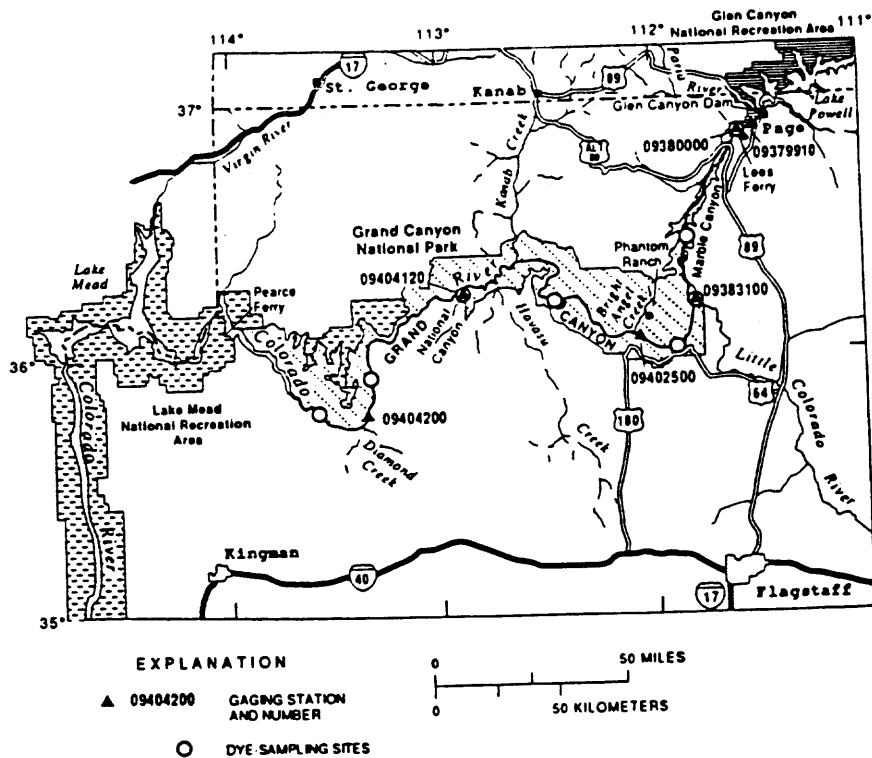


Figure 1.1: Map of the Colorado River in the Grand Canyon National Park, after Schmidt and Graf, 1990 [18].

models, a detailed survey of flow and sediment transport in the Colorado River was carried out by the US Geological Survey at a site located in vicinity of the National Canyon Gaging Station, 166.5 river miles from Lees Ferry, Arizona. The focus of the study presented here is to characterize velocity and suspended sediment concentration profile structure and bottom roughness, using measurements collected at the National Canyon site.

Flow in the Grand Canyon stretch of the Colorado River is controlled by the Glen Canyon Dam, because the tributaries to the Colorado River between the dam and Lake Mead have discharges that are only a small fraction of the total discharge in the main stem. Thus the river provides a laboratory-like setting in the sense that discharge in the reach can be controlled at the dam. The measurements were made at National Canyon during a period of controlled dam releases in July 1991, where the flow fluctuated in diurnal cycles between a high discharge of $710 \text{ m}^3/\text{sec}$ and a low discharge of $280 \text{ m}^3/\text{sec}$.

Velocity and suspended sediment profiles were measured by the US Geological Survey from a cableway suspended across the river. Each of these variables were measured at seven points in the vertical, at ten stations across the river and each profile was replicated 8-9 times. The channel at the study site was sand bedded, so bedforms were found in abundance on the channel bottom.

The analysis of the measured velocity and suspended sediment profiles presented in this study has three components. First, the velocity measurements made at both high and low discharge were analyzed to determine values of shear velocity and bottom roughness pertaining to the exterior flow region. This approach was motivated in part by the need to derive water surface slope (which was not measured) from the velocity measurements. Second, the velocity profile was theoretically extrapolated to the bottom through an interior flow region of strong wake influence, and a characteristic shear velocity and a roughness parameter pertaining to the interior flow region was determined. Third, the Rouse number characteristic of the concentration profile measurements in the exterior flow was found, and the velocity structure derived in the first and second steps was used to extrapolate the concentration profile through the interior flow region to the bedload layer.

The velocity measurements were made during two different discharges, and have been analyzed statistically to determine empirical values of bedform roughness and shear velocity of the flow. The analysis also permitted identification of a region of uniform flow in the central portion of the channel. The statistical analysis was performed by determining the best fit, in a least squares sense, of model velocity profiles to the velocity measurements. A quasi-logarithmic model profile was chosen for the analysis. This model profile describes velocity as increasing with the logarithm of the depth in the bottom 20 % of the flow and with the square of the depth in the remaining 80 %. The slope of the velocity profile is controlled by the shear velocity, and the intercept with zero velocity defines the roughness parameter z_{0T} . The measurement derived value of shear velocity was then used to determine channel slope.

A flow over bedforms can be divided into two regions, an interior flow region and an exterior flow region. The interior flow region includes the flow in the near boundary region, where wake effects related to the presence of bedforms are strong. The interior flow region is thin relative to the total depth of flow (approximately 5 % of the flow

depth at National Canyon), but the conditions in the wake region determine the effective roughness for the exterior flow. The exterior flow region describes the region where the flow is very nearly spatially uniform (Arya, 1975 [2]).

All velocity profile measurements were made in the exterior portion of the flow. It was therefore necessary to describe the flow in the interior flow region using a theoretical model, such as the one developed by *Smith and McLean*, 1977 [20] that considers flow over bedforms in a spatially averaged sense. *Smith and McLean* obtained good results by assuming that the velocity profile, averaged over the length of a bedform, could be approximated as logarithmic in the interior flow with a profile slope determined by the skin friction shear velocity, and a roughness associated with a grain scale roughness parameter. Recent experiments performed by *Wiberg and Nelson*, 1992 [23] suggested that the spatially averaged velocity profile of the interior flow may not be logarithmic. However, these authors also found that, in the case of asymmetric ripples such as the bedforms observed at National Canyon, the shear velocity obtained by assuming a logarithmic interior flow structure led to a reasonable estimate of the average boundary shear stress.

In the case of flow over bedforms, two scales of roughness can be identified. In the near boundary region, the roughness scale is related to mean sediment size. This roughness scale is referred to as the skin friction roughness, z_{0F} . Further away from the boundary, the flow has adjusted to the bedforms and the roughness scale of the outer flow is related to the ratio of height to length of the bedforms and the degree of flow separation around them. This roughness scale is referred to as the bedform roughness or the total roughness, z_{0T} . The roughness parameter derived from analysis of the velocity measurements corresponds to the bedform roughness, z_{0T} , since the velocity measurements were all made in the exterior flow. The bedform roughness is typically orders of magnitude greater than the skin friction roughness but much less than the bedform height. The measurement derived value of z_{0T} allows one to determine values of the parameters that scale the roughness of the exterior flow, and to evaluate how these parameters vary with change of velocity.

Sediment transport in the Colorado River is dominated by suspended load transport. Locally derived sand sized sediment is transported at discharges above approximately $320 \text{ m}^3/\text{s}$. The sand is locally eroded and re-deposited with fluctuations in discharge, and these variations are instrumental in modifying the local channel envi-

ronment. During tributary floods, large amounts of silt are typically introduced into the river. The settling velocity of silt is low, so the sediment remains in suspension, and is transported over great distances as washload.

While suspended sediment concentration profiles were measured in the exterior portion of the flow during high and low discharges only the high discharge samples contained sufficient sediment for laboratory analysis. The high discharge concentration profiles were also analyzed statistically to determine empirical values of Rouse numbers and concentration of sediment at the top of the bedload layer. The statistical analysis of the concentration profile measurements is analogous to the analysis of the velocity profile measurements. The model concentration profile used for the analysis also has a two part structure, and the slope of the profile is controlled by the Rouse number.

Once a best fit model profile had been identified, the profile was extrapolated to the top of the bedload layer, using the shear velocity of the interior flow obtained from the velocity profile analysis. The extrapolation provided an empirical value of concentration at the top of the bedload layer. From this empirical concentration, a value of the coefficient γ was derived. It was found to be of the order of magnitude expected of this parameter (10^{-3}) (*Smith and McLean, 1977 [20]* and *Wiberg, Pers. Comm.*). The analysis of both the velocity and sediment profiles indicates that the structures of the selected model velocity and concentration profiles are in good agreement with the structures of the respective measured profiles in the central portion of the river. Consequently, the high discharge measurement derived values of shear velocity and Rouse number were combined to calculate a settling velocity. The grain size that corresponds to this settling velocity, i.e. $D=0.015$ cm, is in good agreement with grain sizes estimated from grain size analysis of the suspended sediment samples.

The measured concentration profiles display a structure that corresponds well to the structure expected if the sediment in suspension consists of only one grain size. However, grain size analyses of the suspended sediment samples indicated that the sediment in suspension was in fact represented by a distribution of grain sizes.

The concentration profiles corresponding to three different likely sediment distributions were calculated, and it was found that in all three cases the volume of sediment in suspension was greatly over-predicted relative to the measured volume of suspended sediment. The over-predicted sediment volume was explained by lim-

ited availability of the fine grain sizes in the bed. Concentration profiles that match the measured profiles were constructed for each of the three distributions of bottom sediment by segmenting each distribution into seven size classes and then limiting the availability of the finest size classes. The over-predicted volume of sediment in suspension may also be an artifact of considering a sediment distribution that is too broad, but due to uncertainties in the grain size analysis a more precise determination of sediment size distribution is not possible.

Chapter 2

THE NATIONAL CANYON FIELD STUDY

The site just upstream of the National Canyon gaging station was selected as a primary study reach because the river at this location is uncomplicated. The uncomplicated nature of the river at National Canyon was thought to provide a manageable environment for a field study and to increase the likelihood of collecting a data set that could be interpreted in a relatively straight forward manner. The cableway at National Canyon is located approximately 500 meters upstream from a minor rapid, and the surveyed reach extends approximately 1500 meters upstream from the cableway. In this reach, the river has limited curvature and in-channel bars do not exist. The reach in vicinity of the cableway is illustrated in Figure 2.1.

The nature of large rivers complicates field surveys considerably. The Colorado River at National Canyon is 80 meters wide, 8 meters deep and has a surface velocity of 2 meters per second at a discharge of $710 \text{ m}^3/\text{sec}$, which was the peak discharge during research flow G in July 1991. The National Canyon Gaging Station can only be reached by a three day float trip from Lees Ferry, which severely complicates the logistics of field work at that site. The data collection at National Canyon took place during 9 months of controlled dam releases in the period from December 1990 through August 1991, but in this document, only the measurements made during research flow G are presented.

2.1 *The Research Flows*

Flow in the Colorado river below Glen Canyon Dam can be effectively controlled by the amount of water released from the dam, since the tributaries contribute only a small fraction of the total discharge of the river. The research flow release schedule included both fluctuating flows with a specified fixed amplitudes and extended periods of constant discharge. Six, eleven-day study periods were reserved for studies of water released in diurnal cycles. To provide a wide range of conditions, the low and high amplitudes of the released discharge were varied between each study period. In

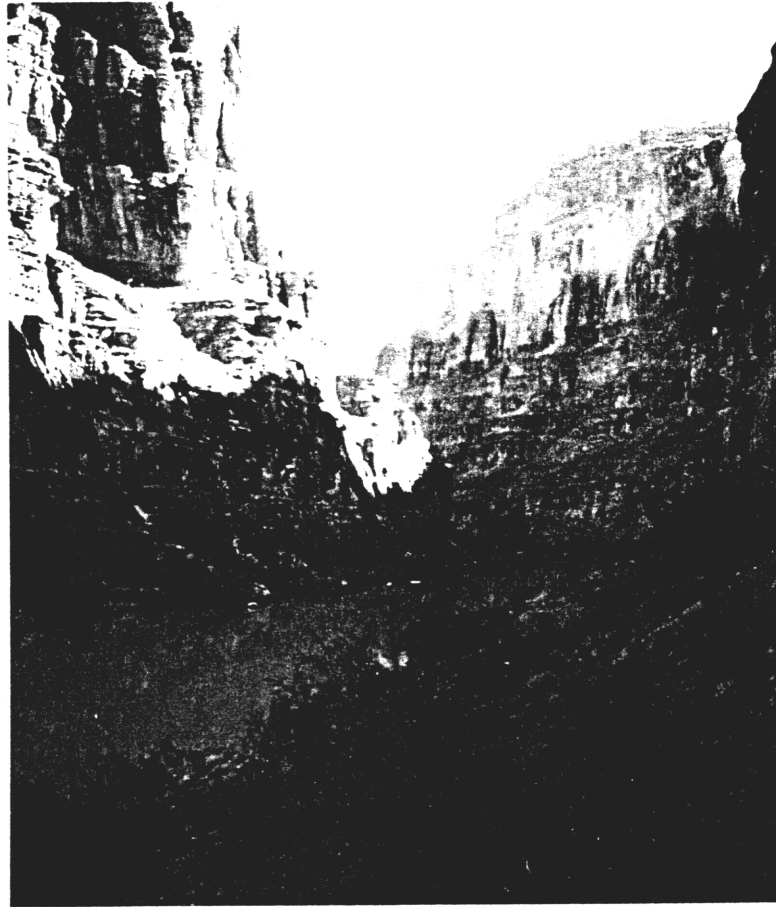


Figure 2.1: The National Canyon Study Reach. The photo is taken from a platform where the cable is anchored on the left bank. The view is approximately 1000 meters upstream.

in addition two, eleven-day study periods of constant discharge were monitored. Each study period was followed by a 3-day period of constant low discharge ($140 \text{ m}^3/\text{sec}$). The downstream travel time to Lake Mead of the wave released at Glen Canyon Dam is approximately three days, depending on the peak discharge. The 3-day period of constant low discharge served to define an end to the research flow period, that would be observed in the research flow record, prior to resuming normal dam operation or beginning a new research flow period.

The National Canyon studies were conducted between December 1990 and July 1991, as described in Table 2.1. Research flows A, B, and C were used for preliminary studies to establish sampling schemes used during research flows D, E, F, and G.

Start Date	End Date	High Discharge	Low Discharge	Research Flow
		m^3/sec (<i>cfs</i>)	m^3/sec (<i>cfs</i>)	
Dec. 17 1990	Dec. 27 1990	311 (11,000)	Steady Flow	A
Dec. 31 1990	Jan. 10 1991	566 (20,000)	283 (10,000)	B
Jan. 28 1991	Feb. 7 1991	425 (15,000)	142 (5,000)	C
May 6 1991	May 16 1991	736 (26,000)	85 (3,000)	D
May 20 1991	May 30 1991	425 (15,000)	Steady Flow	E
July 1 1991	July 11 1991	920 (32,500)	85 (3,000)	F
July 15 1991	July 25 1991	708 (25,000)	283 (10,000)	G

Table 2.1: Research flow schedule from December 1990 to July 1991.

The data collection process described herein is the process that was used during the fluctuating flow period between July 15 and July 26, 1991, research flow G. All measurements were made using standard USGS techniques (*Marchand et. al.*, 1984 [9] and *Interagency Committee on Water Resources*, 1963 [14]) and were made in English units. The measurements have since all been converted to metric units.

2.2 Measurements Made During the Study Period in July, 1991

The National Canyon Gaging Station is equipped with a pressure gage that permanently records the water surface elevation (stage) every 15 minutes and a Manning sampler that automatically collects water samples. At many USGS gaging stations, measurements of discharge of water and suspended sediment are made on a daily basis. These measurements, however, require an operator and due to the remote location of the National Canyon site, it is not feasible to collect these properties on

a regular basis. During the National Canyon studies, a permanent camp was established at the gage. The camp was equipped with a small fuel driven generator that produced sufficient electricity for the few electrical instruments, a portable computer to record data as it was collected and a scale for weighing the suspended sediment samples.

A grid of 20 cross-sections was established upstream from the cableway, and in the vicinity of the cableway these cross-sections were tied together with 5 longitudinal passes made near the center of the channel (see Figure 2.38). In Figure 2.4 the grid of cross-sections is shown. In Figure 2.4, the curvature of the reach appears greater than it actually is, due to different scales of the x and y axes on the diagram. The study reach begins at the cableway and extends approximately 1500 meters upstream.

During research flow G the flow fluctuated in diurnal cycles between a low discharge of $280 \text{ m}^3/\text{sec}$ and a high discharge of $710 \text{ m}^3/\text{sec}$. Suspended sediment and velocity profiles were measured from a cableway suspended across the river at the National Canyon gaging station during peak and trough discharge. The cableway was equipped with two cablecars and a smaller cable with stay lines to stabilize the instruments in the flow. Sampling from the cableway is illustrated in Figure 2.2.

Eleven permanent measuring positions were established across the river, as shown in Figure 2.5. The position of each station was marked on the cable. Each cablecar had a brake to secure the vehicle at one of the permanent positions on the cable while measuring at that location and a machine driven winch to hoist the instruments. The instruments were attached to a steel wire. Each time a series of measurements was made from a new position on the cableway, the length of the wire between the winch and the surface of the river was registered with a precision of 2.5 cm , to provide a reference for the following measurements. A series of measurements was started from each bank and the cablecars would meet at the center of the river. All cablecar measurements were made by professional hydro-technicians with experience in using the sampling techniques.

2.3 Velocity Measurements

Velocity measurements were made from the cableway, using a Price AA current meter with open cups attached to a fish shaped 25 kg weight. The weight was tethered to a line parallel to the cableway, to secure its position during measurements. For

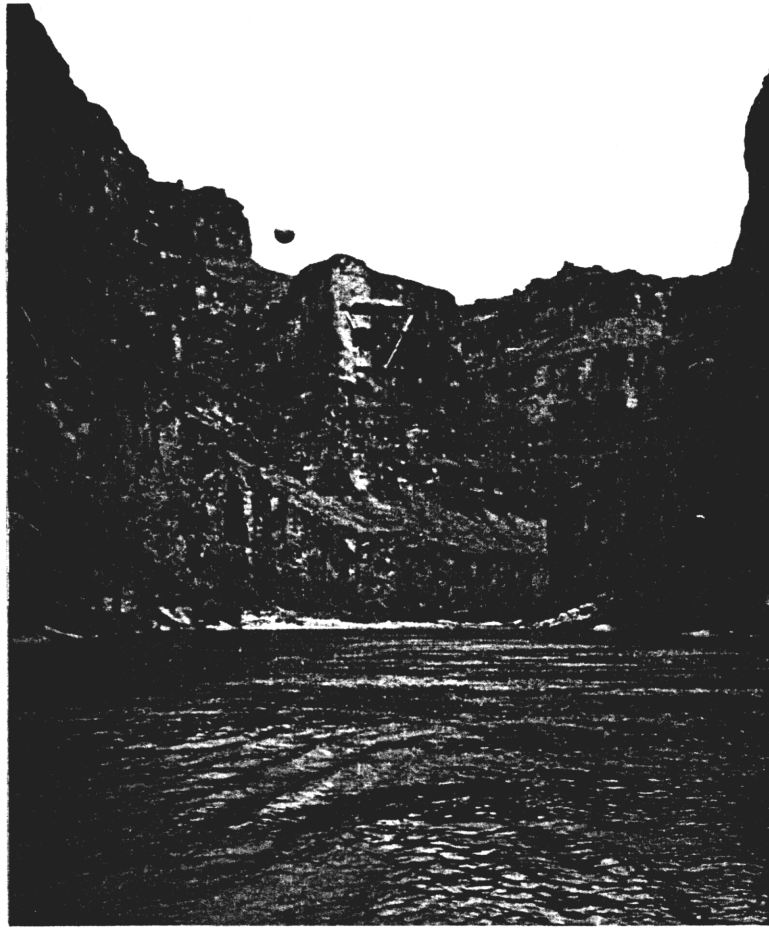


Figure 2.2: Suspended sediment sampling from the cableway. The view is approximately 800 meters downstream.

each rotation of the current meter a click was registered, and the meter was held at each position in the vertical for approximately one minute. Number of revolutions per unit time is related to velocity through the current meter conversion table. Each measurement period lasted for approximately 60 seconds, providing 80 to 150 revolutions. The clicks were counted by the operator. Velocity was measured twice daily, during peak flow at seven points in the vertical and during the trough, at six points in the vertical, and at 11 stations across the river. The vertical distances between measurements were spaced closer towards the bottom of the river. The velocity measurements made at both high and low discharge are plotted as a function of height above the bottom, and are shown in Figures 2.6 to 2.16. The difference in water surface elevation between high and low discharge is approximately 1.6 meters. Each

plotted point represents a velocity measurement at a specific elevation above the bed. The curve through the data is the average of all velocity measurements made at a specific elevation above the bed, at that station.

One cross-section of velocity measurements was completed in approximately 1.5 hours at lower stage, with a change in surface elevation of 20 *cm* or 4 % of the total depth and in approximately 2 hours during upper stage with an elevation change of 25 *cm*, equivalent to 3 % of the total depth. The difference in total sampling time is due to more samples being collected during the peak discharge. The variations in stage during the measurements were too small to be considered. An average depth during the measurement period was calculated instead for each station across the river. As seen in Figures 2.6 through 2.16, the measured velocity profiles display a significant amount of scatter. Small variations in velocity due to depth changes are clearly not resolved in the data-set.

The variability that is observed in the data set is primarily due to turbulent fluctuations of a larger scale than the sampling time. The data set would display less scatter if the sampling time had been longer. Ideally measurements should have been made for 3 or 4 minutes, but under such circumstances it would take almost a day to make one set of velocity measurements. The average profiles, particularly towards the center of the channel, are close to logarithmic in structure.

2.4 Suspended Sediment Measurements and Analysis of Samples

Point measurements of suspended sediment were made using a P-61 milk bottle suspended sediment sampler. A drawing illustrating the instrument is shown in Figure 2.17. Inside a 45.4 *kg* cast bronze fish-shaped weight is a bottle that holds one liter of water and sediment. The weight is spherical pointing against the current and a nozzle with an 4.8 *mm* opening is attached. An electrical device in the cablecar permits the operator to open and close the valve controlling inflow through the nozzle. The instrument is designed with a pressure-equalizing chamber that permits the pressure inside the instrument to adjust to the pressure in the surrounding flow between measurements, allowing the water to flow through the nozzle with undisturbed velocity. When the intake valve is closed, the bottle is connected to the pressure-equalizing chamber, and the pressure in the bottle adjusts to that in the pressure-equalizing chamber which is the same as that in the surrounding flow. When the intake valve is

opened, the bottle is switched to a connection with an exhaust opening in order to let air out of the bottle as water comes in. (*Interagency Committee On Water Resources*, 1963 [14]) The bottle was replaced between each point measurement. Concentration of suspended sediment was measured at seven points in the vertical at 11 stations across the river, twice daily, which came to a total of 1276 samples during trip G. A substantial part of the field work consisted of taring bottles and weighing, labeling and packing the suspended sediment samples.

Analysis of the suspended sediment samples was carried out at the US Geological Survey sediment laboratory facilities in Vancouver, Washington. The sediment distribution in each sample was determined using a VA-tube. For this analysis a 120 *cm* glass tube filled with water is utilized. Prior to the analysis, the sediment was sieved to separate the silt fraction (sizes smaller than 0.0625 *mm*) from the sand fraction (sizes greater than 0.0625 *mm*) and the water temperature was measured to enable determination of the water viscosity. The sand fraction was introduced at the surface of a water column and had to settle 120 *cm*. The material settles at a velocity that is approximately proportional to particle size, where coarse material settles the fastest. The height of the settled sediment column was measured at time intervals, corresponding to the time it takes for sediment of a given size to settle 120 *cm*. The tube is connected to a device that recorded the column height automatically as a function of time. An example of a chart generated during the analysis is shown in Figure 2.18. When sediment of 0.0625 *mm* has settled, the height of the sediment column is measured. This height is equivalent to the weight of the sand fraction. To determine the fraction of size 0.0625 *mm* and smaller in the sediment distribution, the ratio of the weight of sand to the total weight of silt and sand is found and subtracted from 1 (*Dan Gooding, USGS, Vancouver, Washington, Pers. Comm.*).

The VA-tube analysis provides information on 3 points in the sediment grain-size distribution, the fractions finer than 0.25 *mm*, 0.125 *mm*, and 0.062 *mm*. Sediment sizes typically follow a lognormal distribution. It has been chosen to estimate the distribution of sediment at 3 levels in the vertical, 15 *cm* above the bed, 183 *cm* above the bed, and 60 *cm* below the surface. Based on data from the VA-tube analysis of samples taken at these 3 levels, a lognormal distribution function has been estimated at each level, Figures 2.19 to 2.21. The function is an estimate rather than an actual fit, which was considered appropriate due to the large scatter in the data which is

related to small sample size.

In a VA-tube grain size analysis, grain size is inferred from settling velocity of sediment, and sediment settling velocity must be known accurately in order to have confidence in the analysis. However, the result of the analysis is dependent on the specific method used to determine settling velocity of a grain size and the settling velocity of a grain may vary depending on whether the grain is settling close to the walls or in the center of the VA-tube. Furthermore the sample size used for the analysis is generally very small (less than a gram of sediment) which increases the uncertainty of the analysis. The errors associated with the VA-tube analysis tends to broaden a narrow grain size distribution (*J. Dungan Smith, Pers. Comm.*).

Based on the sieve analysis the percentage of material finer than 0.062 mm in the sediment sample is known. This fine material moves as wash load. The concentration of fine material has been extracted from the total concentration and is plotted as concentration of silt on Figures 2.22 to 2.31. The remaining material is plotted as concentration of sand on these figures. It is interesting to note that the concentration of silt is uniform with depth as expected for wash load. During the study period, a small flood occurred in one of the upstream tributaries. The flood introduced a large amount of silt in the river which is seen in the data set as one day with significantly higher concentration of silt, whereas no significant change in sand concentration can be detected for that same day.

While sampling with a P-61 milk bottle sampler, the nozzle of the instrument must point directly into the flow. In large rivers three-dimensional flow features as boils or circulation eddies are relatively common and the flow direction can differ substantially from the main direction of flow when these features occur. The measuring technique was not set up in a manner that allowed determination of the main direction of flow and positioning the instrument accordingly, partly because this is not feasible from a cablecar far above the river.

Suspended sediment is related to the turbulent structure of the flow and as in the case of the velocity measurements, the turbulent time scale may not be resolved over the sampling period. The bottle inside the sampler holds one liter and is filled in less than a minute. In a sample with large concentration of sediment, about 0.5 gram of sediment is collected. A larger sample would increase the probability of collecting a statistically representative sample.

The sampling method assumes that sediment in suspension moves with the same velocity as the surrounding flow. The sample will be skewed if sediment moves with a higher or lower velocity, where a higher sediment velocity would result in a sample with a higher concentration.

2.5 National Canyon Bathymetry

A grid of 20 cross-sections in a 1460 meter reach was established upstream from the cableway. The first 180 meters above the cableway were surveyed in great detail. Cross-sections were measured every 60 meters and were tied together with longitudinal bottom surveys (Figure 2.38). From 180 meters to 850 meters upstream from the cableway, cross-sections were measured every 60 meters and above 850 meters and below 1460 meters, cross-sections were measured every 120 meters. The locations of cross-sections are shown in Figure 2.4.

The cross-sections were surveyed using an echo-sounding instrument placed on a raft. The output of the instrument is a strip chart, displaying the measured bottom topography as a function of time. To determine the shape of each cross-section, 10 passes were made across the river. A tag line was tied across the river between the two end points defining the cross-section, and 10 passes were made along the tag line. The tag line was marked in 10 foot increments and each time an increment was passed the chart was marked. An example of an echo-sounding chart is shown in Figure 2.32

The echo-sounding records were digitized manually using an electronic digitizing table connected to a main-frame computer system. The data were entered as distance from a defined origin in the direction of the y - axis, and as distance above a datum in the direction of the z - axis. Approximately one point per 0.5 mm of echo-sounding chart was registered. For each recorded pass across the river, two files were recorded, one file that included the digitized trace of the pass and another that included the position of the 10 foot marks on the record. The digitized trace was then scaled by the 10 foot increments, and a point every foot was extracted from the record. Furthermore the passes were adjusted to variations in stage, so that the cross-sections are all equivalent to a water surface elevation at stage 12.2 meters at the cableway which corresponds to a discharge of $370 \text{ m}^3/\text{sec}$. The cross-sections were then tied together with the surveyed positions of the cross-sectional end-points, and converted into a local, rectangular, metric coordinate system of the National Canyon

area, where the x - axis is directed along the river, the y - axis is directed across the river, and the z - axis is height above mean sea level (ASL). This coordinate system is used in Figure 2.4 and Figure 2.37. The 10 scaled records for a cross-section were then averaged to provide the final cross-sectional shape as displayed in Figures 2.33 to 2.36, demonstrating the channel structure in the vicinity of the cableway. In addition to these four cross-sections the remaining 16 cross-sections were digitized and analyzed in the manner described. The twenty cross-sections were combined to produce a contour map of the channel bathymetry. The map is seen in Figure 2.37.

Longitudinal drifts were made between cross-section 600 and the cableway. During the drifts, tag lines were tied across the river at cross-sections 200 and 400. When the boat passed under a tag line, the chart was marked, and the cross-stream distance from the LEW was noted on the chart. These records provided very good information of the structure of the bottom. The signal from the echo-sounder is of sufficient detail to register the shape of bed forms on the river bed. An example of this is shown in Figure 2.39. From these records it is also possible to distinguish occasional boulders on the river bed from bedforms. Due to the difficulty of locating the same position twice, longitudinal passes were not averaged if repeated over the same section of the river. Passes were made at 10 meter intervals across the river to capture the variations in bottom topography not otherwise resolved. In the vicinity of the cableway 8 longitudinal profiles were recorded at 5 locations, 3 of the passes were repeated twice. A digitized example of a pass made at each of the five locations is shown in Figures 2.40 to 2.44.

The vertical scale of the strip chart is 1:100. The vertical digitizing accuracy of the strip chart is one millimeter, which is equivalent 10 *cm* in nature. This digitizing accuracy is based on the ability of the operator to evaluate the precise position of a point when the signal is fuzzy. The accuracy of the digitizing equipment is greater. The purpose of defining each cross-section from 10 passes is to provide a cross-sectional shape that is corrected for differences in boat position relative to bottom features and stretching and shrinking errors due to short term variations in boat speed. The longitudinal profiles are also subject to stretching and shrinking error if the boat does not follow a straight line between two marked cross-sections. The echo-sounding instrument distorts sharp edged features into rounded features.

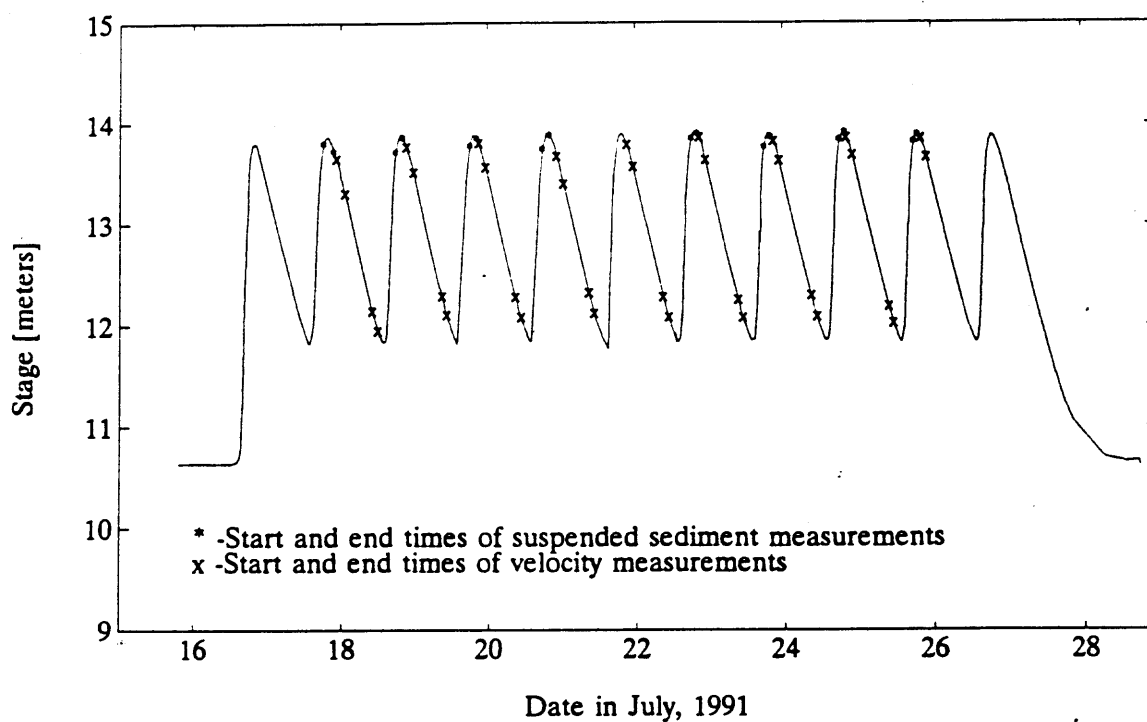


Figure 2.3: Variation in stage during trip G. Low stage corresponds to a discharge of $280 \text{ m}^3/\text{sec}$. High stage corresponds to a discharge of $730 \text{ m}^3/\text{sec}$. Start and end times of suspended sediment and velocity measurements are marked on the curve to indicate stage variation over the sampling period. The time at which the measurements were made was determined by the water surface elevation, rather than by the time of day, to ensure that the measurements were made under approximately the same flow conditions every day, which at times meant sampling at night.

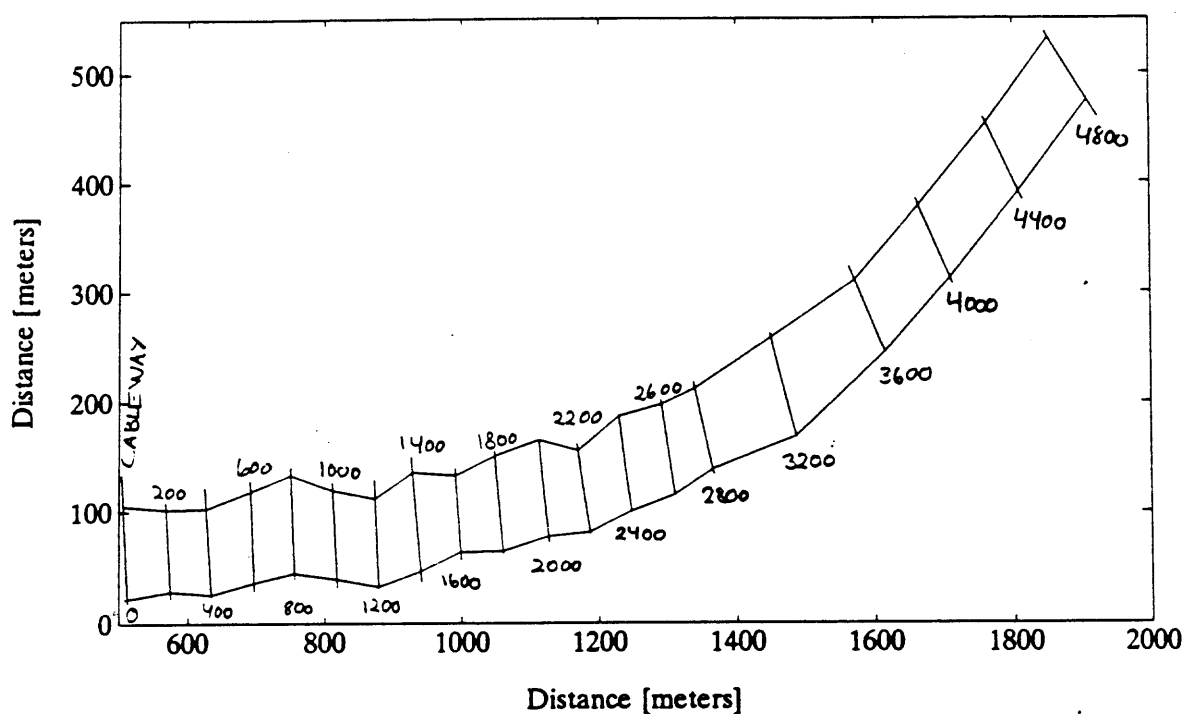


Figure 2.4: Location of cross-sections in the National Canyon Reach. The cross-sections are numbered corresponding to their distance in feet upstream from the cableway. (e.g. cross-section 200 is located 200 feet upstream from the cableway). On this figure, the curvature of the reach appears greater than it is in reality due to different scales of the x and y - axes. A scaled topographic map of the reach is presented in Figure 2.37.

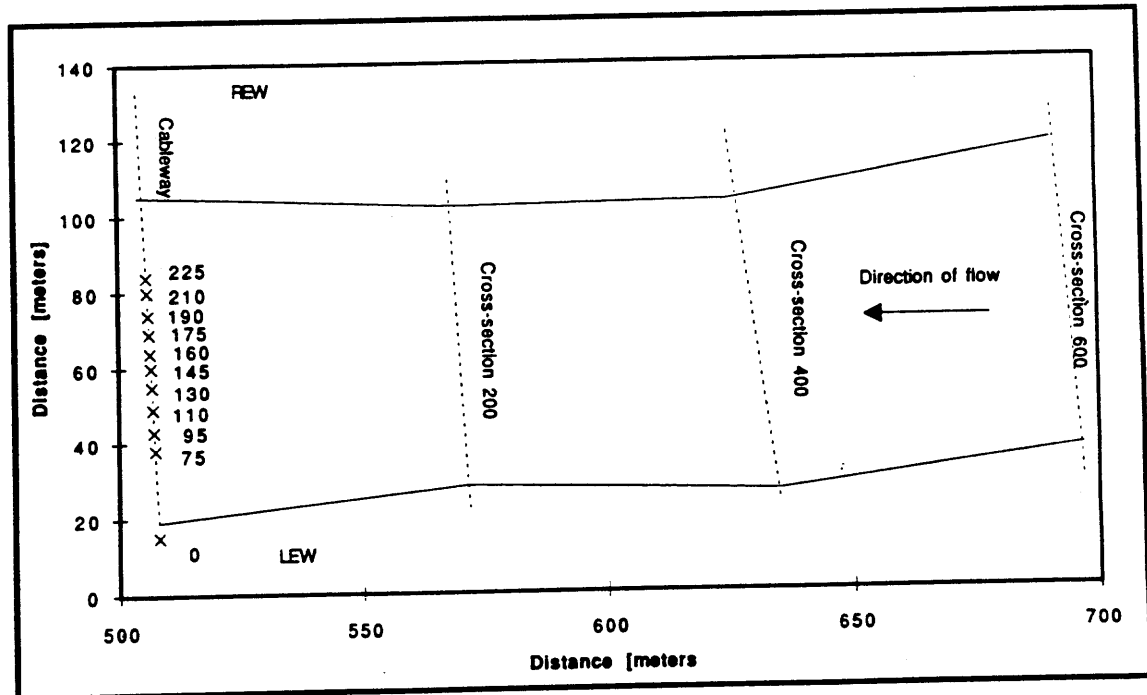


Figure 2.5: Location of stations on the cableway. The stations are numbered corresponding to their distance in feet from the left edge of water, when looking downstream (LEW), (e.g. station 75 is located 75 feet from the left edge of water). REW refers to right edge of water. Solid lines mark the approximate location of the banks. The stipled lines indicate position of cross-sections.

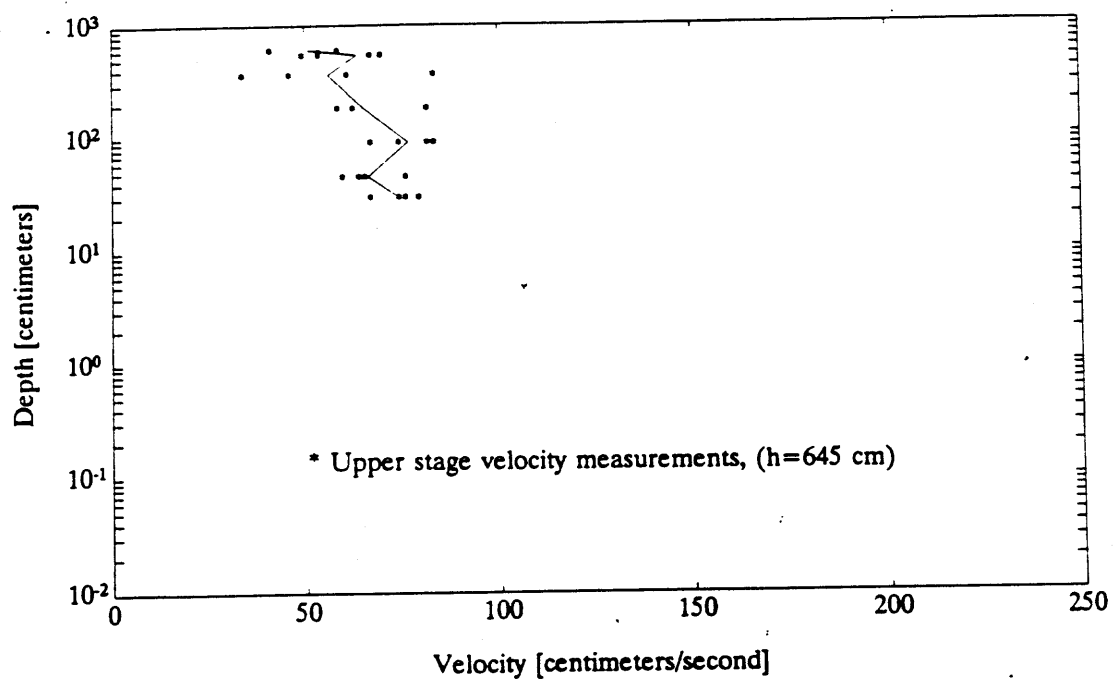


Figure 2.6: Velocity measurements at station 60. Local water depth is h .

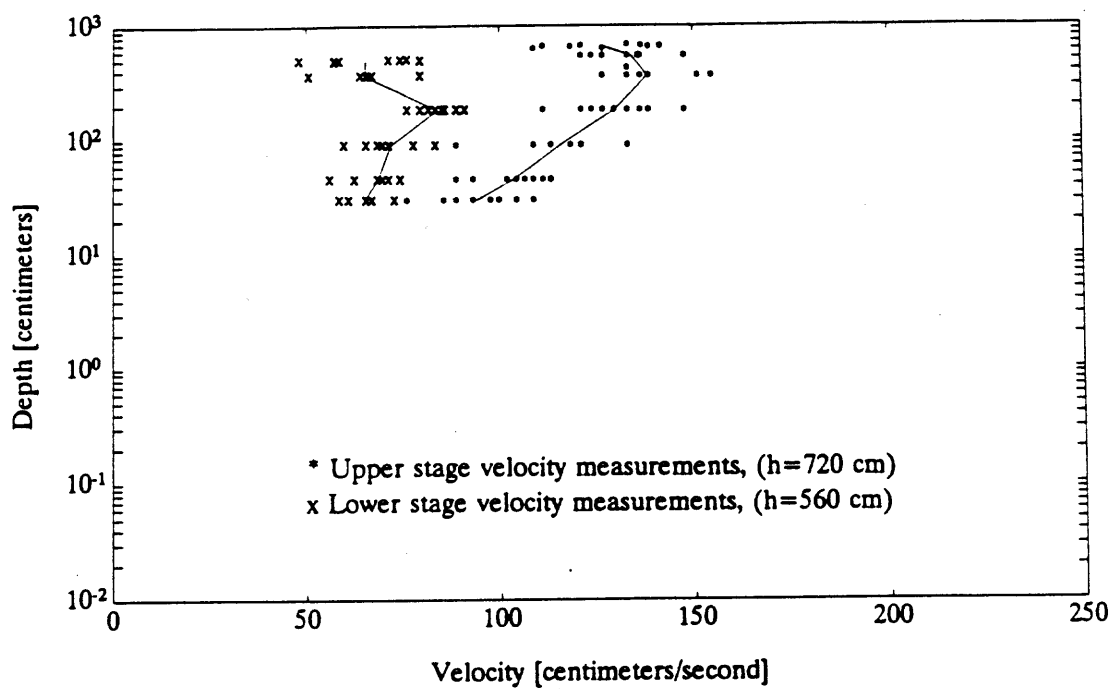


Figure 2.7: Velocity measurements at station 75. Local water depth is h .

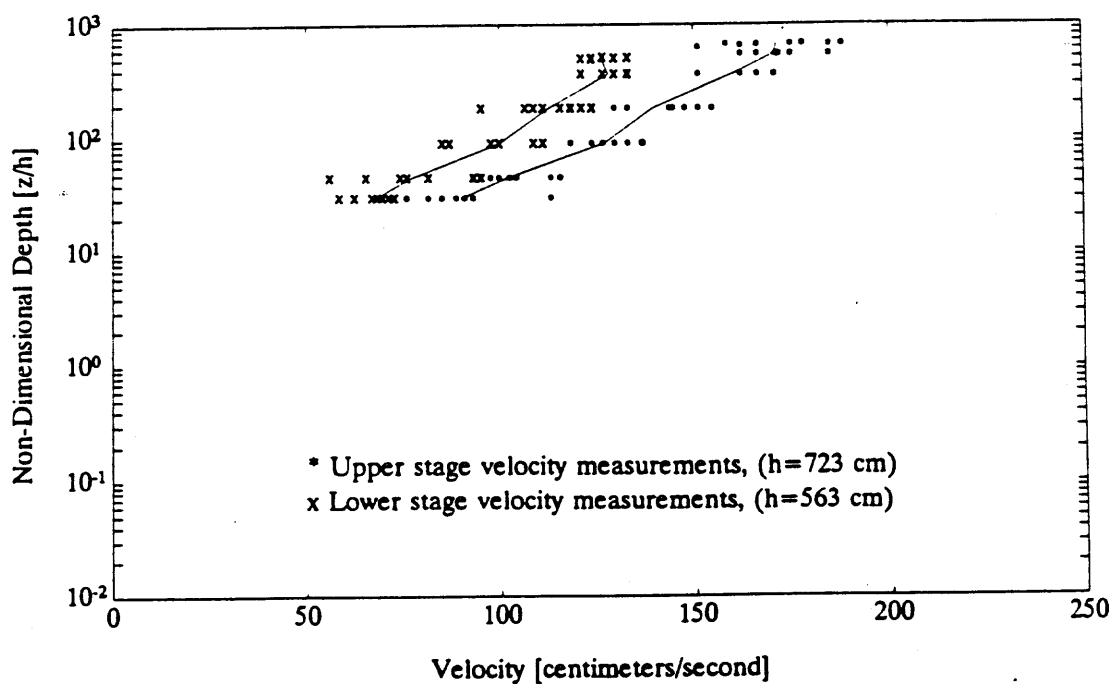


Figure 2.8: Velocity measurements at station 95. Local water depth is h .

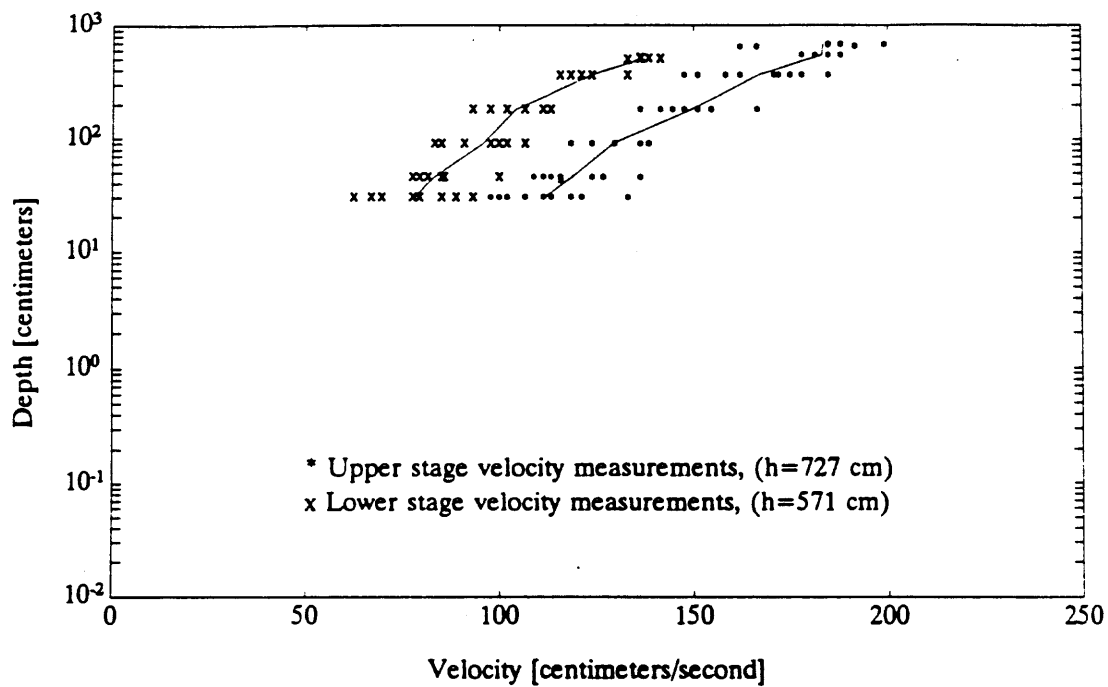


Figure 2.9: Velocity measurements at station 110. Local water depth is h .

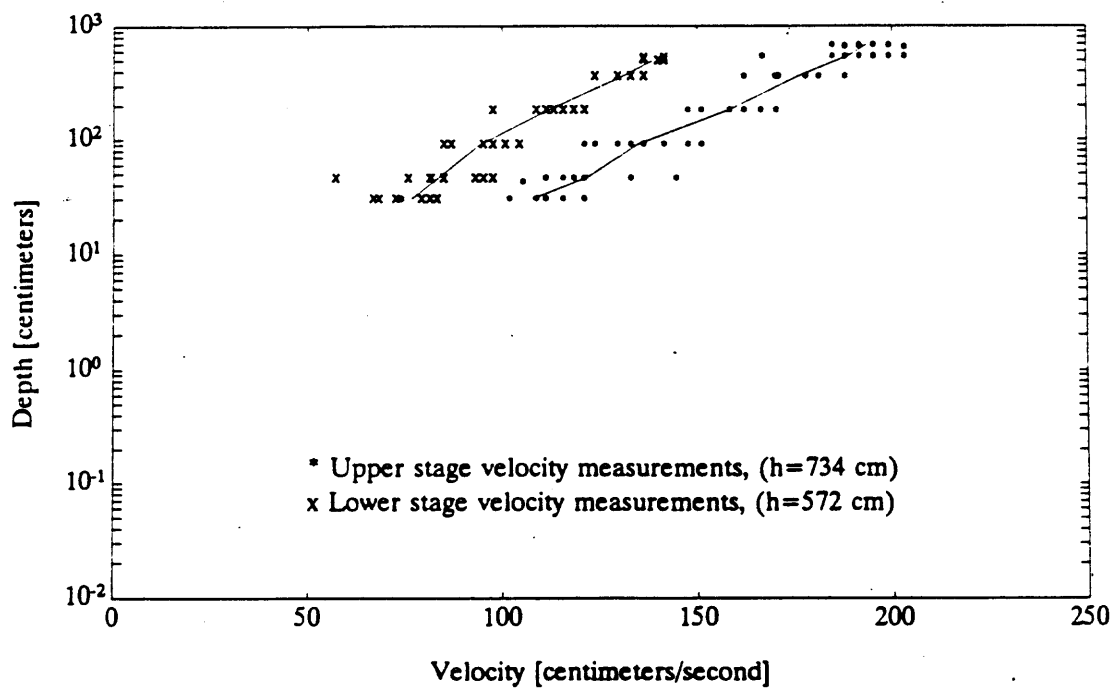


Figure 2.10: Velocity measurements at station 130. Local water depth is h .

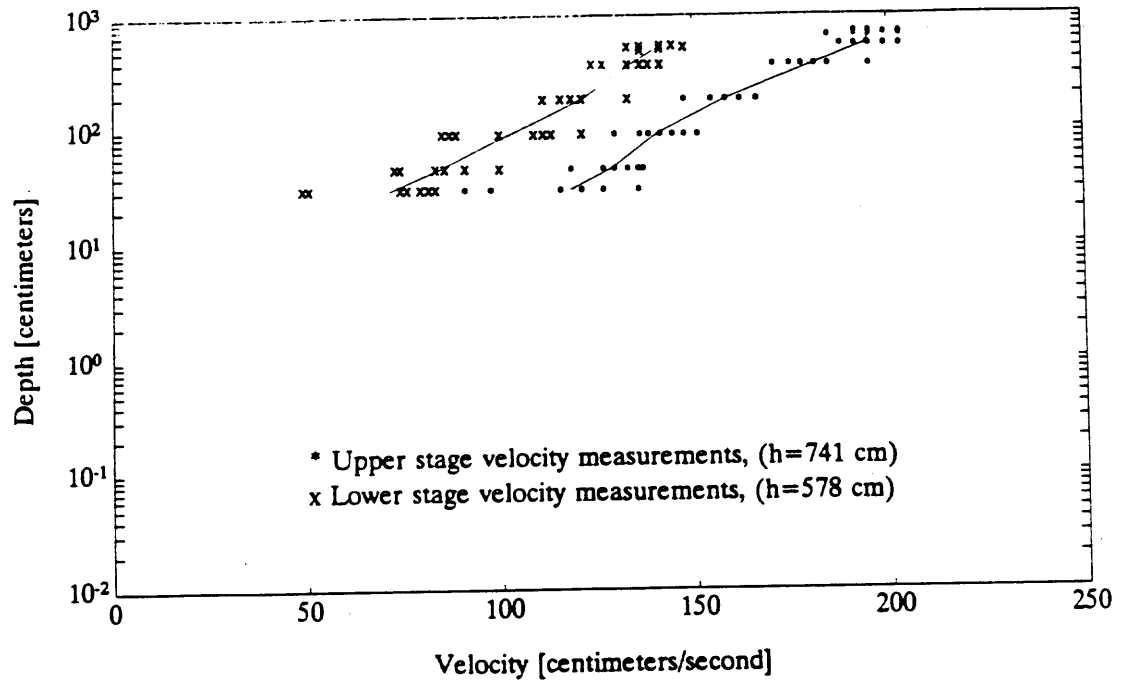


Figure 2.11: Velocity measurements at station 145. Local water depth is h .

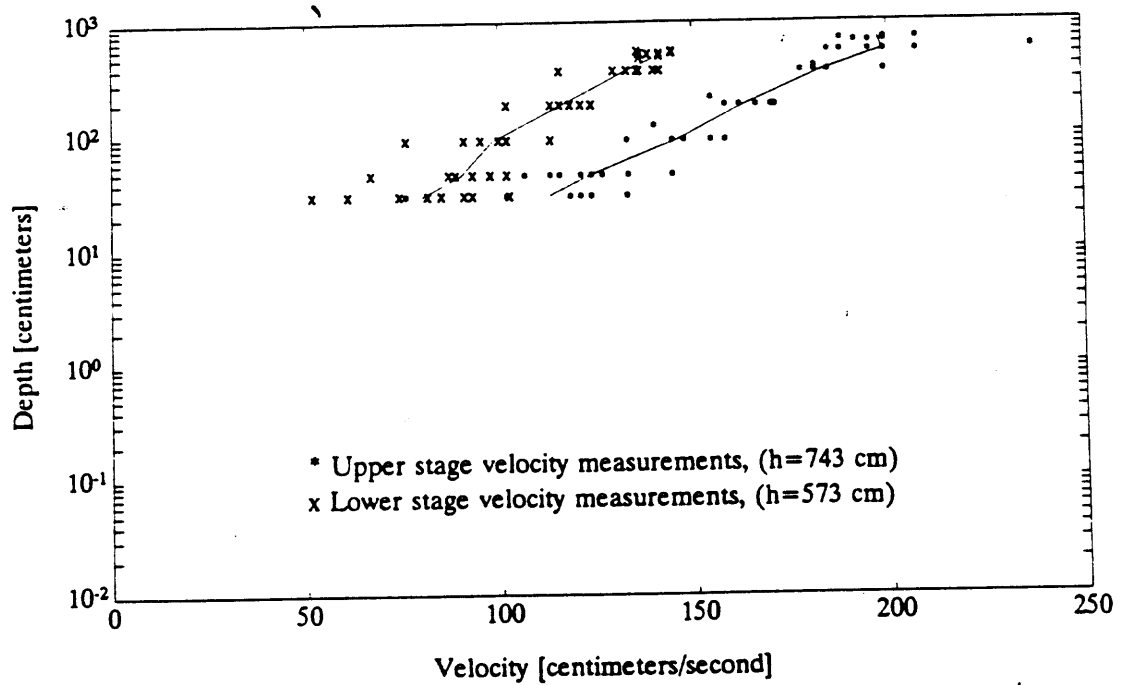


Figure 2.12: Velocity measurements at station 160. Local water depth is h .

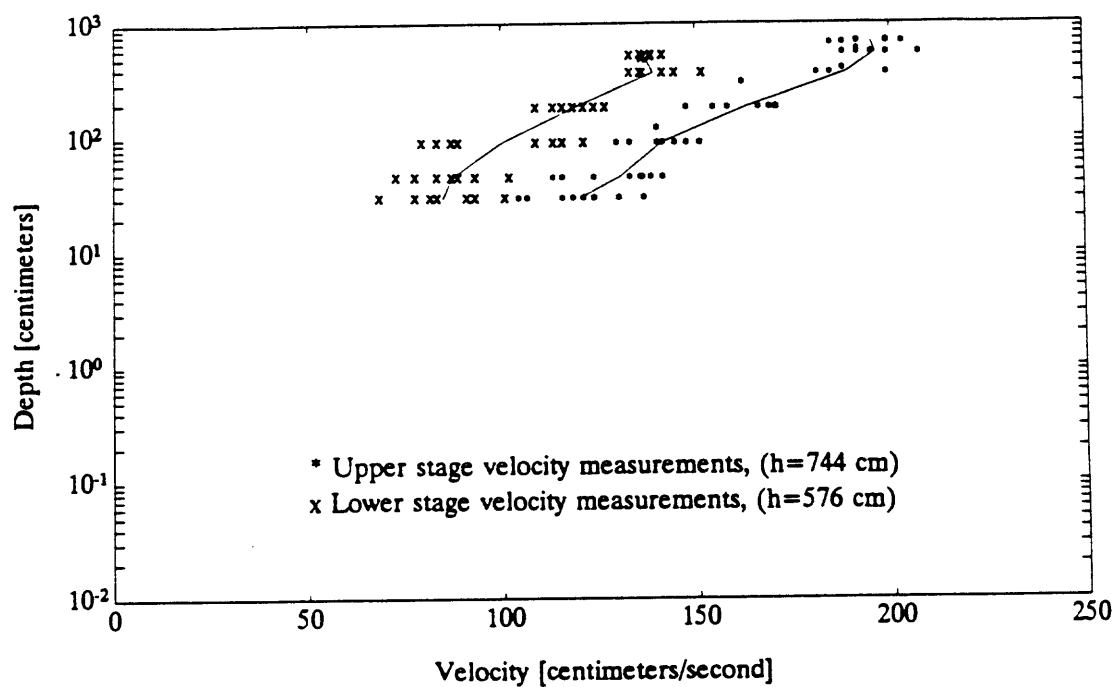


Figure 2.13: Velocity measurements at station 175. Local water depth is h .

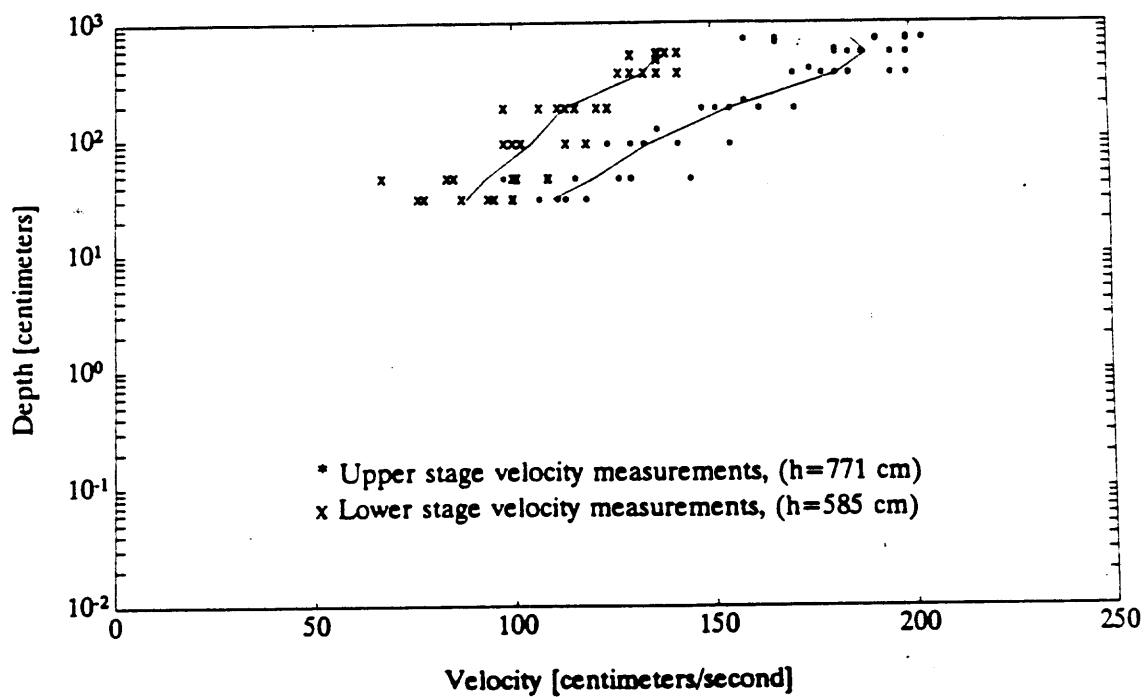


Figure 2.14: Velocity measurements at station 190. Local water depth is h .

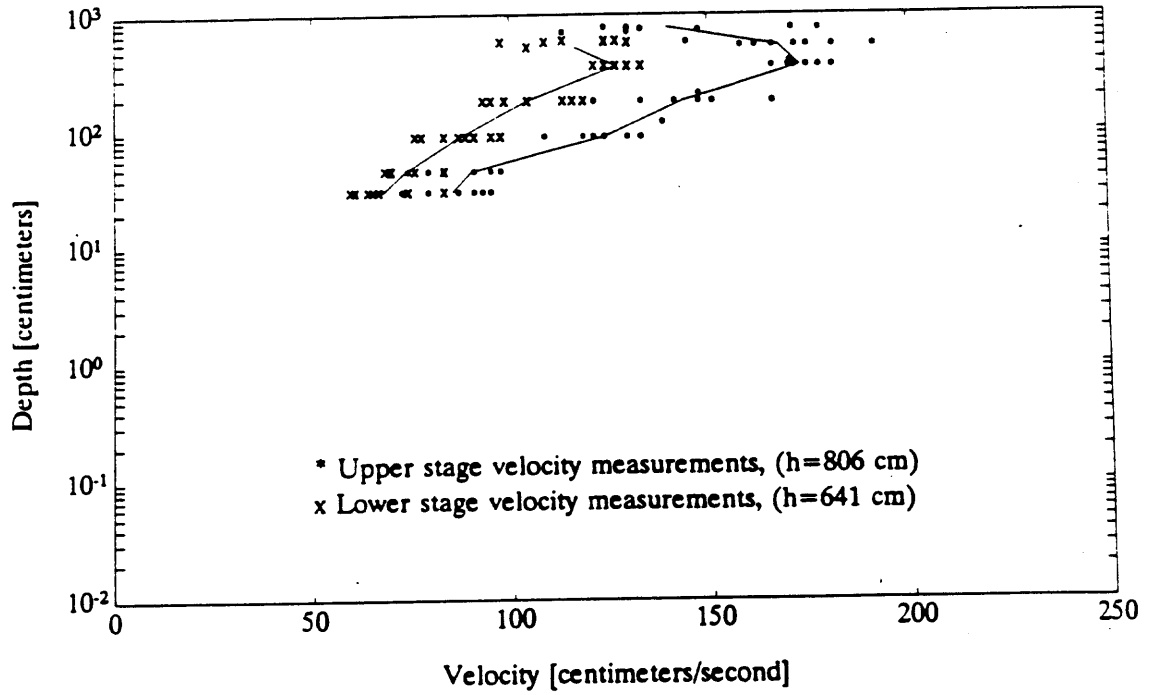


Figure 2.15: Velocity measurements at station 210. Local water depth is h .

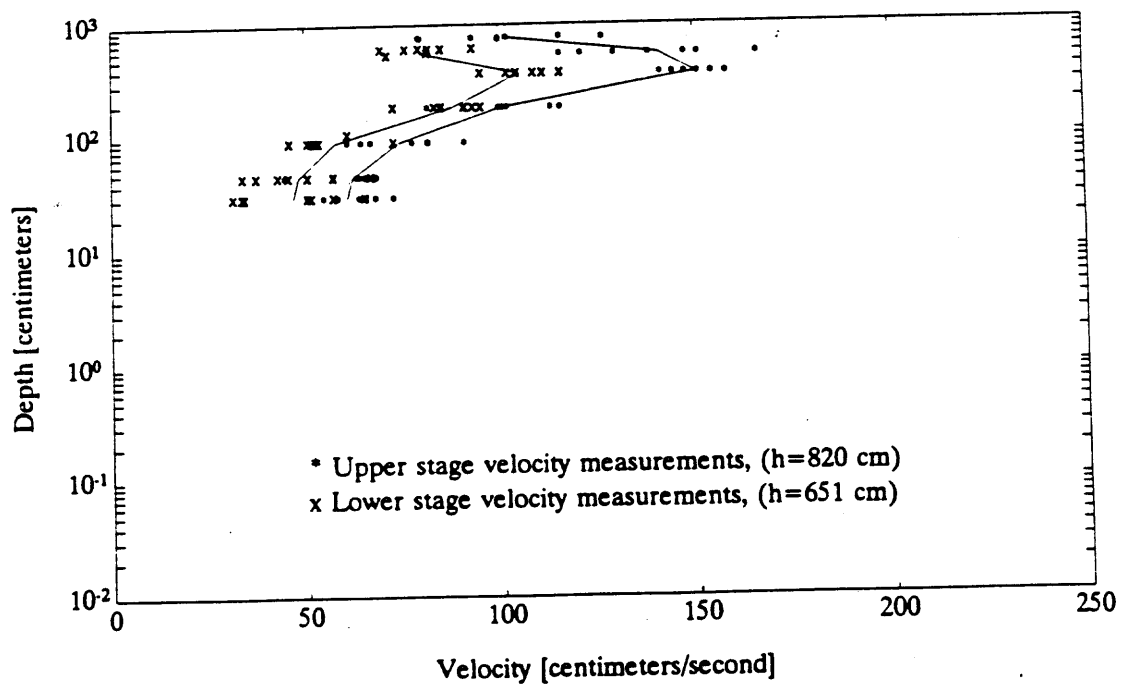


Figure 2.16: Velocity measurements at station 225. Local water depth is h .

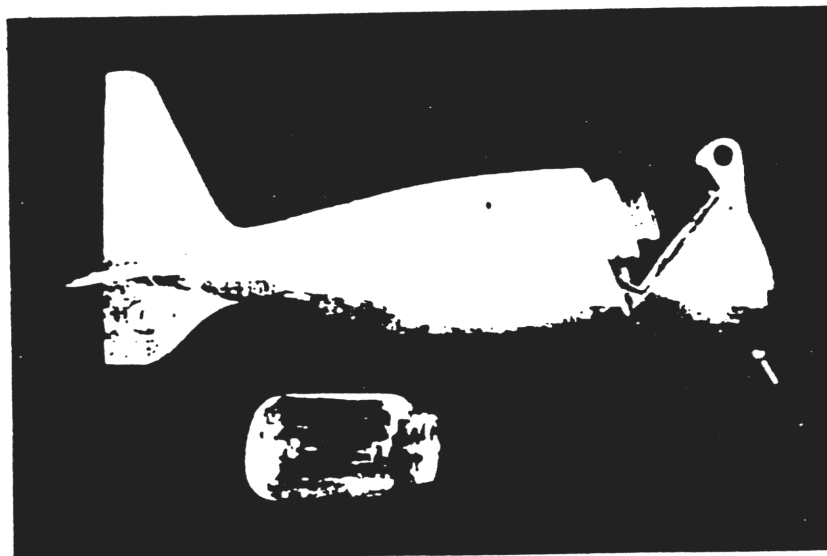
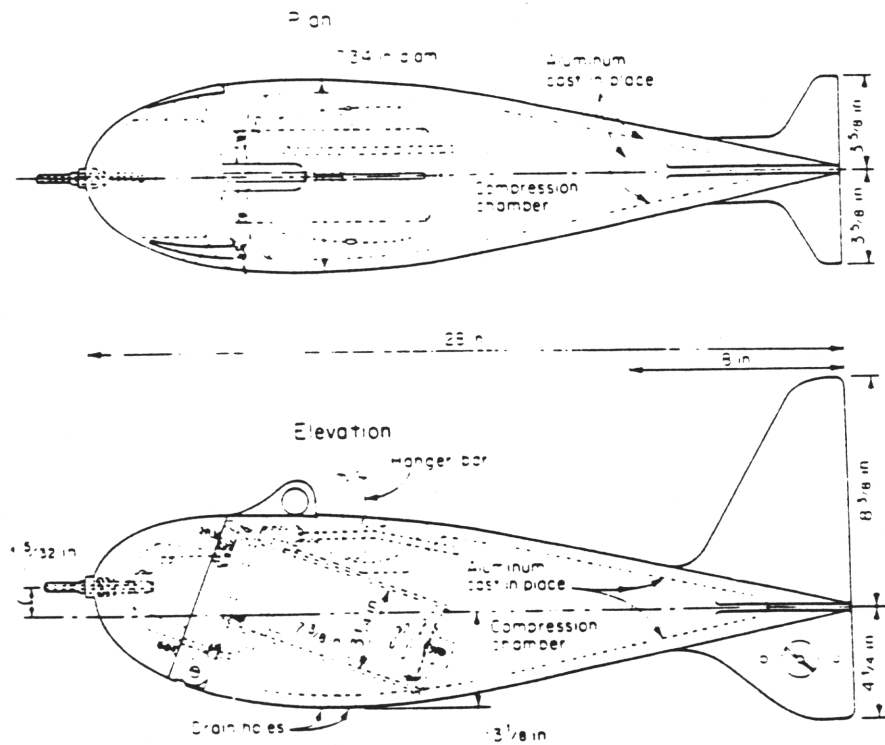
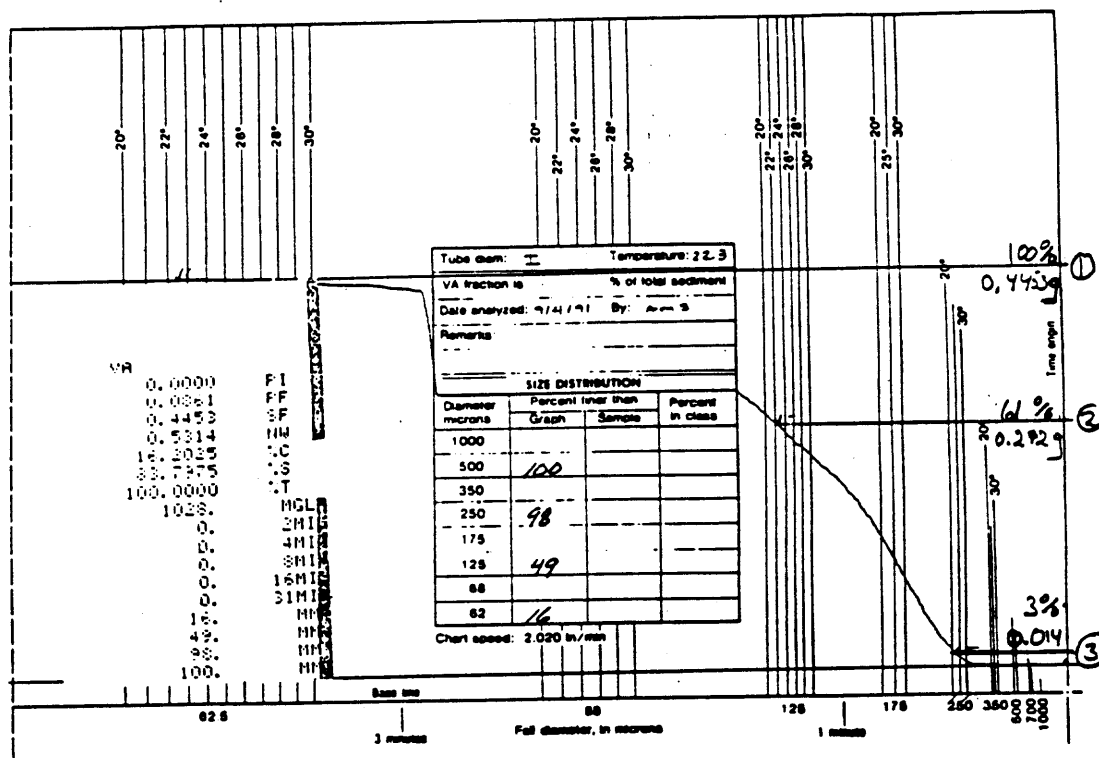


Figure 2.17: P-61 suspended sediment sampler. After *Inter Agency Committee on Water Resources*[1963].



Total weight of sediment sample : 0.5314 g
 Weight of sand fraction : 0.4453 g
 Weight of silt fraction : 0.0861 g

- ① Fraction of 0.062 mm in distribution : $1 - \frac{0.4453}{0.5314} = 0.16$
 ② Fraction of 0.125 mm in distribution : $1 - \frac{0.272}{0.5314} = 0.49$
 ③ Fraction of 0.250 mm in distribution : $1 - \frac{0.014}{0.5314} = 0.97$

Figure 2.18: Example of chart generated during VA-tube analysis.

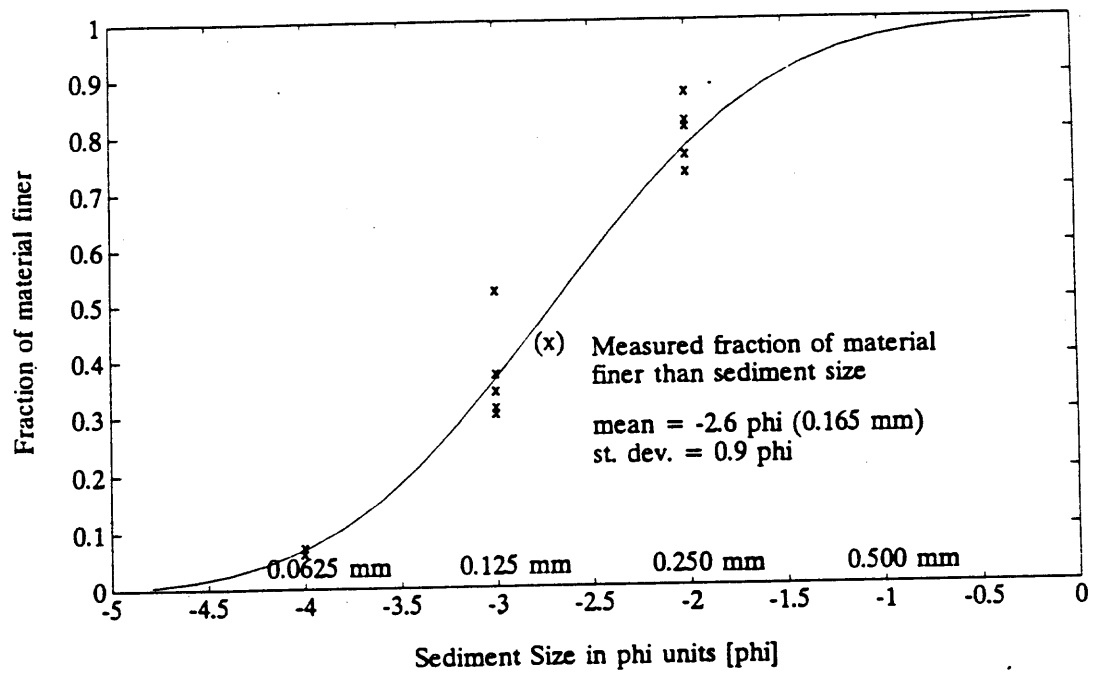


Figure 2.19: Distribution of sediment 15 *cm* above the bed.

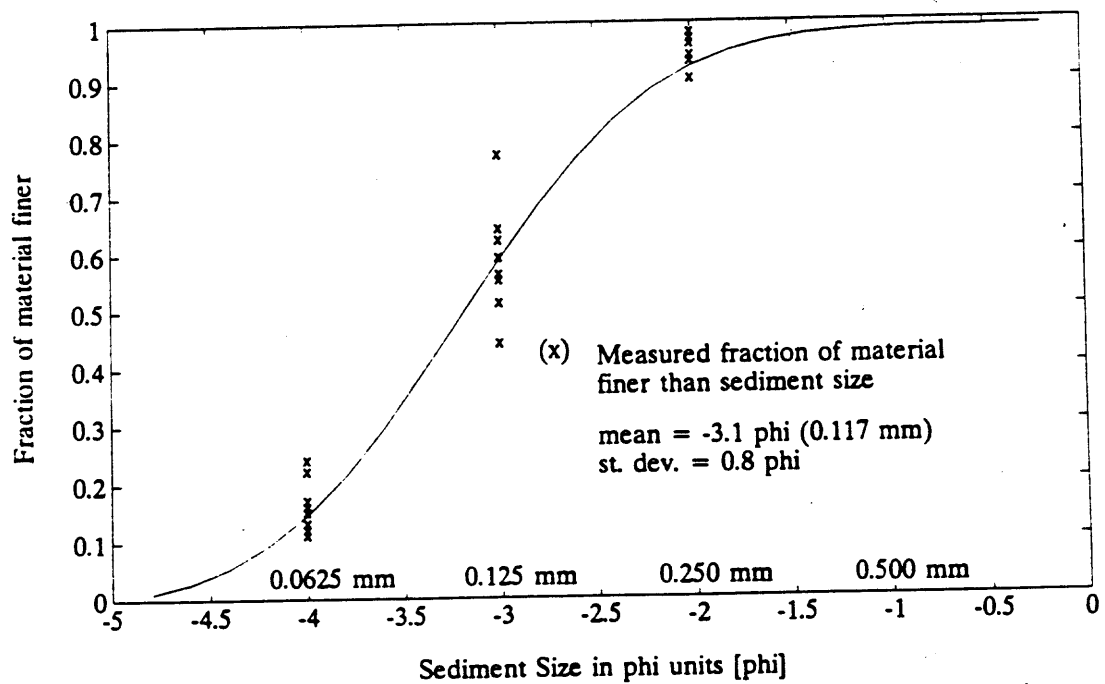


Figure 2.20: Distribution of sediment 180 *cm* above the bed.

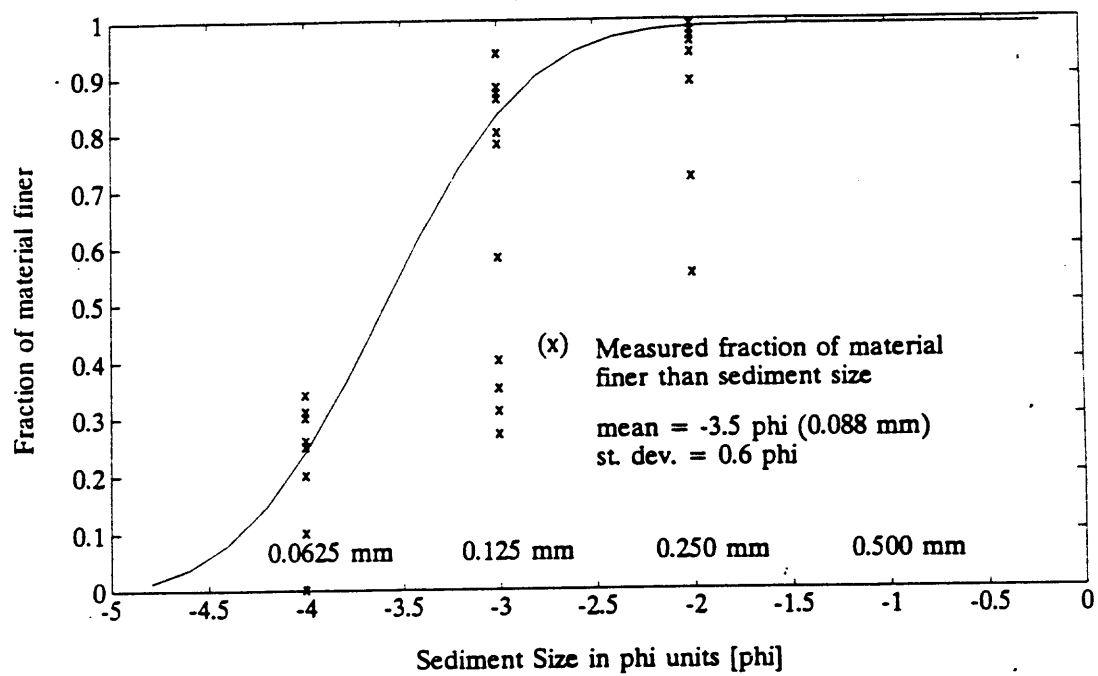


Figure 2.21: Distribution of sediment 60 cm below the water surface.

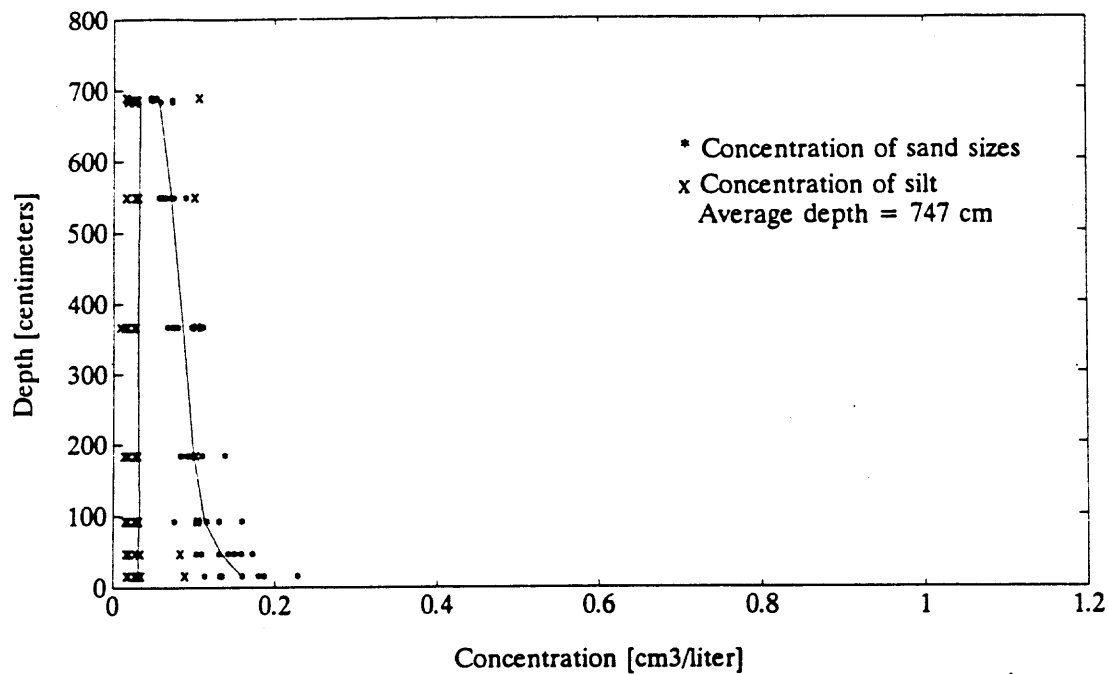


Figure 2.22: Suspended sediment concentration measurements at station 75.

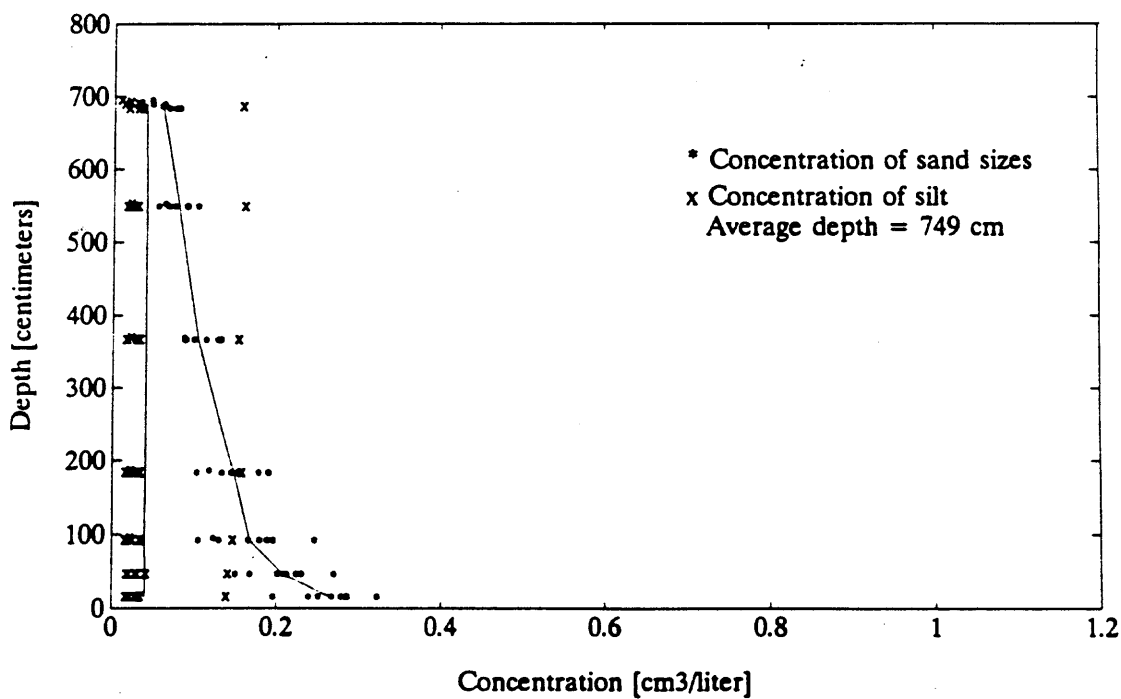


Figure 2.23: Suspended sediment concentration measurements at station 95.

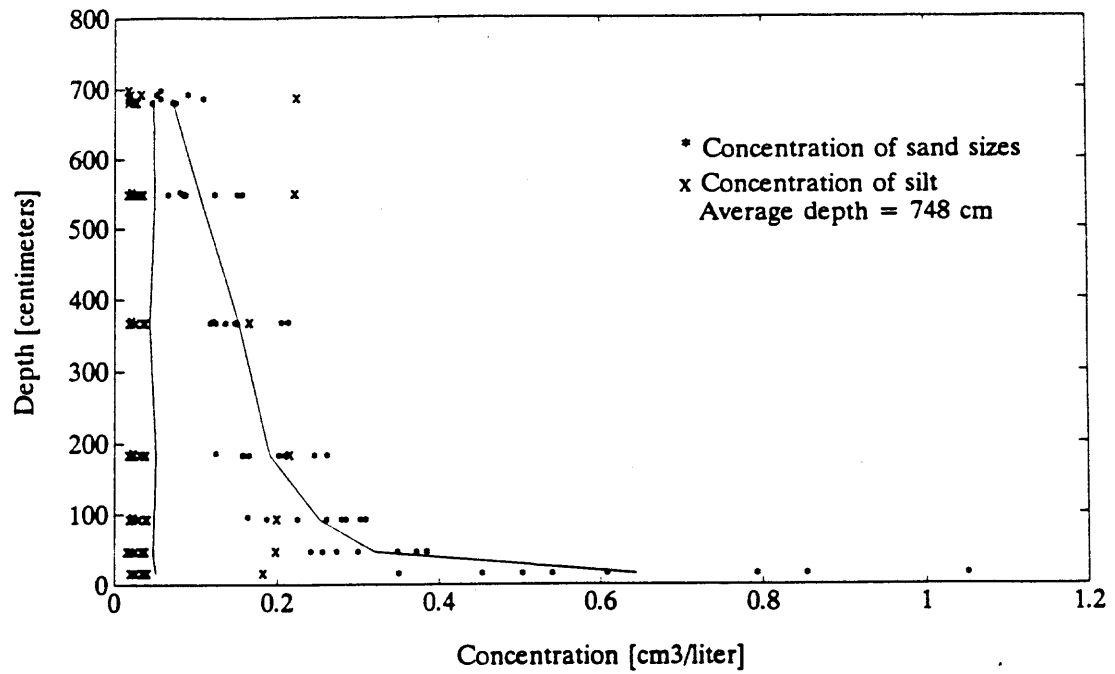


Figure 2.24: Suspended sediment concentration measurements at station 110.

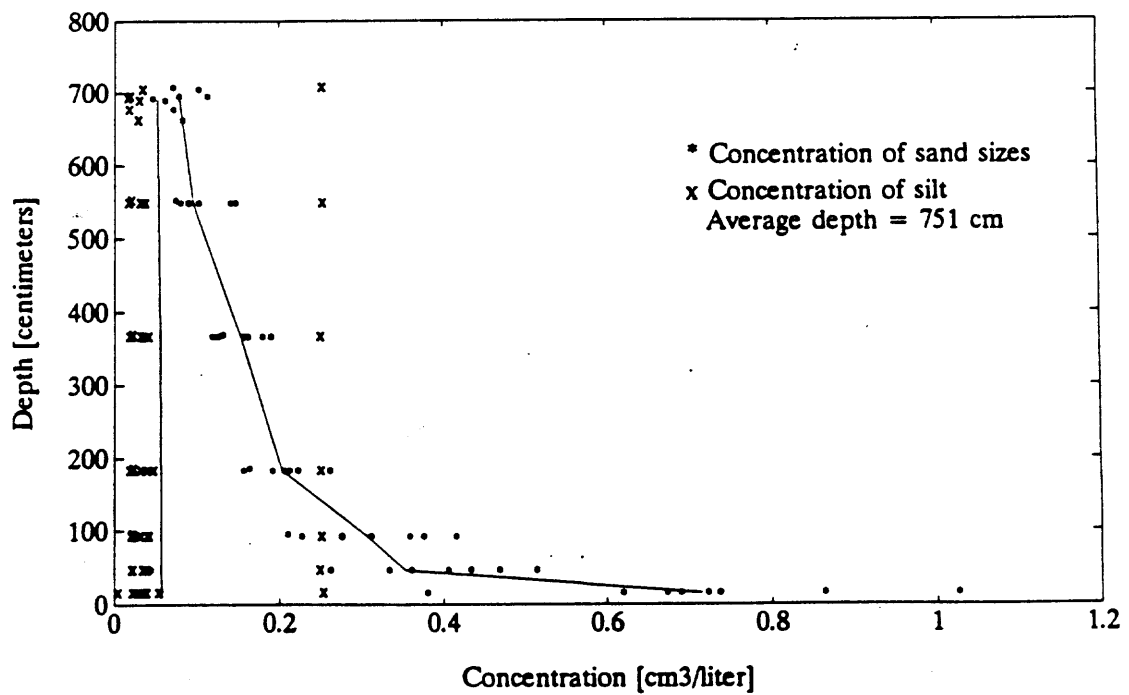


Figure 2.25: Suspended sediment concentration measurements at station 130.

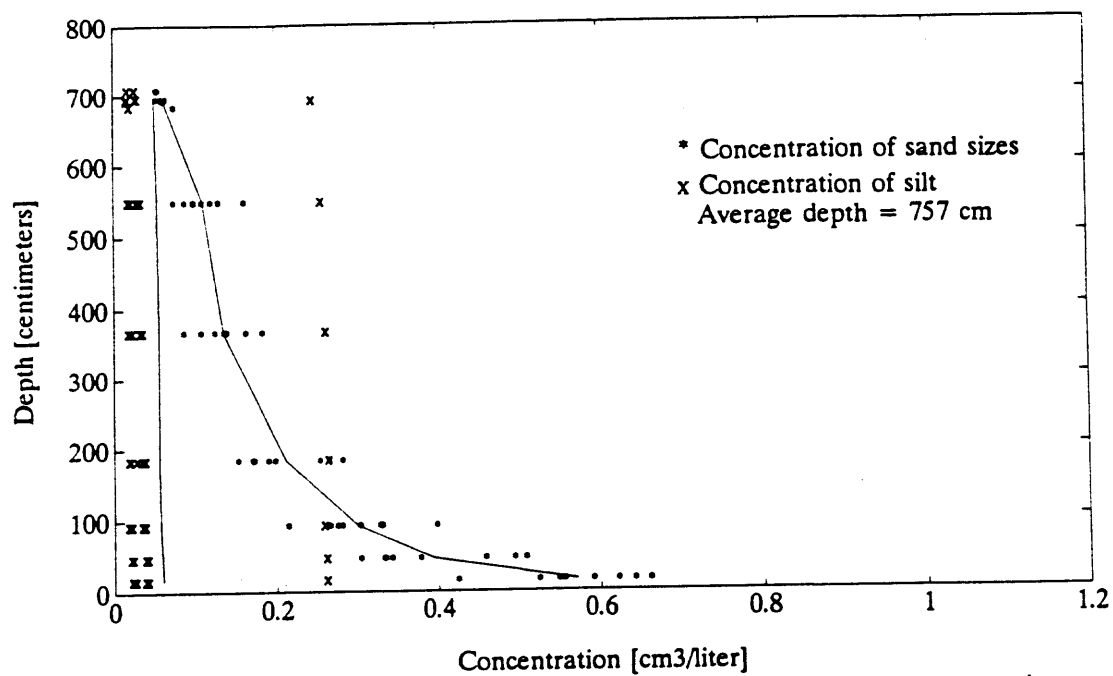


Figure 2.26: Suspended sediment concentration measurements at station 145.

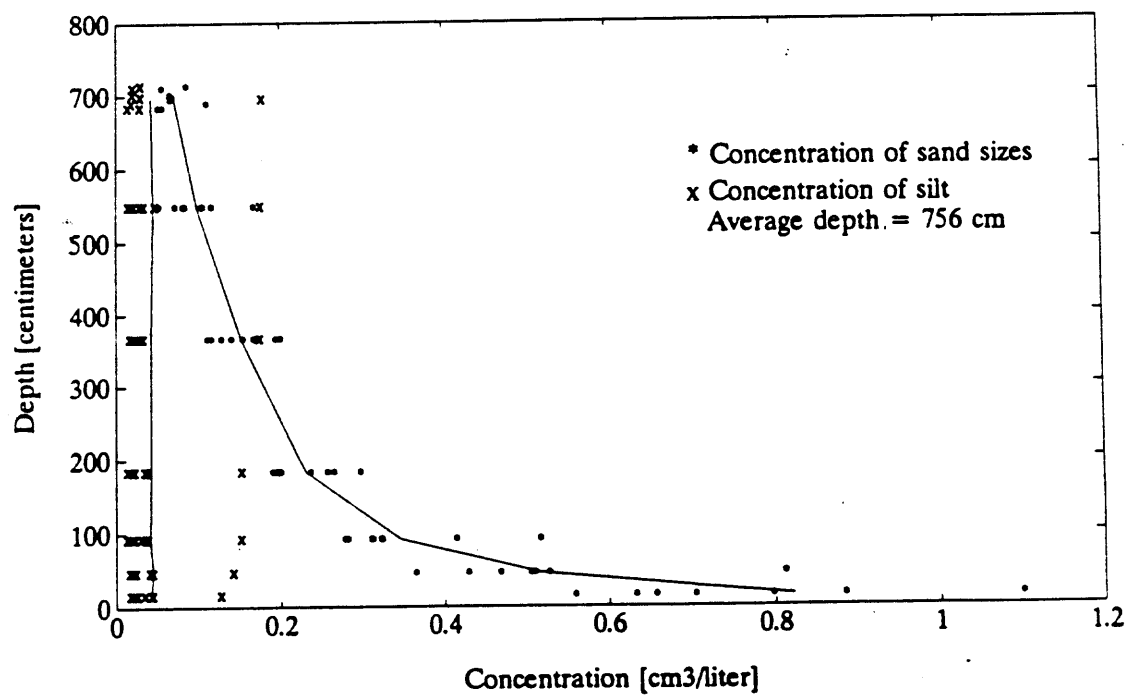


Figure 2.27: Suspended sediment concentration measurements at station 160.

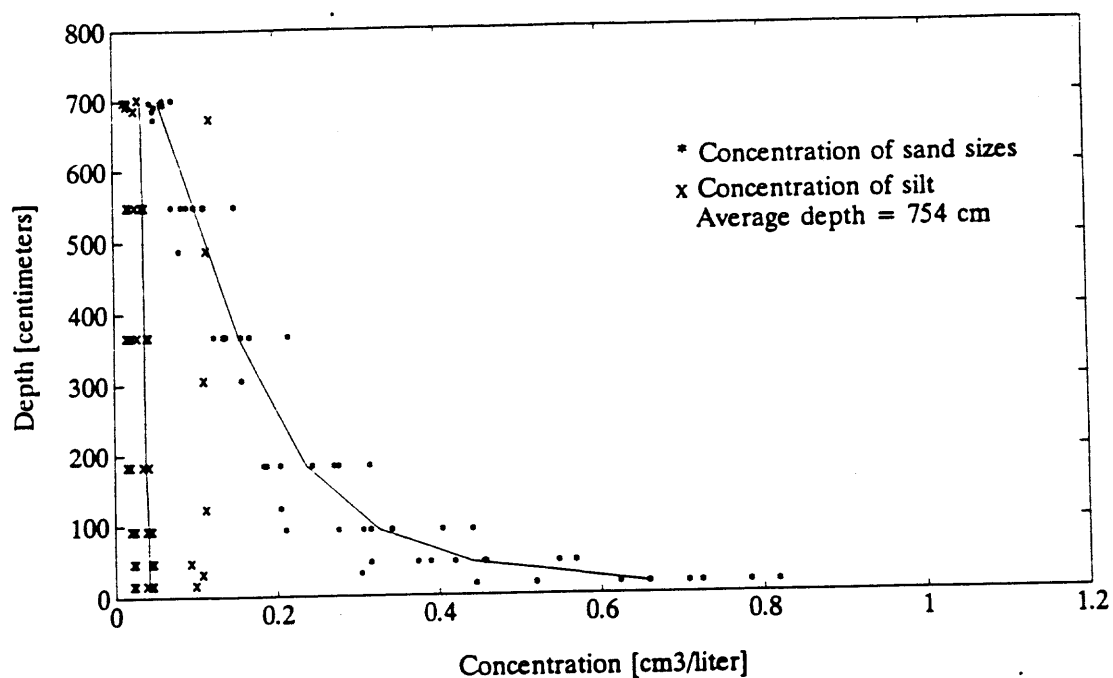


Figure 2.28: Suspended sediment concentration measurements at station 175.

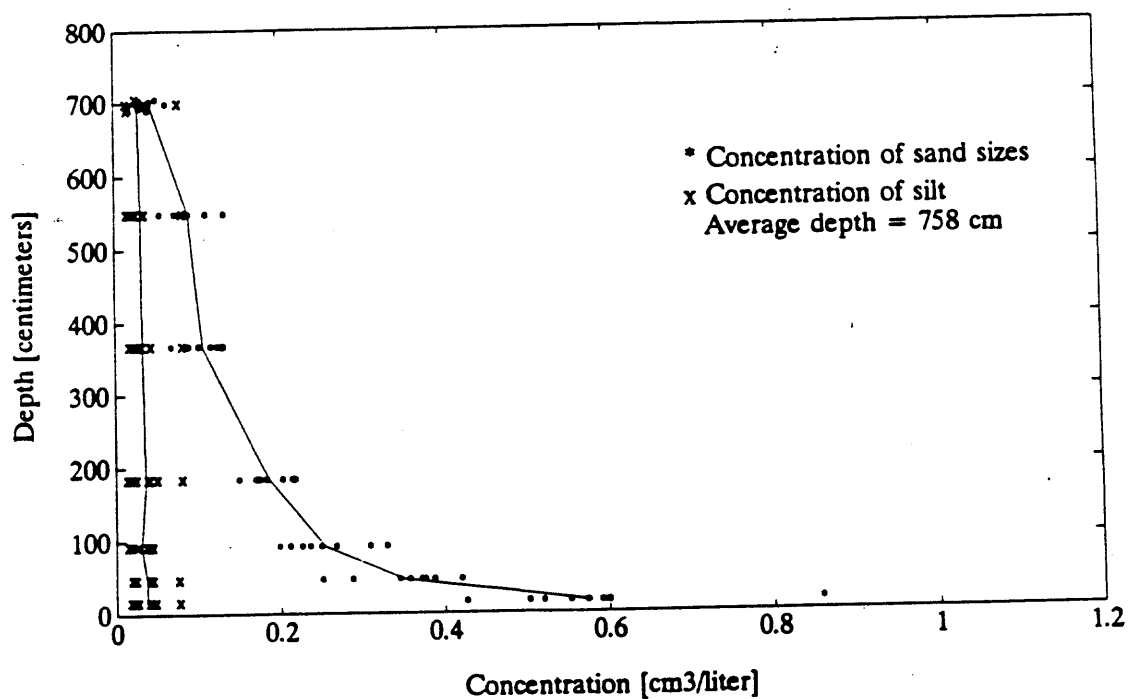


Figure 2.29: Suspended sediment concentration measurements at station 190.

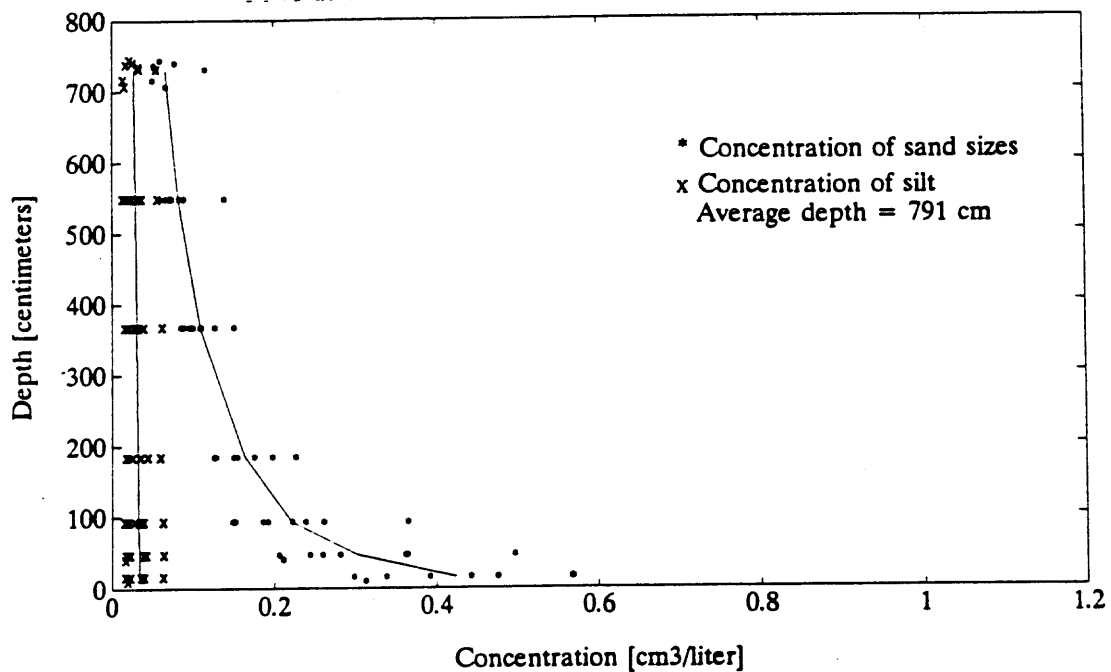


Figure 2.30: Suspended sediment concentration measurements at station 210.

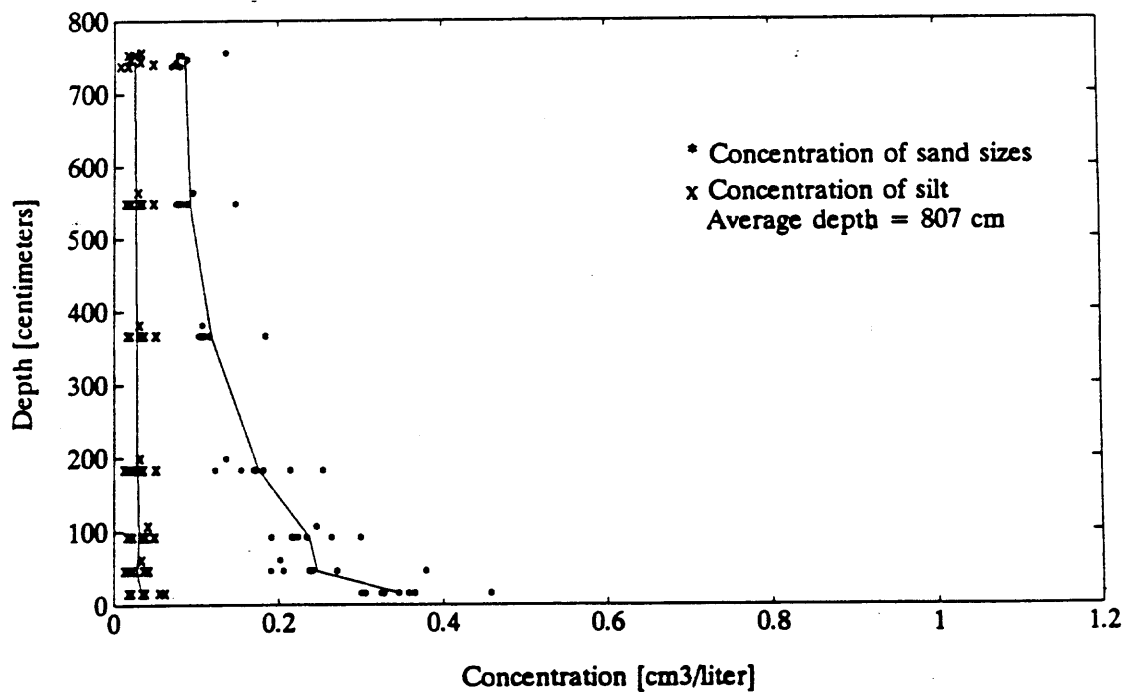


Figure 2.31: Suspended sediment concentration measurements at station 225.

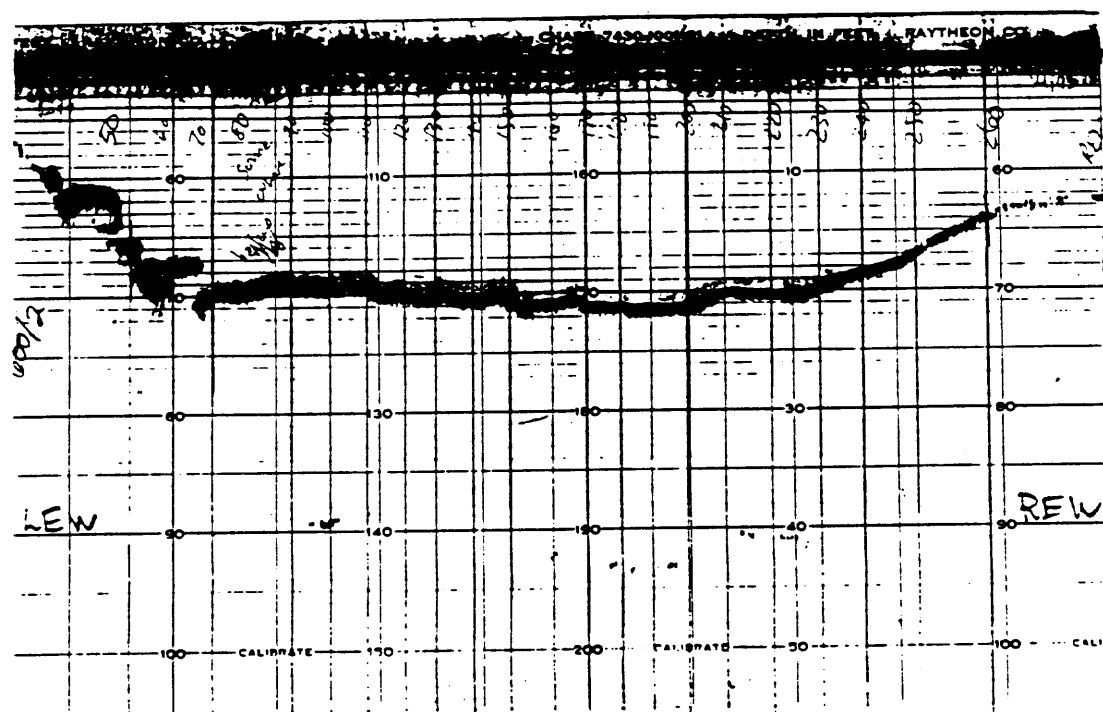


Figure 2.32: Example of echo-sounding chart from cross-section 600. The irregular structure at the left edge of water indicates that there are boulders present near the bank. The right edge of water and the center of the channel show only gradual variations, indicating a layer of sand on the bed and bank.

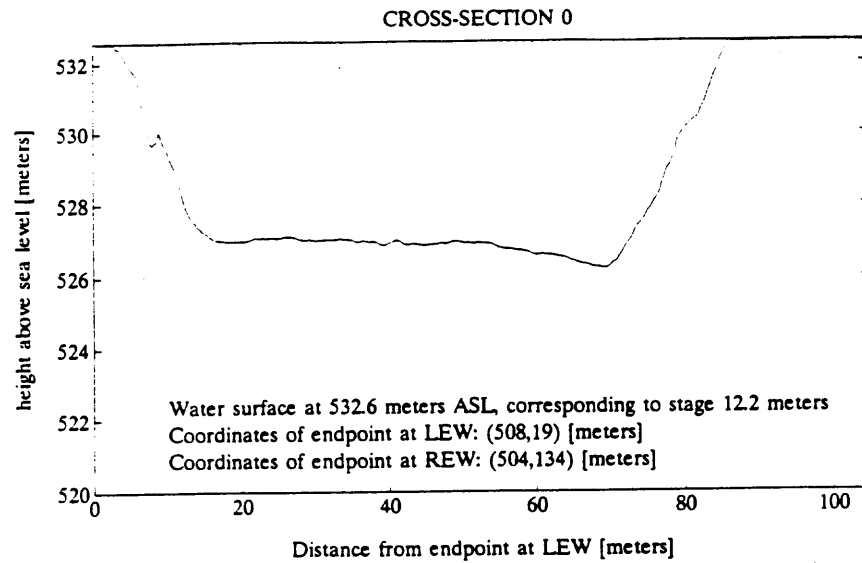


Figure 2.33: Cross-section 0. The x - axis is distance in meters from the bank at the left edge of water, and the distance does not correspond to the local coordinate system of National Canyon. ASL refers to height above mean sea level. The discharge at the cableway, at stage 12.2 meters is $370 \text{ m}^3/\text{sec}$.

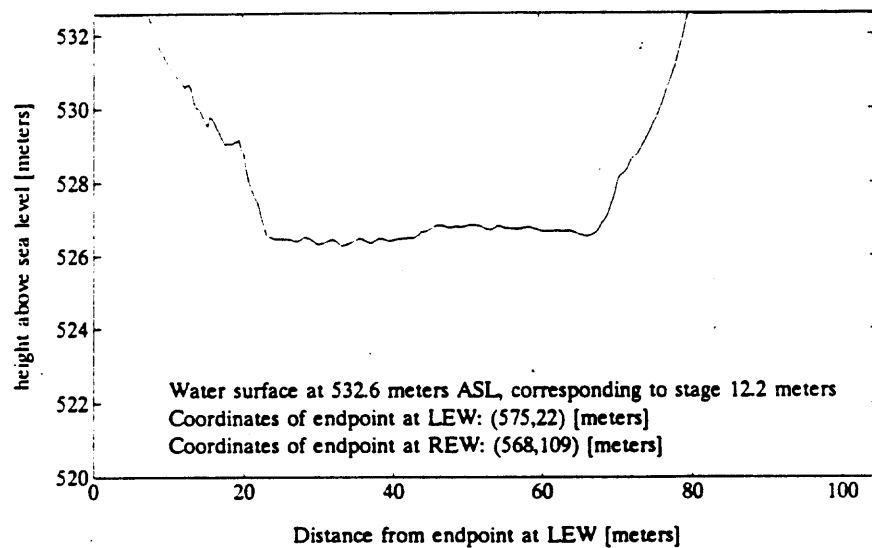


Figure 2.34: Cross-section 200. The x - axis is distance in meters from the bank at the left edge of water, and the distance does not correspond to the local coordinate system of National Canyon. ASL refers to height above mean sea level. The discharge at the cableway, at stage 12.2 meters is $370 \text{ m}^3/\text{sec}$.

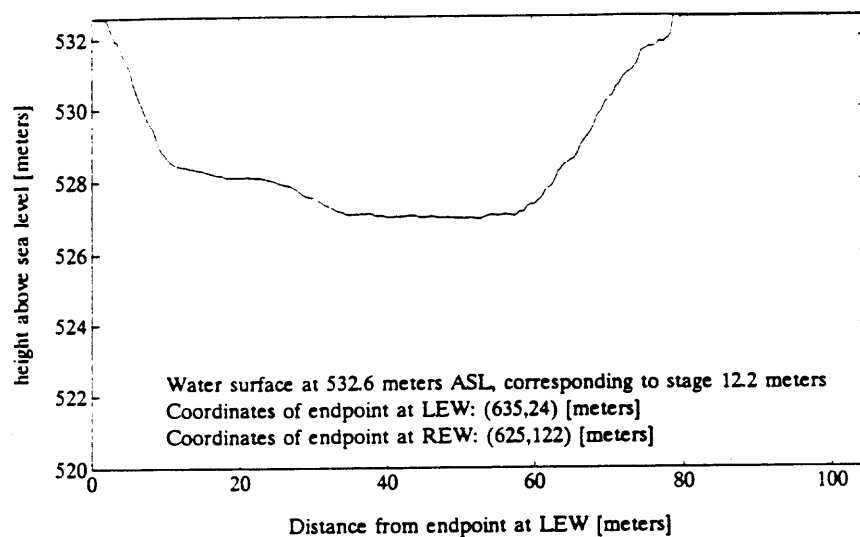


Figure 2.35: Cross-section 400. The x - axis is distance in meters from the bank at the left edge of water, and the distance does not correspond to the local coordinate system of National Canyon. ASL refers to height above mean sea level. The discharge at the cableway, at stage 12.2 meters is $370 \text{ m}^3/\text{sec}$.

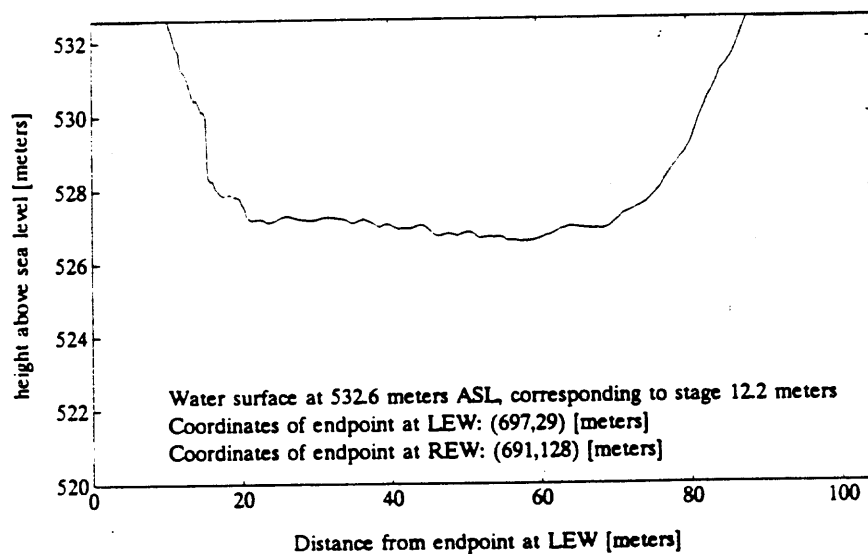


Figure 2.36: Cross-section 600. The x - axis is distance in meters from the bank at the left edge of water, and the distance does not correspond to the local coordinate system of National Canyon. ASL refers to height above mean sea level. The discharge at the cableway, at stage 12.2 meters is

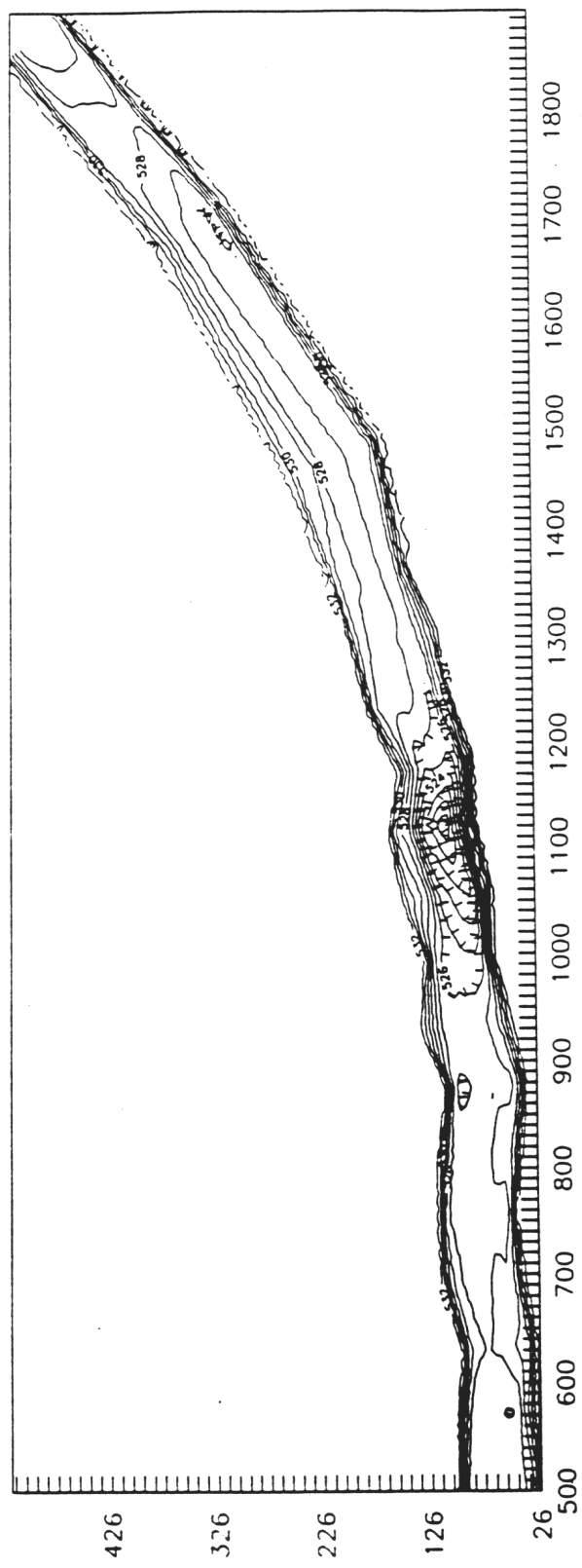


Figure 2.37: Map of the National Canyon Reach. The map is a scaled contour map in the local coordinate system of National Canyon, the units of both the x - and y -axes are in meters. The contours are distance in meters above mean sea level.

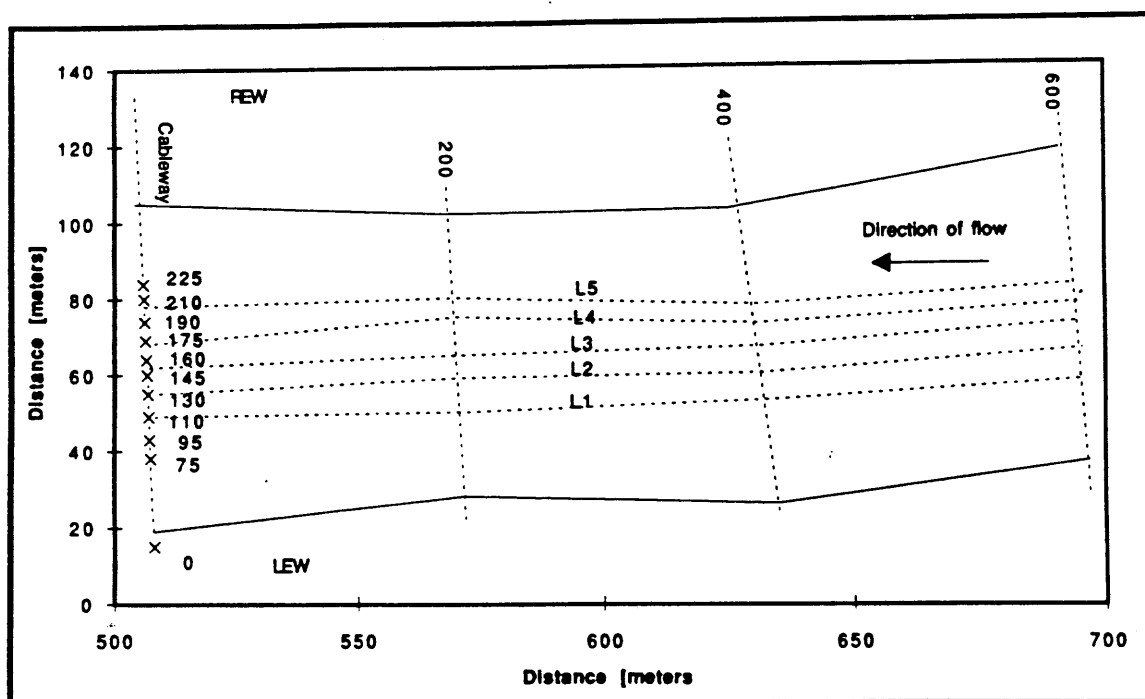


Figure 2.38: Location of longitudinal passes and stations on the cableway, relative to cableway, cross-sections 200, 400, and 600. The solid line indicates the approximate location of the banks.

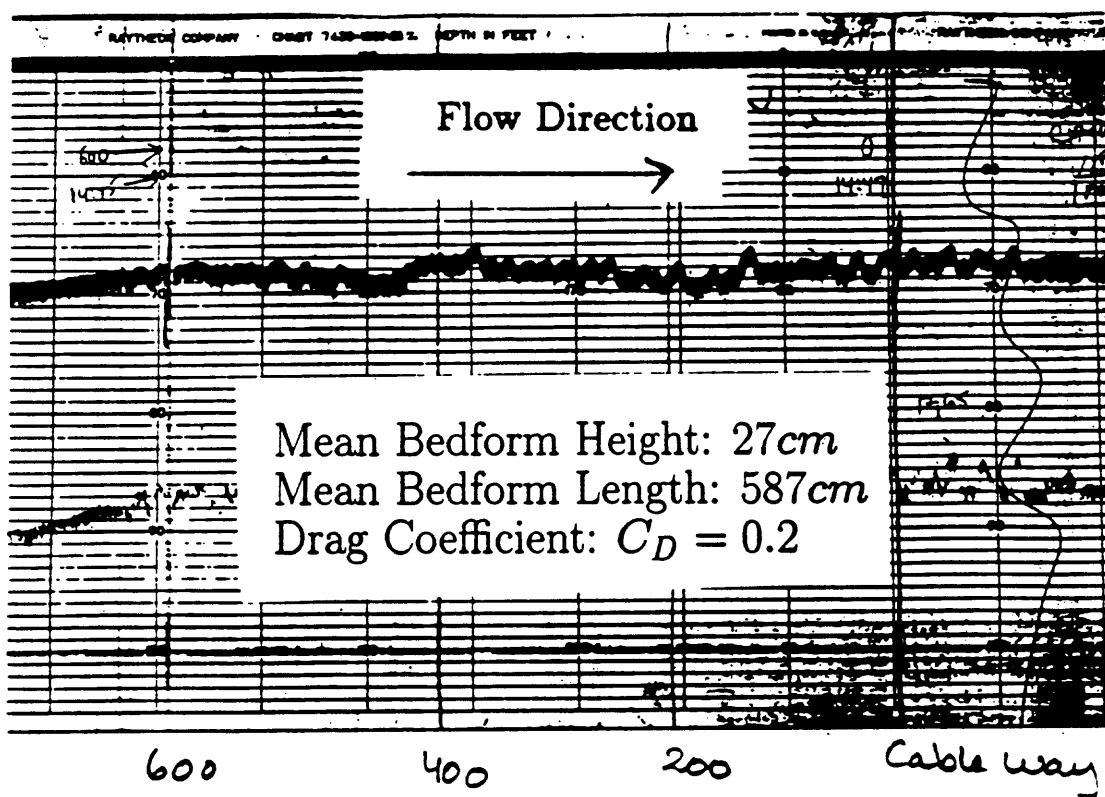


Figure 2.39: Example of a longitudinal echo-sounding record. This record is equivalent to L3 on figure 2.38. Note the regular array of sharp crested, asymmetrical bedforms.

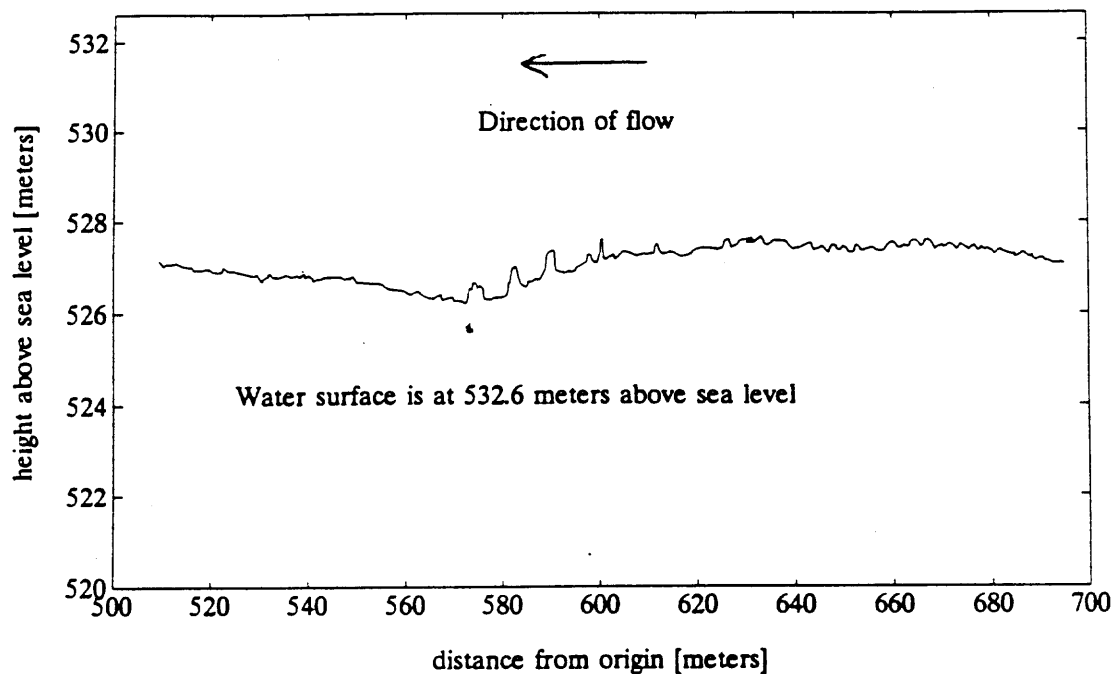


Figure 2.40: Pass L1 on figure 2.38. Water surface elevation is measured at the cableway.

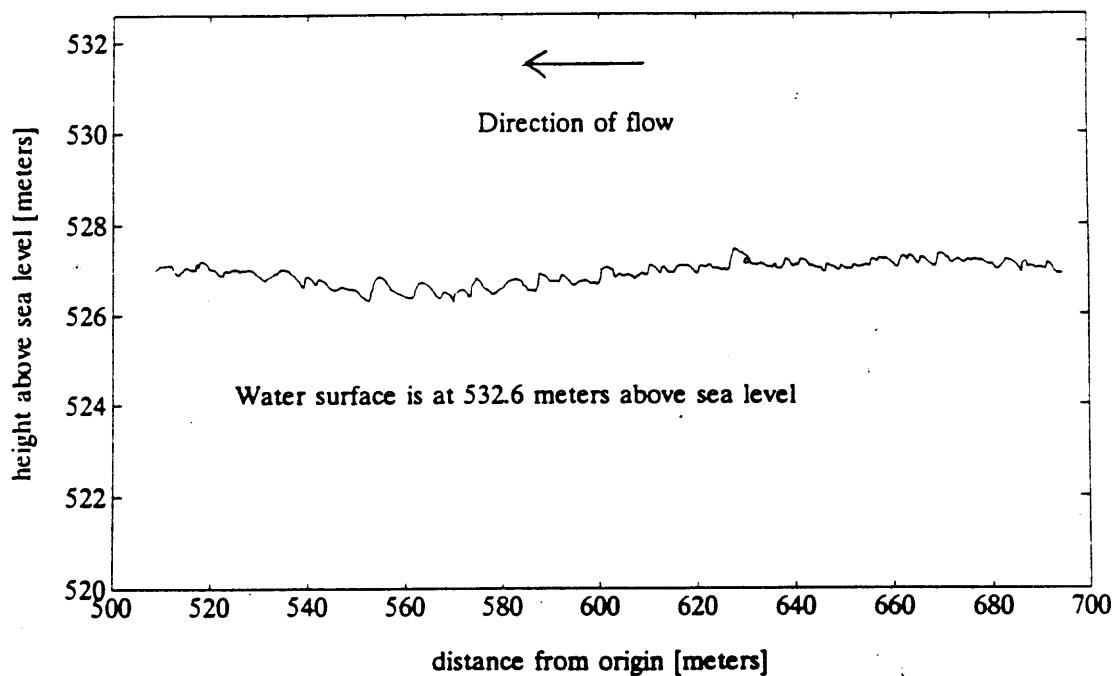


Figure 2.41: Pass L2 on figure 2.38. Water surface elevation is measured at the cableway.

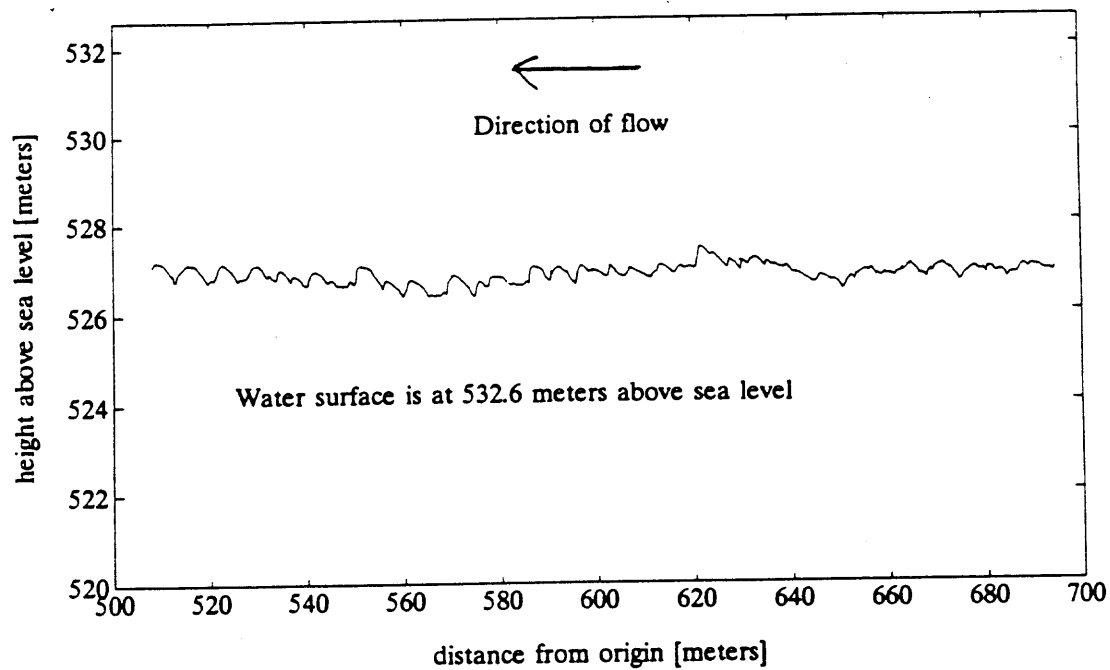


Figure 2.42: Pass L3 on figure 2.38. Water surface elevation is measured at the cableway.

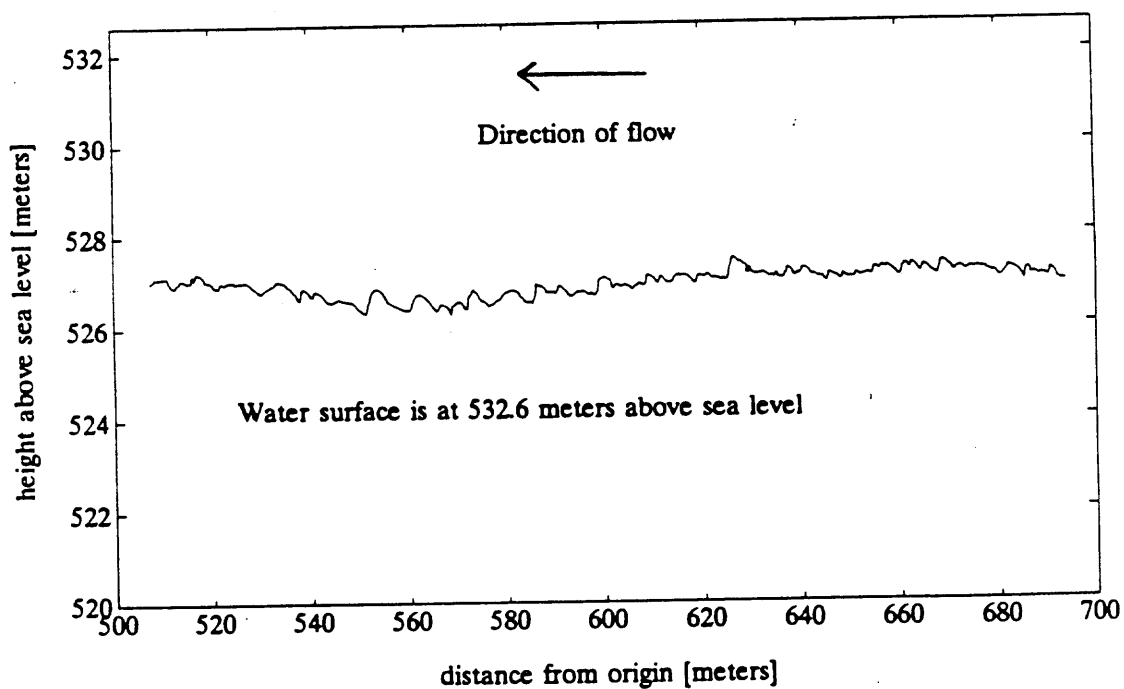


Figure 2.43: Pass L4 on figure 2.38. Water surface elevation is measured at the cableway.

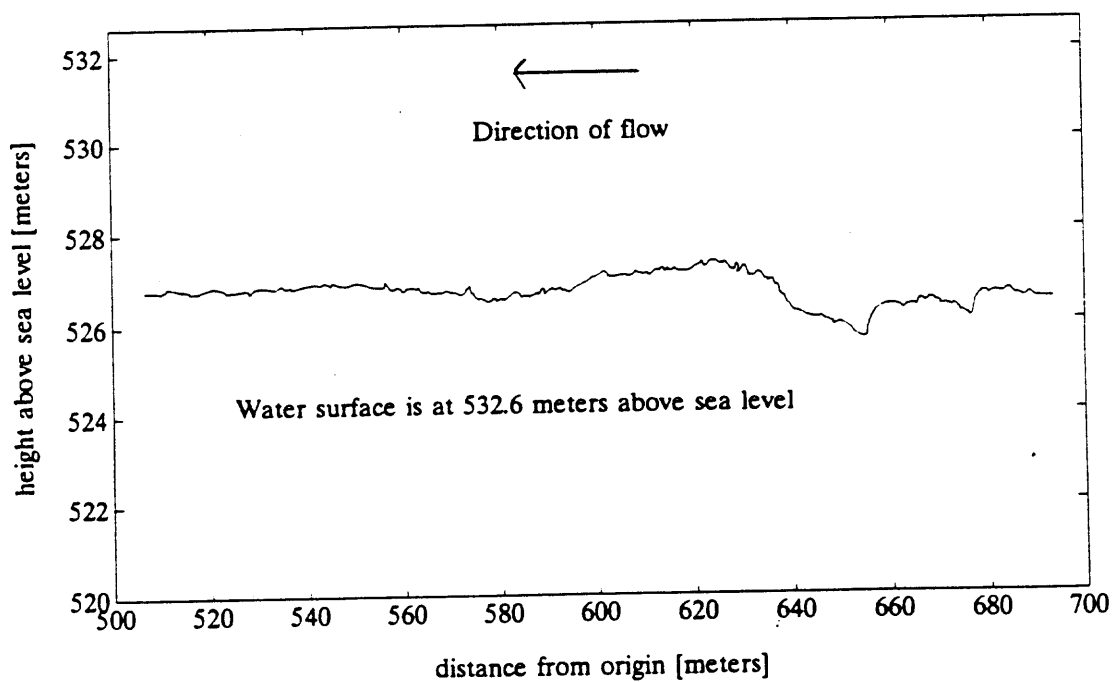


Figure 2.44: Pass L5 on figure 2.38. Water surface elevation is measured at the cableway.

Chapter 3

VELOCITY PROFILE ANALYSIS

3.1 The Velocity Profile Model

The roughness and shear velocity of the exterior flow are derived from the velocity profile measurements. These two parameters are determined by matching a quasi-logarithmic velocity structure to the measured profiles to determine the best fit velocity profile in a least squares sense. The shear velocity is used to determine channel slope at National Canyon which was not measured accurately during the field survey, and the measurement derived bedform roughness is compared to a calculated value of this parameter.

In steady, uniform flow in a wide channel over a planar bed of well sorted sediment and small relative roughness, the stress acting on the boundary is given by the component of the gravitational force of water in the direction of flow per unit area of the bed and it is proportional to the depth-slope product:

$$\tau_b = \rho g h \sin(\alpha) = \rho g h S \quad (3.1)$$

In this expression ρ is fluid density, g is the gravitational acceleration, h is the flow depth and α is the angle of the channel surface to horizontal. Since this angle normally is small, $\sin(\alpha) \approx \tan(\alpha) \approx \alpha \approx S$, where S is the water surface slope (*Richards, 1982 [16]*).

Furthermore, fluid shear stress decreases linearly with height above the bottom in steady uniform flow (*Fredsøe, 1989 [6]*). Stress is zero at the surface and is equivalent to the boundary shear stress τ_b at the bottom.

$$\tau_T(z) = \tau_b(1 - z/h) \quad (3.2)$$

It is reasonable to assume that the flow near National Canyon, at least in the central segment of the river is uniform on large scale, since the river in this reach is relatively straight. Though the discharge varies in time, the period of these fluctuations is long

relative to the length of time it takes a parcel of water to pass through the study reach, and the flow can be considered quasi-steady.

Downstream velocity u may be related to fluid stress through the constitutive equation for turbulent flow (Fredsoe, 1989 [6]). Fluid stress $\tau_T(z)$ is proportional to the turbulent eddy viscosity $K(z)$, fluid density ρ , and velocity gradient:

$$\tau_T(z) = \rho K(z) \frac{\partial u}{\partial z} \quad (3.3)$$

By combining equation 3.2 and 3.3 an expression for velocity gradient is obtained:

$$\frac{\partial u}{\partial z} = \frac{u_{*T}^2(1 - z/h)}{K(z)} \quad (3.4)$$

Where $u_{*T}^2 = \frac{\tau_b}{\rho}$ defines the shear velocity.

It has been found that vertical velocity structure is well described when a two part eddy viscosity structure is used, which is parabolic in the near boundary region and constant in the upper 80 % of the flow (Rattray and Mitsuda 1974 [15]). The structure is scaled by u_* , a non-dimensional depth parameter $\xi = z/h$, the coefficient $\beta = 6.24$, and von Karmans constant $\kappa = 0.41$.

$$K(\xi) = \begin{cases} u_{*T} \kappa h \xi (1 - \xi) & \text{if } \xi < 0.2 \\ \frac{u_{*T} \kappa h}{\beta} & \text{if } \xi \geq 0.2 \end{cases} \quad (3.5)$$

Using the above choice of eddy viscosity, equation 3.4 can be integrated with respect to $\xi = z/h$ to yield an expression for the vertical velocity structure. The bottom part of equation 3.4 is integrated from $\xi_{0T} = z_{0T}/h$ to $\xi = z/h$, where z_{0T} is a bottom roughness parameter. The upper part of equation 3.4 is integrated from $\xi_b = 0.2$ to $\xi = z/h$.

$$u(\xi) = \begin{cases} \frac{u_{*T}}{\kappa} \ln \left(\frac{\xi}{\xi_{0T}} \right) & \text{if } \xi < \xi_b \\ \frac{u_{*T}}{\kappa} \left[\beta(\xi - \xi^2/2) - \beta(\xi_b - \xi_b^2/2) + \ln \left(\frac{\xi_b}{\xi_{0T}} \right) \right] & \text{if } \xi \geq \xi_b \end{cases} \quad (3.6)$$

3.2 Statistical Analysis of Velocity Profiles

During the field study at National Canyon, velocity fluctuated slowly with time between high discharge at $710 \text{ m}^3/\text{sec}$ and low discharge $280 \text{ m}^3/\text{sec}$. Velocity and suspended sediment concentration profiles were surveyed at 10 stations across the

river at both high and low discharge. However, the samples collected during the lower discharge contained insufficient amounts of sediment for laboratory analysis. Both the high and low flow velocity profiles have been analyzed in the same manner, and the information gained from the low flow velocity profiles along with the high flow suspended sediment profiles, provide a check on the results gained from the analysis of the high flow velocity profiles.

The velocity measurements made at different stations across the river are expected to vary from station to station, since the influence of bank effects decreases towards the center of the channel. Close to the banks, the flow is moderated by lateral stresses, and non-uniform bank geometry generates complicated secondary circulation patterns. In the central segment of the river, where bank effects become negligible, the flow conditions are expected to be approximately steady, uniform and two-dimensional. It is assumed here that velocity is adequately modeled using a two-part eddy viscosity, and that the corresponding velocity profile provides an adequate description of the flow in the central segment of the river. Since the majority of the velocity measurements were made in the exterior portion of the flow, only the bottom roughness parameter, z_{0T} and shear velocity, u_{*T} , of the outer flow region are resolved by the measurements.

In order to find the parameters in equation 3.6 that best match the velocity measurements, an iterative scheme was used to determine z_{0T} and u_{*T} . For specified values of z_{0T} and u_{*T} , velocity is calculated according to equation 3.6 at a levels ξ that correspond to the same levels of the flow at which measurements were made. The variance of the measurements around the calculated values of velocity is found. The calculation is repeated using a constant value of z_{0T} but changing values of u_{*T} that produce an increasingly smaller variance, until the value of u_{*T} that produces the smallest variance for a given value of z_{0T} has been found. The calculation is then repeated for a number of values of z_{0T} until a minimum variance, σ_a^2 , has been obtained. This method is in essence a least squares fit of the quasi-logarithmic velocity structure to the data set. It is important to note that the variance, σ_a^2 , of interest here is always the variance of measured values around a specified profile, not the variance at one particular level in the flow. The symbol σ_a refers to the standard deviation of the measurements made at one station (e.g. station 95) around a specified curve.

To get an idea of the extent to which the flow is uniform across the channel,

the mean profile at each station has been determined. First the mean profile was calculated by averaging the velocity measurements made at each level. The mean profiles provide a good picture of the flow structure at each station. Second the best fit velocity profile was found for the measurements using the iterative approach described above. The mean velocity profile is plotted as the dash-dotted line and the best fit profile to the measurements is plotted as the dotted line on Figures 3.1 to 3.10 for the high discharge, and on Figures 3.11 to 3.20 for the low discharge measurements. The dash-dotted line shown on these Figures is equivalent to the solid line on Figures 2.7 to 2.16. At both high and low discharge, the structure of the average profile, at stations 95 through 190, resembles the structure of the selected model velocity profile described previously (Figures 3.2 through 3.8 and 3.12 through 3.18). Close to the left and right banks (station 75, and stations 210 and 225) the flow structure deviates substantially from the structure observed in the central portion of the river (Figures 3.1, 3.9, and 3.10 for the high discharge measurements and Figures 3.11, 3.19, and 3.20 for the low discharge measurements). Figures 3.1 to 3.20 are found at the end of this section.

The results of the least-squares fits are listed in Table 3.1. The smallest variance is expected for profiles where the flow conditions approximate steady, uniform, two-dimensional flow, and in this region the result of the analysis is also expected to provide similar values of z_{0T} , and u_{*T} . Due to large scatter in the velocity measurements, variation of the parameters z_{0T} and u_{*T} , that characterizes the best fit profiles at each station, is expected. In the region where the flow is not steady and uniform, the imposed velocity profile produces a poor fit, and consequently, the variance of the data around the profile is large. Based on the variance, σ_a^2 , indicated in Table 3.1, it is seen that during high discharge, profiles 95 to 190 match the imposed velocity structure well. During low discharge, there is small variability around the model profile of the measurements made from stations 95 to stations 210.

Based on this calculation, it was observed that the measured profiles that matched the quasi-logarithmic velocity structure had similar values of u_{*T} , and values of z_{0T} that are within the same order of magnitude.

Since variations in cross-channel depth are small, and surface slope is constant, little variation in the values found for u_{*T} is expected. It is likely that differences in bottom topography across the river produce variations in bedform roughness, z_{0T} , but

	High Discharge			Low Discharge		
Station	z_{0T}	u_{*T}	σ_a^2	z_{0T}	u_{*T}	σ_a^2
	<i>cm</i>	<i>cm/sec</i>	<i>cm²/sec²</i>	<i>cm</i>	<i>cm/sec</i>	<i>cm²/sec²</i>
75	0.001	4.0	148	0.01	3.0	181
95	0.44	9.2	105	0.61	7.6	88
110	0.14	8.4	93	0.34	6.9	60
130	0.27	9.6	101	0.57	7.8	51
145	0.14	9.0	64	0.73	8.3	104
160	0.29	9.9	112	0.34	7.3	103
175	0.13	8.8	95	0.30	7.3	92
190	0.25	9.3	126	0.08	6.0	69
210	0.43	8.6	374	0.51	6.9	100
225	1.70	8.5	496	1.25	6.0	218
Lumped Data Set	0.18	9.1	120	0.37	7.3	95

Table 3.1: Characteristics of the imposed velocity profile that produces the smallest variance, σ_a^2 . Mean depth during high flow is 740 *cm* and mean depth during low flow is 570 *cm*.

these variations are also likely to be small relative to the resolution of the measured profiles. Constant values of shear velocity and bottom roughness parameter imply that it is likely that uniform flow conditions existed in the central portion of the flow, and thus one velocity profile exists that describes the flow in the central segment of the river.

Consequently, to enable evaluation of the bulk properties of the flow, the velocity profiles that displayed similar structure were lumped into a single data set, representing the flow conditions in the central part of the river. The lumped data set for high flow consists of velocity measurements made at the six stations 110, 130, 145, 160, 175, and 190. For low flow the measurements made at the seven stations 95, 110, 130, 145, 160, 175, and 190 were lumped into one data set.

In the iterative manner described previously the statistically best fit profile was found to the lumped data sets. This profile is shown as a solid line on all velocity profile plots, at high discharge, Figures 3.1 to 3.10 and at low discharge, Figures 3.11 through 3.20, and the curve is the same for all profiles across the river. To

determine whether the best fit profile to the lumped data set actually matches the velocity profile measured at a given station, this profile is compared to the measured profiles at individual stations, by computing the variance σ_b^2 between the imposed profile and the measurements. The symbol σ_b refers to the standard deviation of measurements made at a station (e.g. station 95) around a curve that corresponds to the best fit curve to measurements made at several stations (e.g. stations 110 through 190). If the profile that matches the lumped data set resembles the best fit at a given station, the difference in variance between the two profiles will be small. The statistical similarity of the two fits is tested using an F-test to test the difference in variance. An F-test is used to compare the variances of two different samples. If the variances compare within an upper and a lower limit, determined by the sample size, the null-hypothesis, $\sigma_a^2 = \sigma_b^2$ is true. The range between the upper and lower limit decreases with sample size and with the degree of confidence wanted in the final result. The variance of the measured velocity profiles are compared within a 98% confidence interval. Since fewer measurements were made at low flow, the range is slightly greater. If the null-hypothesis is true, the measurements of a specific profile can be approximated by the best fit curve to the lumped data set. If it is false, the measurements of velocity at a specific station do not match the best fit curve to the lumped data set. If the null-hypothesis is true for all lumped measurements, it can be concluded that one velocity profile exists that describes the flow in the central segment of the river. The results of the F-test are listed in Tables 3.3 and 3.4. The high discharge value are listed in Table 3.3 and the low discharge values are found in Table 3.4. The statistical method and limits of the F-test were obtained from *Devore*, 1987 [4].

In the analysis of the velocity profile structure, the quality of the velocity measurements has not been evaluated. All measurements have been included. When conducting a least squares fit on a large data set, singular outlying values do not make a large difference in the actual position of the velocity profile. Due to the variability within the data set it is difficult to assess which measurements are subject to error. It is not unlikely that error is attached to some data points, since the measurements were made by an operator who counted the number of revolutions of the current meter.

The resolution of the measurements at hand does not allow for anything but a

	High Discharge			Low Discharge		
Station	σ_a^2	σ_b^2	$\frac{\sigma_a^2}{\sigma_b^2}$	σ_a^2	σ_b^2	$\frac{\sigma_a^2}{\sigma_b^2}$
	cm^2/sec^2	cm^2/sec^2		cm^2/sec^2	cm^2/sec^2	
75	148	1789	0.08	182	2002	0.09
95	105	491	0.21	88	115	0.76
110	93	173	0.54	60	77	0.78
130	101	108	0.94	51	55	0.92
145	64	73	0.88	105	116	0.90
160	112	140	0.80	103	108	0.95
175	95	107	0.89	92	106	0.87
190	126	136	0.93	69	97	0.71
210	374	1021	0.37	100	218	0.46
225	494	3856	0.13	218	1544	0.14

Table 3.2: Variance of measured velocity profiles around two imposed velocity profiles, where σ_a^2 represents the minimum variance, and σ_b^2 , represents the variance of the measured values around the best fit profile to the lumped data set.

qualitative interpretation of the near bank processes. During the National Canyon survey, large eddies were observed in the vicinity of the banks, and it is likely that such secondary circulation would alter the flow structure from the quasi-logarithmic structure typical of steady, uniform flow. Furthermore the profiles at the right bank stations 210 and 225 (Figures 3.9 and 3.10) have a convex structure, typical of flow over beds of large scale roughness (*Wiberg and Smith, 1991 [25]*). The measured profiles indicate that the bank effects extend further into the center of the channel during high flow than during low flow. The convex structure observed at stations 210 and 225 is more distinct during high flow. At low flow, the velocity structure at station 95 matches that of the stations in the central part of the river, whereas at high discharge, the apparent roughness is significantly higher than the roughness observed for the stations in the central part of the river.

High Discharge				
Station	$F_{0.99,62,62}$	$\frac{\sigma_a^2}{\sigma_b^2}$	$F_{0.01,62,62}$	null-hypothesis
75	0.54	0.08	1.84	False
95	0.54	0.21	1.84	False
110	0.54	0.54	1.84	True
130	0.54	0.94	1.84	True
145	0.54	0.88	1.84	True
160	0.54	0.80	1.84	True
175	0.54	0.89	1.84	True
190	0.54	0.93	1.84	True
210	0.54	0.37	1.84	False
225	0.54	0.13	1.84	False

Table 3.3: Testing the null-hypothesis, is the ratio of σ_a^2 to σ_b^2 within the limits of the F-statistics.

Low Discharge				
Station	$F_{0.99,47,47}$	$\frac{\sigma_a^2}{\sigma_b^2}$	$F_{0.01,47,47}$	null-hypothesis
75	0.5	0.09	2.0	False
95	0.5	0.76	2.0	True
110	0.5	0.78	2.0	True
130	0.5	0.92	2.0	True
145	0.5	0.90	2.0	True
160	0.5	0.95	2.0	True
175	0.5	0.87	2.0	True
190	0.5	0.71	2.0	True
210	0.5	0.46	2.0	False
225	0.5	0.14	2.0	False

Table 3.4: Testing the null-hypothesis, is the ratio of σ_a^2 to σ_b^2 within the limits of the F-statistics.

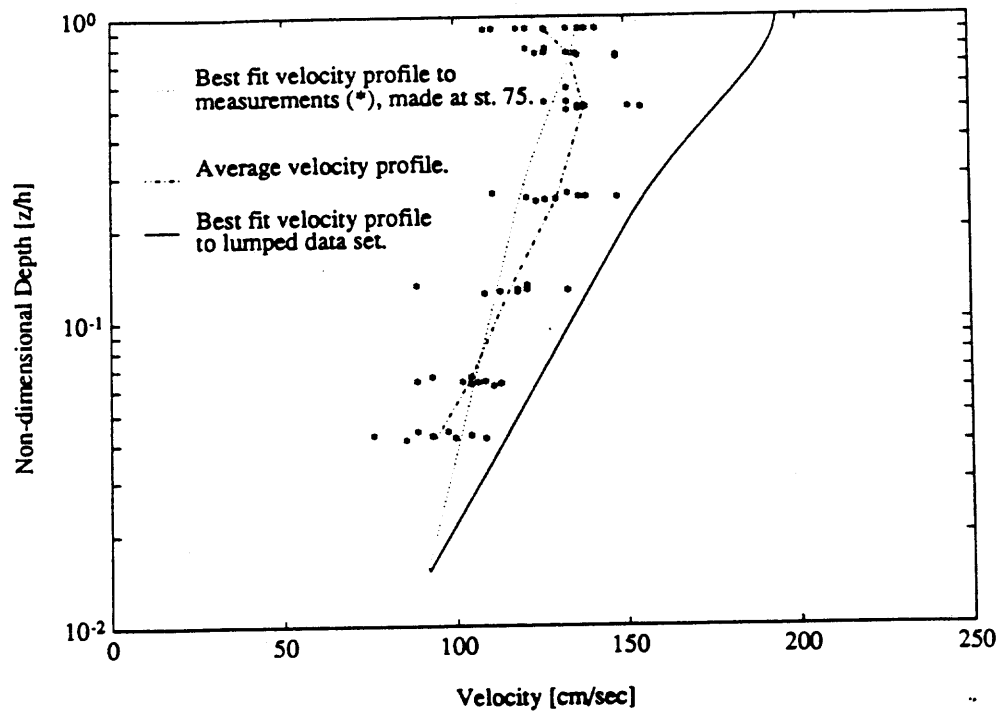


Figure 3.1: Velocity profile measured at station 75 during high discharge.

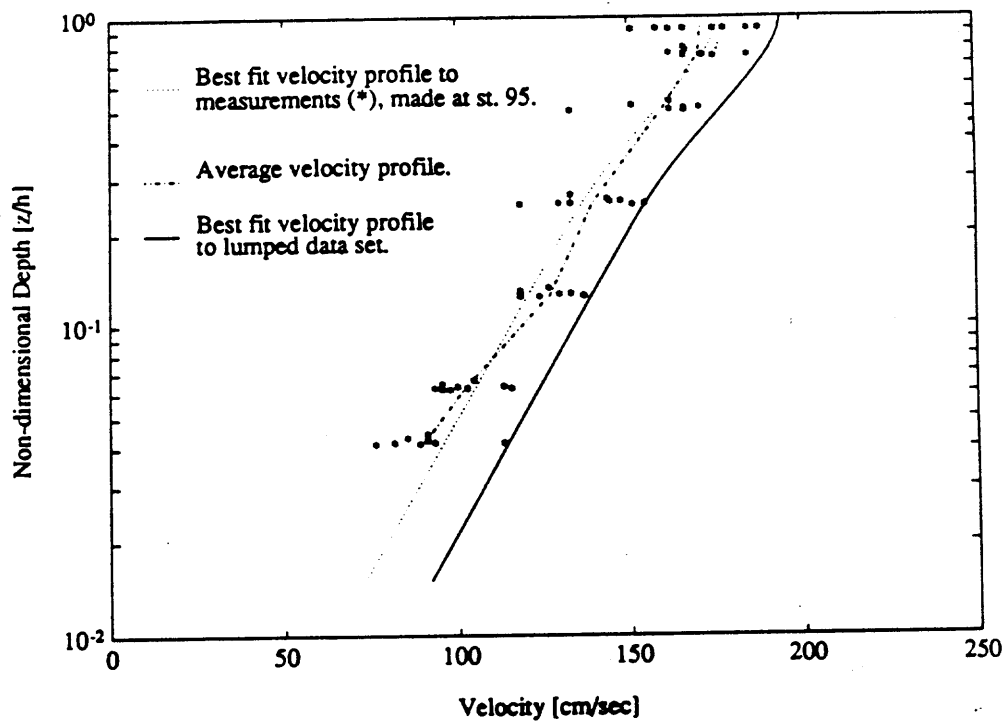


Figure 3.2: Velocity profile measured at station 95 during high discharge.

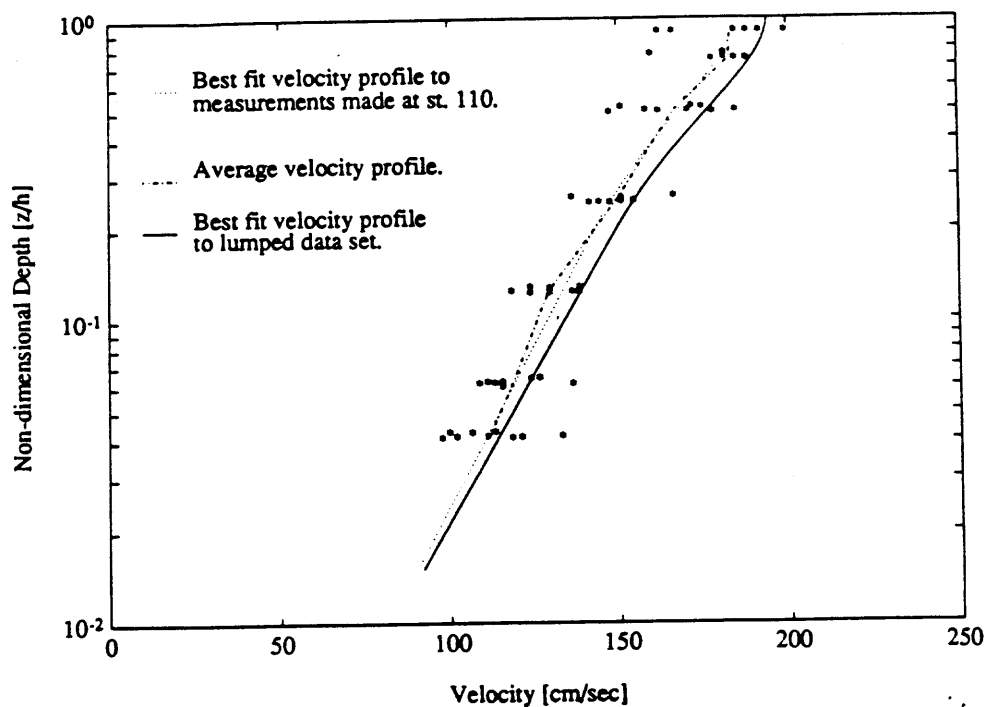


Figure 3.3: Velocity profile measured at station 110 during high discharge.

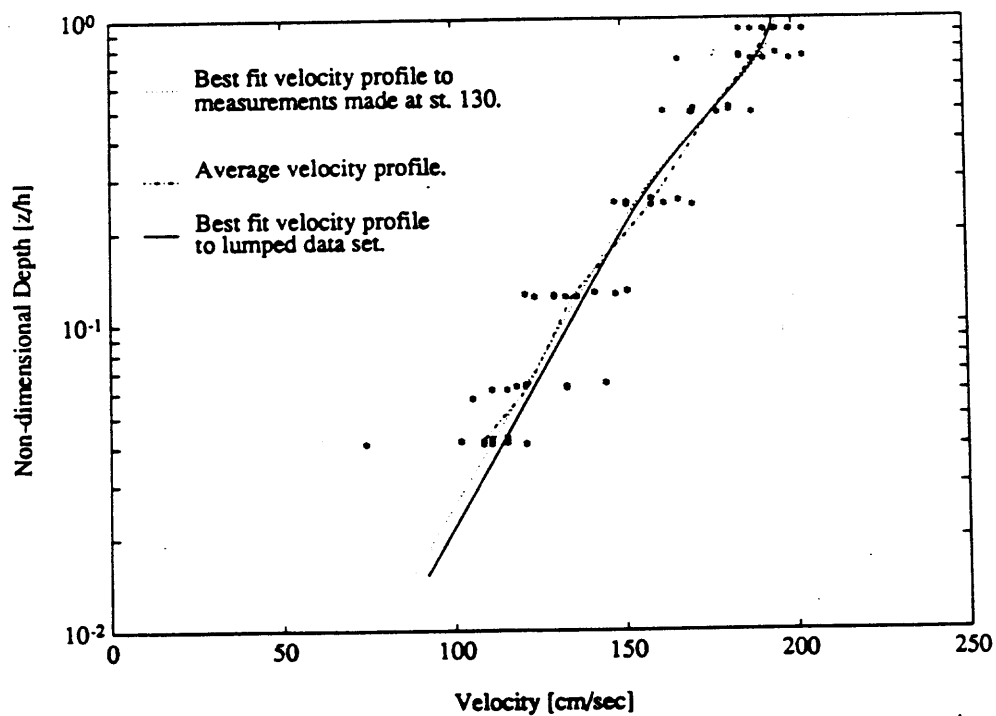


Figure 3.4: Velocity profile measured at station 130 during high discharge.

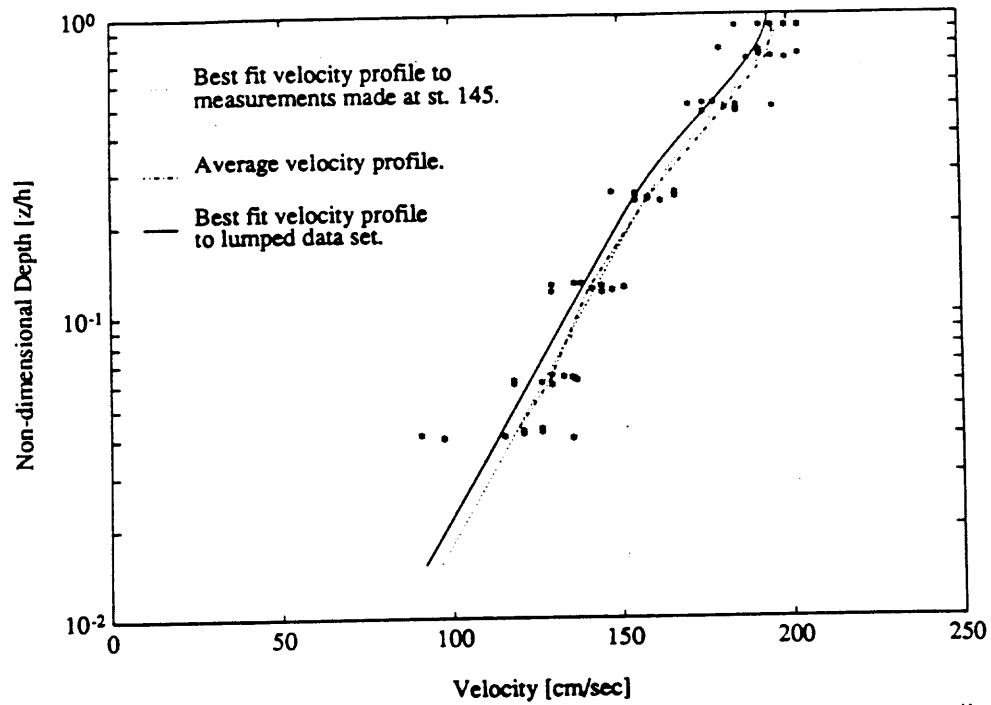


Figure 3.5: Velocity profile measured at station 145 during high discharge.

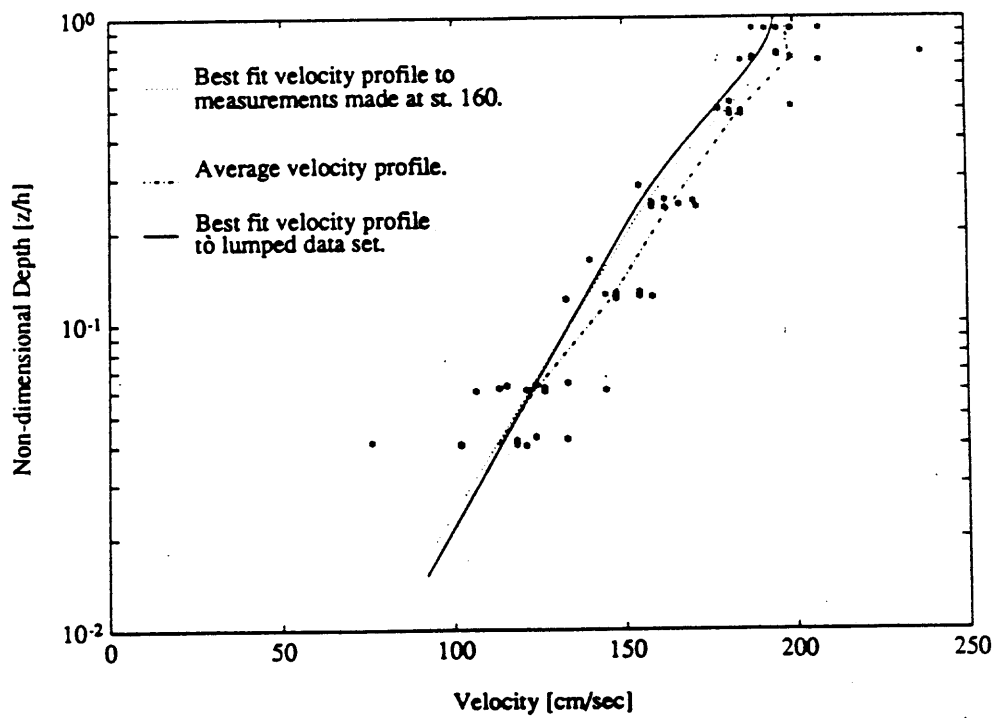


Figure 3.6: Velocity profile measured at station 160 during high discharge.

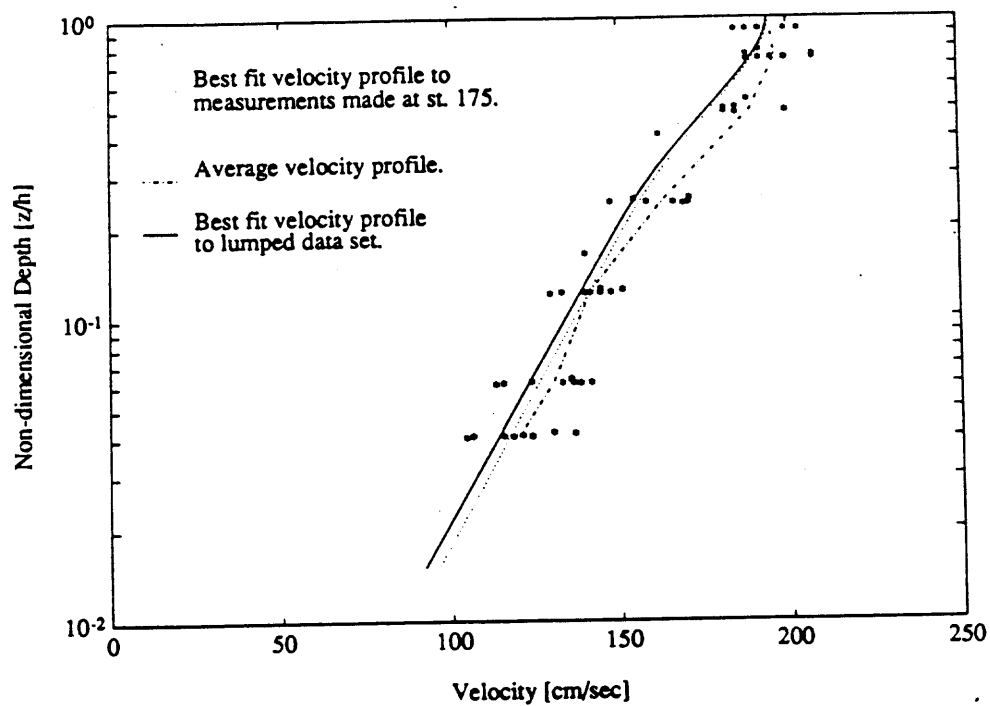


Figure 3.7: Velocity profile measured at station 175 during high discharge.

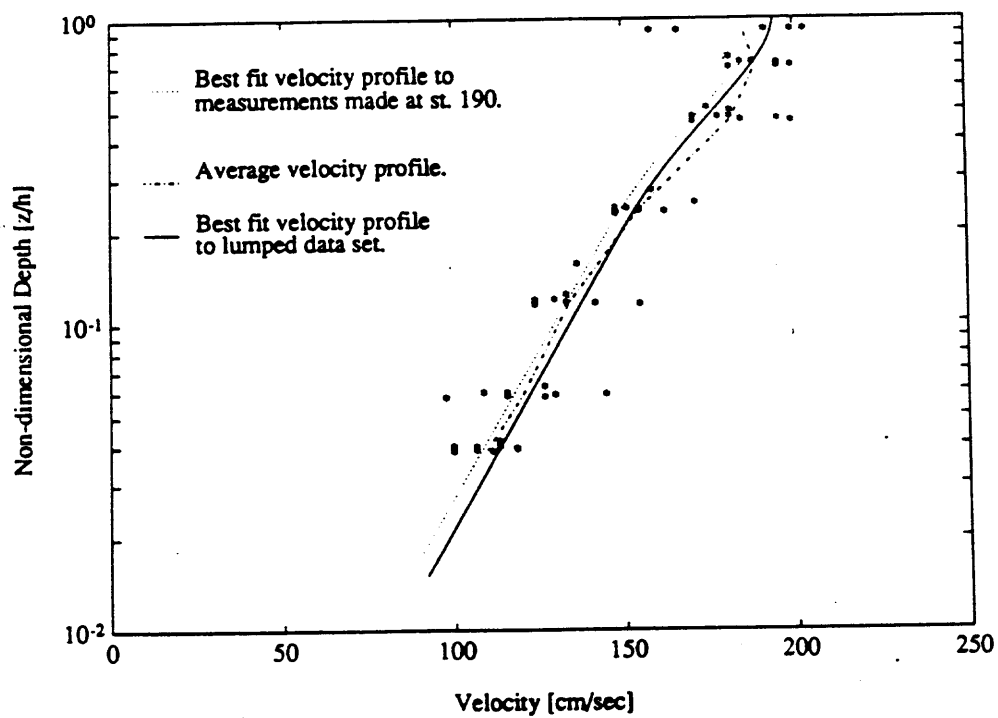


Figure 3.8: Velocity profile measured at station 190 during high discharge.

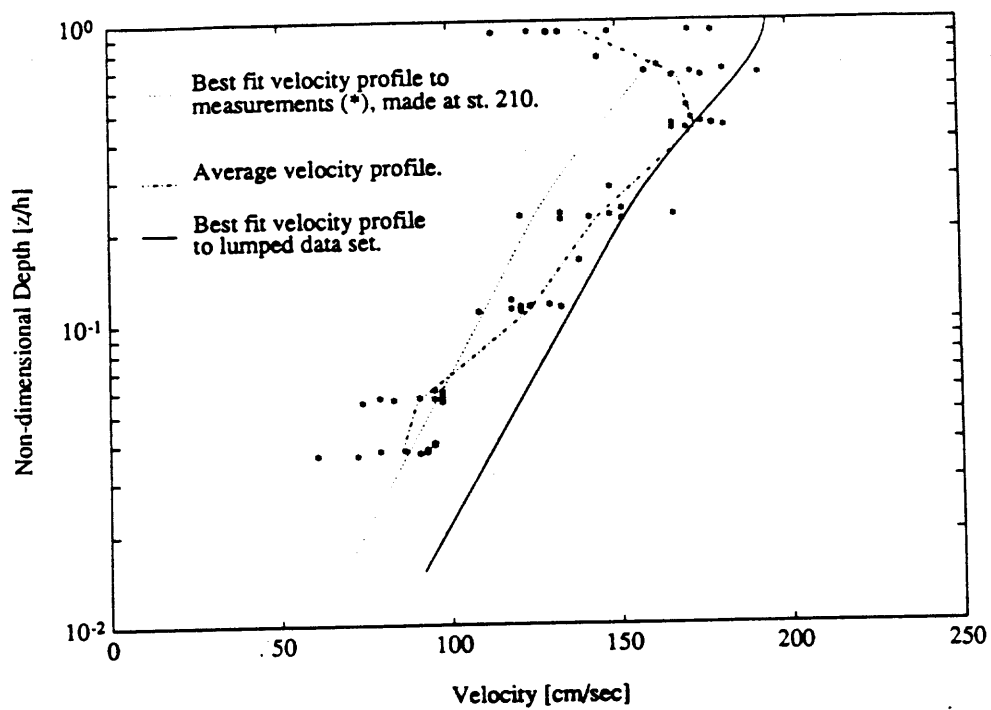


Figure 3.9: Velocity profile measured at station 210 during high discharge.

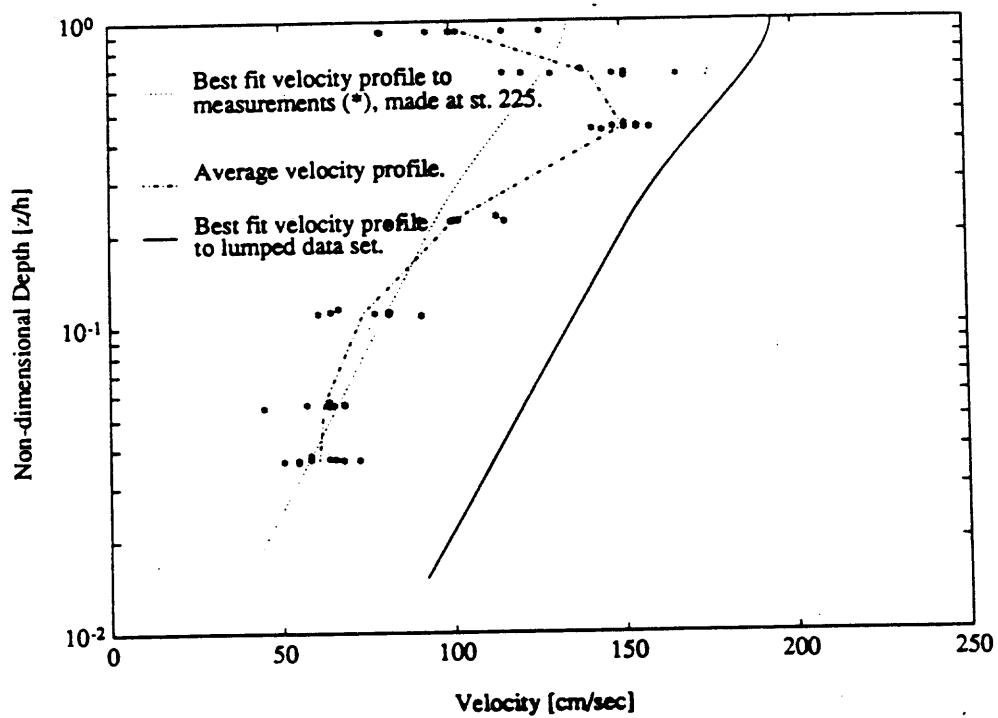


Figure 3.10: Velocity profile measured at station 225 during high discharge.

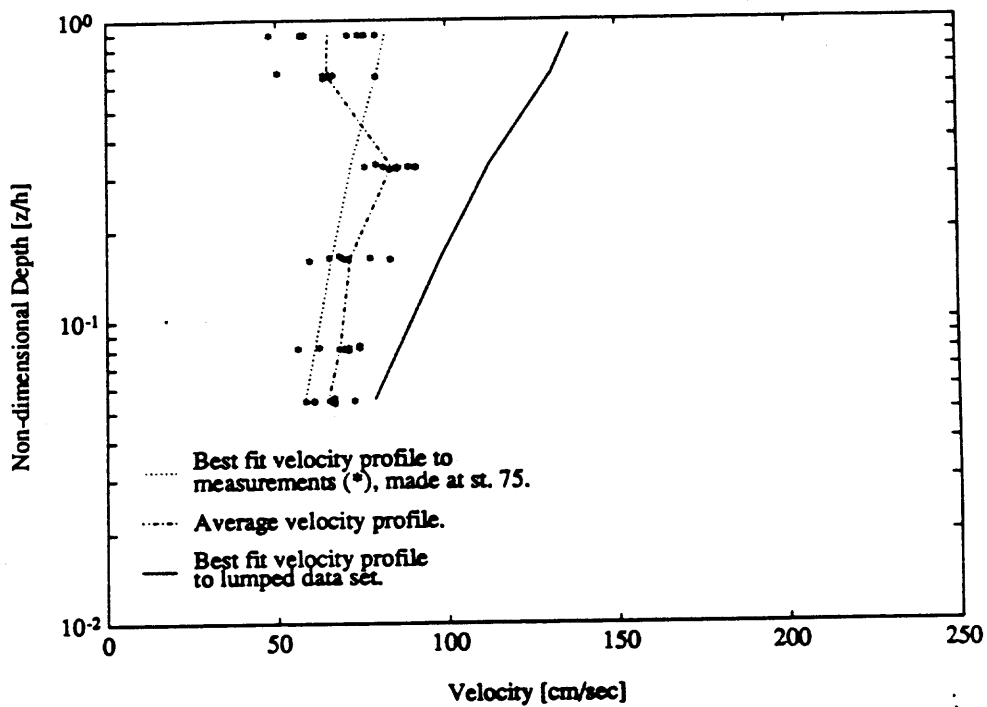


Figure 3.11: Velocity profile measured at station 75 during low discharge.

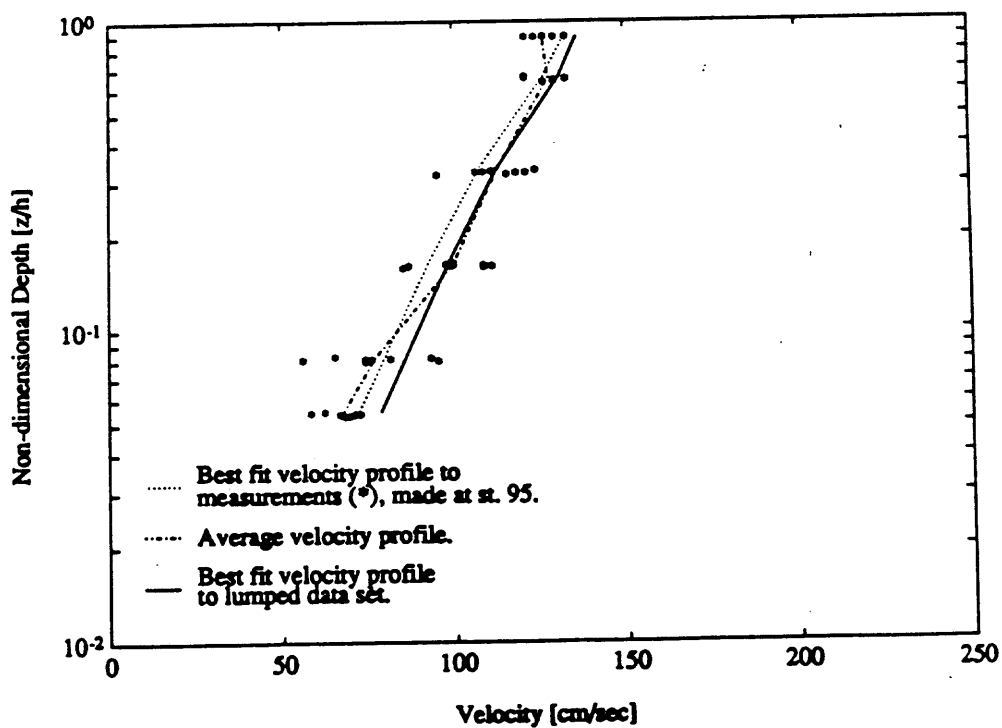


Figure 3.12: Velocity profile measured at station 95 during low discharge.

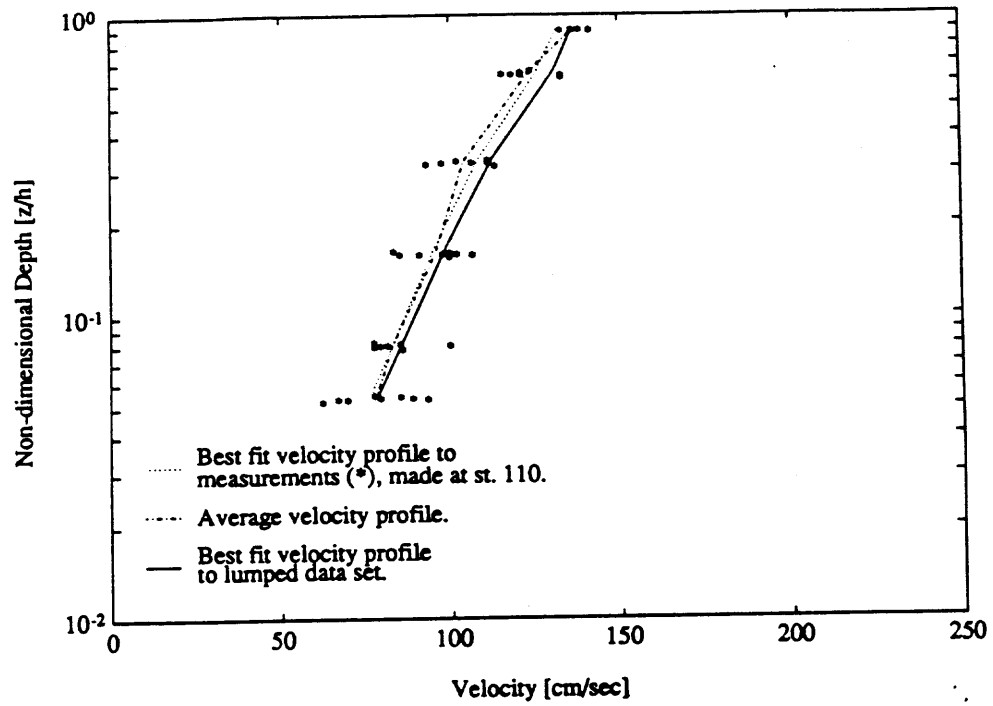


Figure 3.13: Velocity profile measured at station 110 during low discharge.

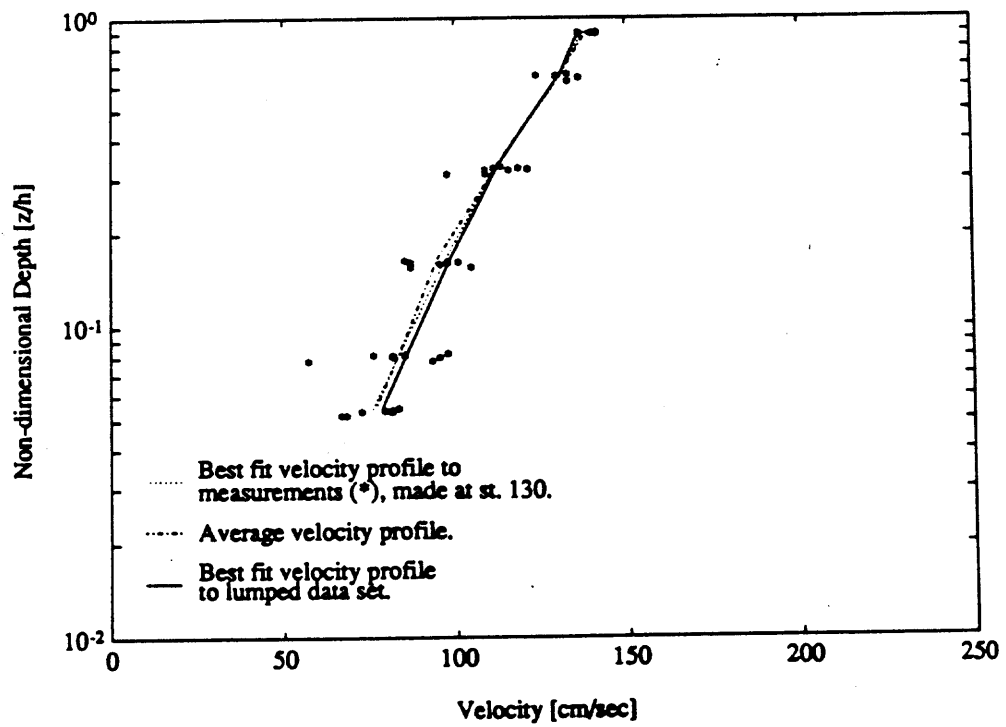


Figure 3.14: Velocity profile measured at station 130 during low discharge.

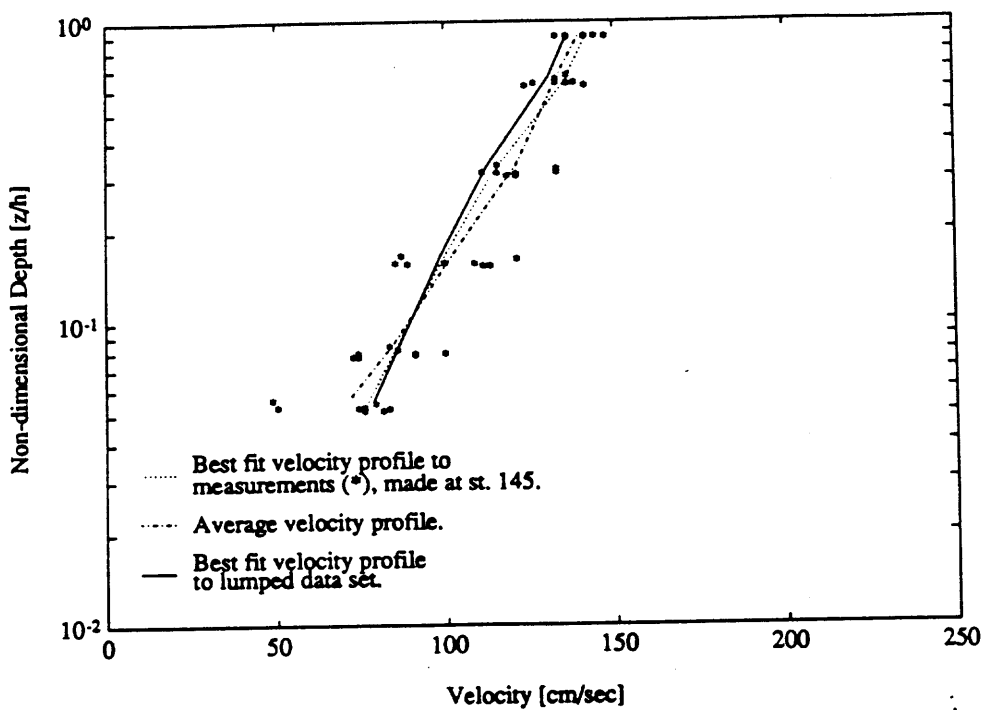


Figure 3.15: Velocity profile measured at station 145 during low discharge.

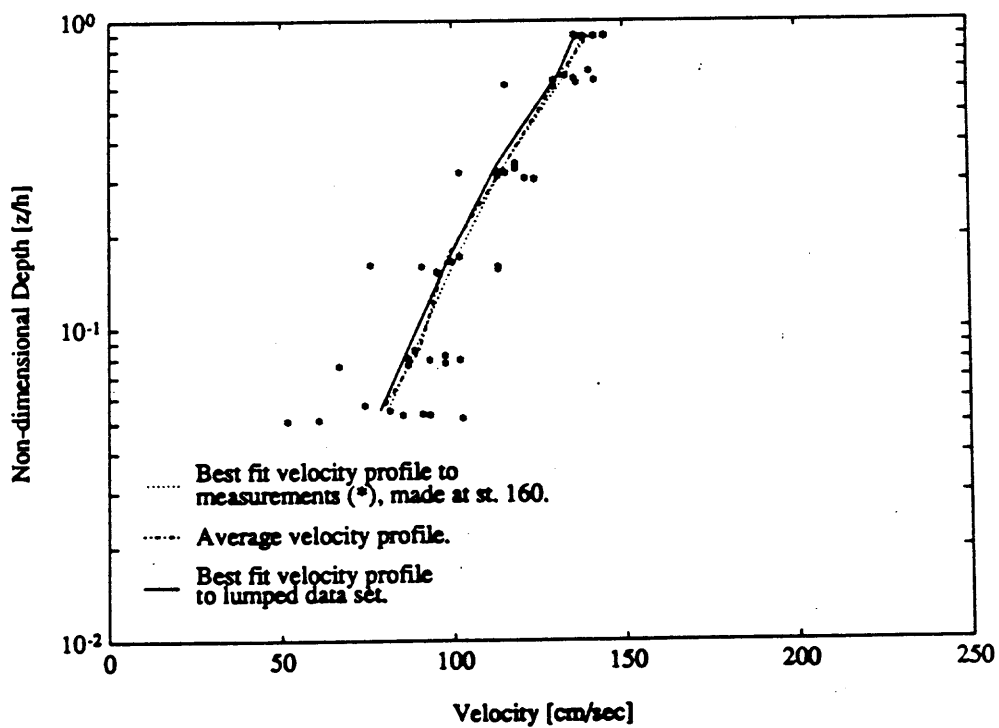


Figure 3.16: Velocity profile measured at station 160 during low discharge.

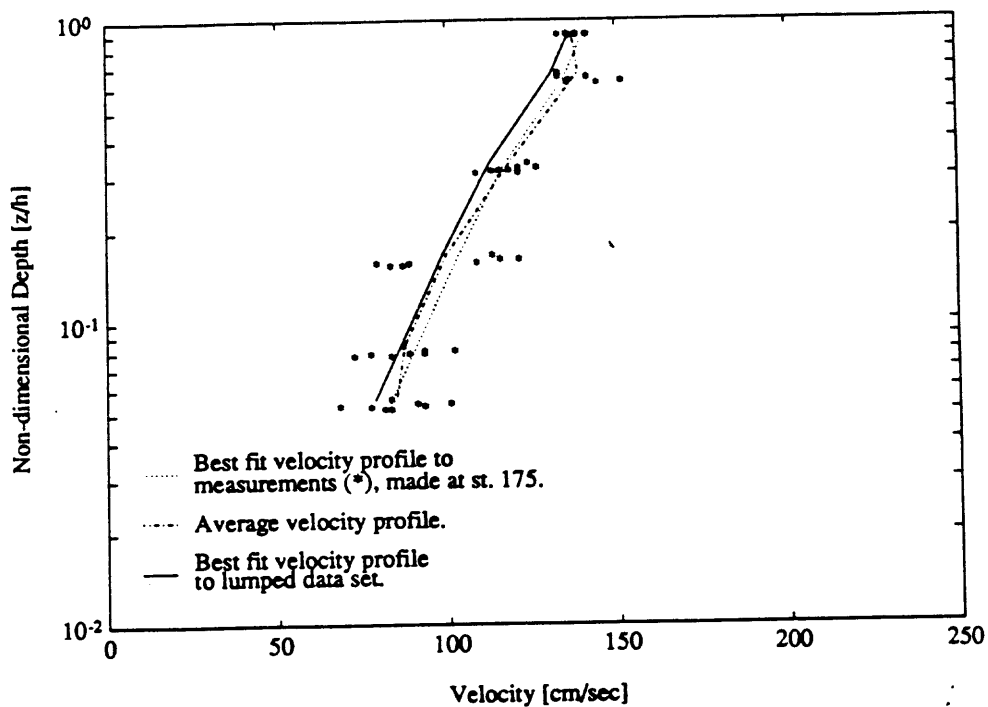


Figure 3.17: Velocity profile measured at station 175 during low discharge.

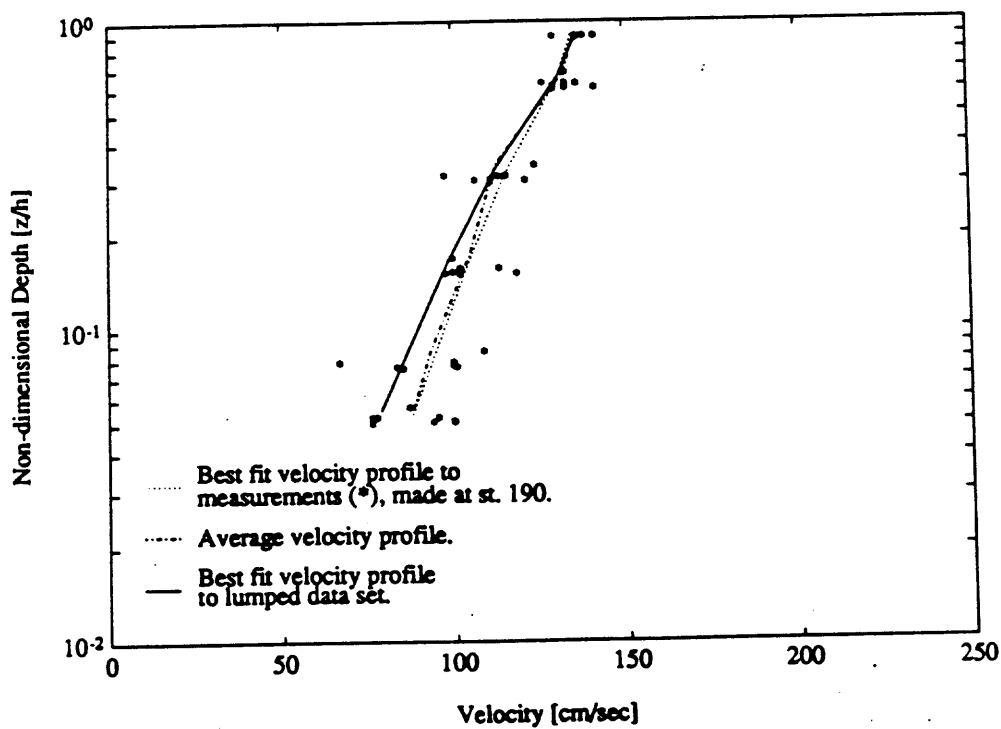


Figure 3.18: Velocity profile measured at station 190 during low discharge.

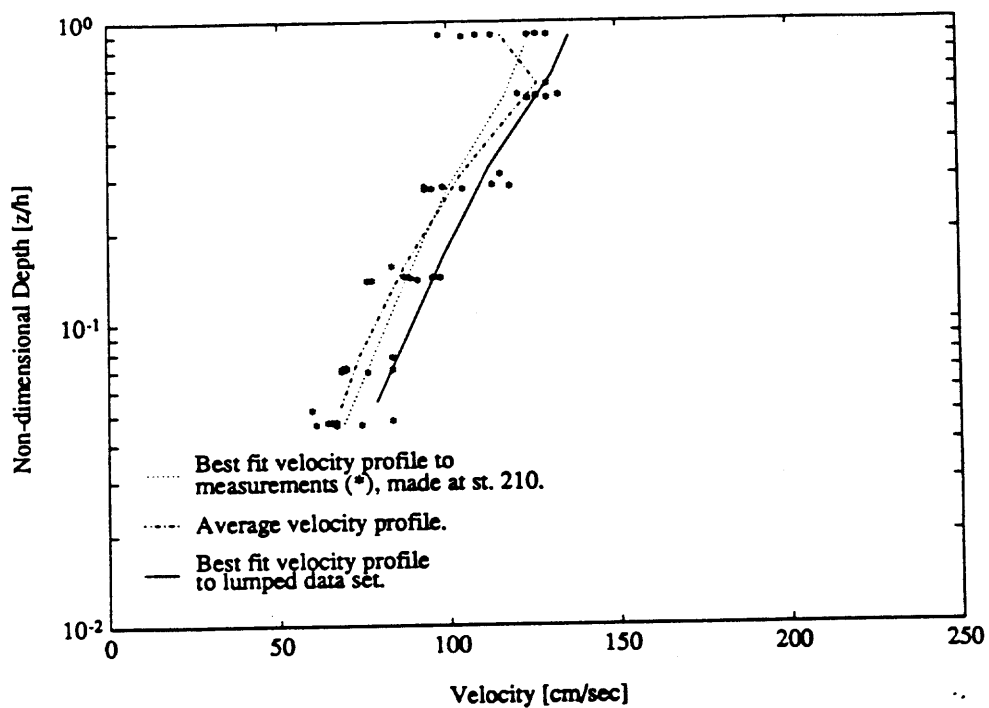


Figure 3.19: Velocity profile measured at station 210 during low discharge.

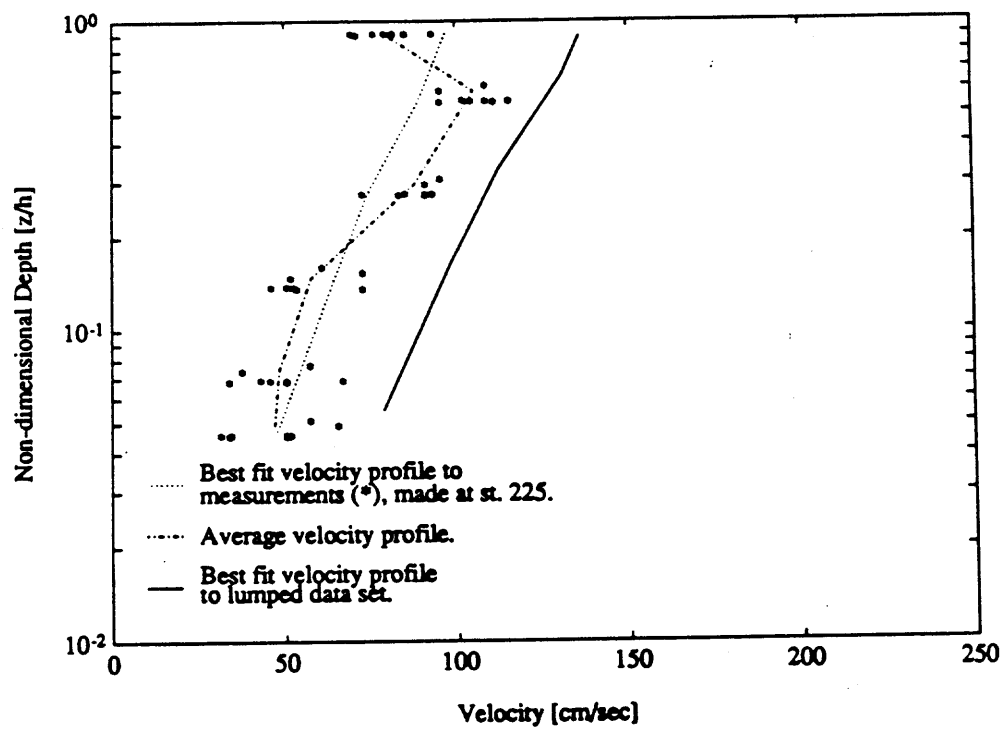


Figure 3.20: Velocity profile measured at station 225 during low discharge.

3.3 Error bars on roughness parameter

The quality of the least squares fit is evaluated by determining the 95 % confidence interval on the values of z_{0T} and u_{*T} . The magnitude of the error bars is determined from the bottom four measurements made in the logarithmic part of the flow. By omitting the top three measurements, the calculated error bars are wider than would be the case if these had been included, but a reasonable estimate of the goodness of fit is still obtained. Since only the logarithmic portion of the velocity profile (the profile structure in the lower 20% of the depth) is included, the confidence limits of the slope κ/u_{*T} and intercept z_{0T} can be estimated from linear regression statistics (Wilkinson, 1984 [26]). The values of κ/u_{*T} and z_{0T} obtained from the linear regression of the measurements made at the bottom four measurements are higher than the values obtained when a quasi-logarithmic profile was fitted to all measurements, but the percent error can be converted into error bars on the values derived. Since z_{0T} is much lower than the level at which the measurements were made, the confidence limit of this parameter is quite wide. The regression coefficients are calculated, and the error on the slope is calculated as

$$\delta u_* = \kappa \delta m \quad (3.7)$$

Where m is the slope of the profile.

The error of z_0 (in log space) is calculated as:

$$\delta \ln(z_0) = \frac{\delta m}{m} \sqrt{X_{rms}^2 + \ln^2(z_0)} \quad (3.8)$$

The value of $X_{rms} = \sum_{n=1}^N \ln^2(z_0)_n / N$ where N is the number of measurements made below $0.2h$.

The results of the error analysis are listed in Table 3.5 and illustrated in Figure 3.21. It is seen that the log-linear regression fit obtained using the bottom four low discharge measurements matches the best fit model profile better than the corresponding high discharge fit, but that the relative magnitude of the error-bar of z_{0T} for the low discharge measurements is almost twice the width of the error-bar of z_{0T} for the high discharge measurements. The low discharge log-linear regression provides a closer fit to the model profile because measurements were made only at six levels as opposed to at seven levels during high discharge, such that the parabolic portion of

the velocity profile is not as well resolved for the low discharge measurements. The error-bar on z_{0T} is wider for the low discharge fit because fewer measurements were used to obtain this value (188 as opposed to 216 measurements for the high discharge value). The result of the error analysis indicates that the statistical uncertainty of u_{*T} is 7-9 %, which converts into an uncertainty of 12-14 % for the boundary shear stress τ_b .

Low Discharge						
Bottom Four Measurements						
u_{*T}	Δu_{*T}	Δu_{*T}	z_{0T}	$\ln(z_{0T})$	$\Delta \ln(z_{0T})$	$\Delta \ln(z_{0T})$
<i>cm/sec</i>	<i>cm/sec</i>	%	<i>cm</i>			%
7.4	0.68	9	0.34	-1.08	-1.65	153
All Measurements						
u_{*T}	u_{*Tmax}	u_{*Tmin}	z_{0T}	$\ln(z_{0T})$	z_{0Tmax}	z_{0Tmin}
<i>cm/sec</i>	<i>cm/sec</i>	<i>cm/sec</i>	<i>cm</i>		<i>cm</i>	<i>cm</i>
7.3	7.9	6.6	0.37	-0.99	1.7	0.081
High Discharge						
Bottom Four Measurements						
u_{*T}	Δu_{*T}	Δu_{*T}	z_{0T}	$\ln(z_{0T})$	$\Delta \ln(z_{0T})$	$\Delta \ln(z_{0T})$
<i>cm/sec</i>	<i>cm/sec</i>	%	<i>cm</i>			%
9.8	0.72	7	0.27	-1.31	-1.07	82
All Measurements						
u_{*T}	u_{*Tmax}	u_{*Tmin}	z_{0T}	$\ln(z_{0T})$	z_{0Tmax}	z_{0Tmin}
<i>cm/sec</i>	<i>cm/sec</i>	<i>cm/sec</i>	<i>cm</i>		<i>cm</i>	<i>cm</i>
9.1	9.7	8.5	0.18	-1.71	0.73	0.096

Table 3.5: Results of error analysis. The percent error calculated using the measurements made at the bottom four levels is converted to provide a minimum and a maximum value of u_{*T} and z_{0T} of the best fit to the lumped data set.

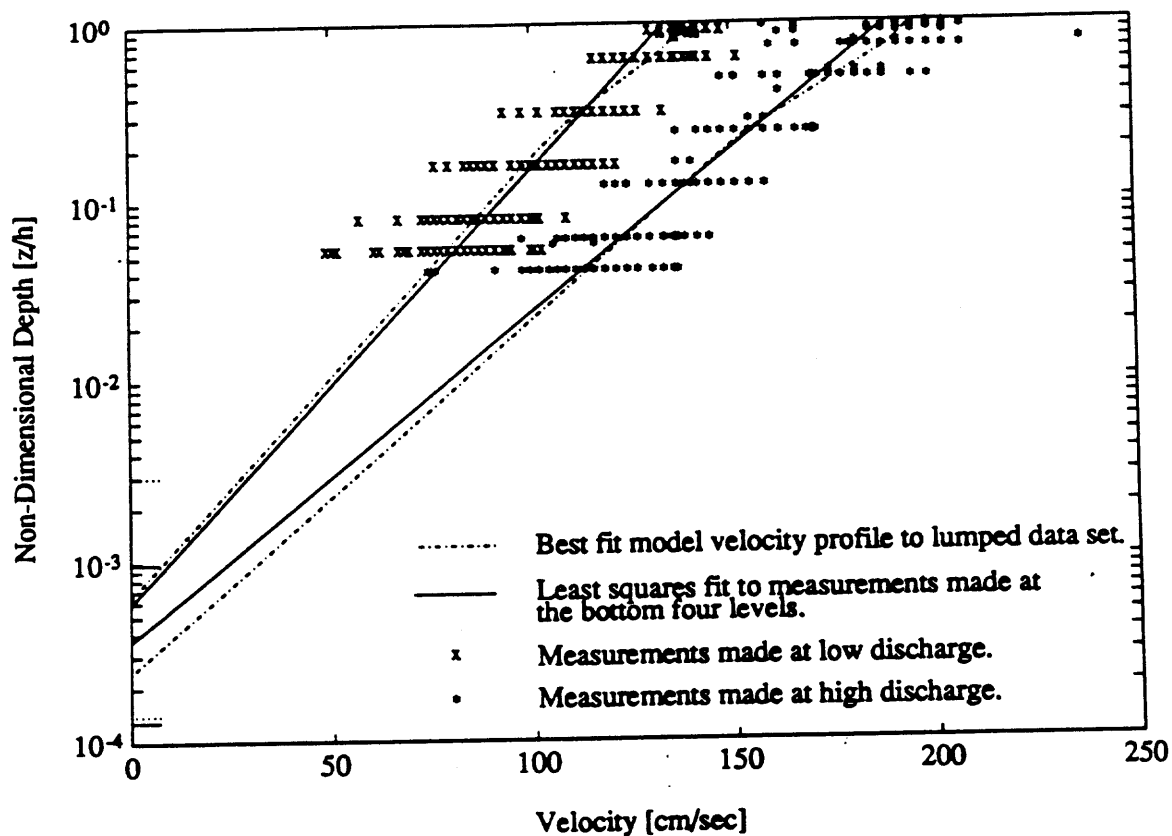


Figure 3.21: Results of error analysis. The best fit velocity profile to the lumped data set is compared to the least squares log-linear fit obtained using the measurements made at the bottom four levels. The errorbars on z_{0T} are indicated by the dotted line for the low discharge measurements and by the solid lines for the high discharge measurements.

3.4 Roughness at National Canyon

The Colorado River is a mixed sand and gravel system. In some reaches along the river, gravel is the predominant bottom material. In other reaches sand covers the bottom. This mixture of sand and gravel creates a channel environment that is patchy with respect to distribution of sediment sizes and bottom conditions (*Smith and Wiele*, 1992 [21]). The boundary shear stress responsible for moving sediment may be derived from the flow conditions in the near boundary region, which differ whether the reach of interest is predominantly a gravel reach, a mixed sand and gravel reach, or a predominantly sand bedded reach (*Wiberg and Smith*, 1991 [25] and *Smith and McLean*, 1977 [20]). While working in the reach at National Canyon a qualitative impression of the bottom was developed. As described in section 2.5 the reach was surveyed using an acoustic depth sounder. The output of the instrument was a continuous strip chart, from which bedforms were observed in abundance in vicinity of the cableway were observed. Since bed forms only develop on a bed that is predominantly sand, it may be concluded that the bottom in vicinity of the cableway was sand bedded. Bedforms were observed from the National Canyon rapid, located approximately 500 meters downstream from the cableway to approximately 500 meters upstream of the cableway, indicating that in a 1000 meter reach the bottom was covered with sand.

In sand bedded streams, bedforms develop in response to the flow when sand is put into motion. Bedform height, H , and wavelength, λ , are functions of the grain size distribution of the bottom material, boundary shear stress, whether sand is moved as bedload or suspended load, the availability of sand, and flow depth (*Middleton and Southard*, 1984 [12]). The presence of bedforms modifies the flow in a manner that gives rise to a high apparent roughness, z_{0T} , of the exterior flow which is one or more orders of magnitude greater than the grain roughness and roughness related to the moving bedload layer, but less than the bedform height (*Smith and McLean*, 1977 [20]).

In a river as deep as the Colorado (approximately 7 meters at high flow) it is not feasible to make velocity measurements sufficiently close to the boundary to resolve the structure of the velocity profile in the interior flow region. The bottommost measurement was made as close to the bottom as possible, which was 15 cm above the bed. Flow measurements closer to the boundary are important because the flow is modi-

fied by the presence of bedforms, and the flow structure in vicinity of the boundary differs from that of the exterior flow. The flow in the near boundary region consists of complex interactions between turbulence, flow separation, wake formation, topographically induced accelerations, and internal boundary layer development (*Wiberg and Nelson, 1992 [23]*). It is currently not possible to model the flow structure in this region in a manner that incorporates all these mechanisms since their interactions are not well understood. However, *Smith and McLean, 1977 [20]* present a model that considers the effect of bedforms on the flow in a relatively straight forward manner. Their model accounts for the spatially averaged form drag over a bedform, and describes the flow in the near boundary region in a spatially averaged sense. The *Smith and McLean, 1977* model has been used to extrapolate the velocity profile of the exterior flow to the bottom, through the region of interior flow and thus determining a value of the skin friction shear stress responsible for moving sediment.

The flow may be divided into three regions: an internal boundary layer, a wake region, and the exterior flow (*Arya, 1975 [2]*). In the *Smith and McLean, 1977 [20]* model, the internal boundary layer and the wake region are considered the interior flow region. In the interior flow region, flow is modified by the presence of bedforms, and roughness is scaled by a characteristic grain diameter of the material moving in the bedload. In the exterior layer, above the bedforms, the effect of flow separation is insignificant, and the flow is controlled by the total stress (see equation 3.2). In the exterior region, the flow has adjusted to a roughness scale that is a function of bedform height and wave length.

The form drag is a force acting on a bedform as a result of flow separation and wake formation on the lee side of the bedform. The separated flow produces a pressure gradient over the bedform, and the resulting force acts on the length scale of a bedform. The form drag is not available to accelerate flow or to move sediment (*McLean, 1990 [10]*), and it is particularly important in the interior flow region where the wake influence is strong.

The total stress acting in the downstream direction can be partitioned into two components, form drag, τ_D , and skin friction stress, τ_F .

$$\tau_T = \tau_D + \tau_F \quad (3.9)$$

The stress associated with form drag, τ_D , is determined by considering the drag force on a bedform relative to the area of the bed affected by that bedform. The drag

force is related to the mean velocity of the undisturbed flow field (the velocity that would be observed if bedforms were not present). The mean velocity \bar{u} , is obtained by integrating the velocity profile of the undisturbed flow field over the height of a bedform. In addition, form drag is related to bed form length, and a drag coefficient C_D .

$$\tau_D = \frac{\rho C_D \bar{u}^2 H}{\lambda} \quad (3.10)$$

The magnitude of C_D is related to the degree of flow separation over the bedforms which in return is a function of the shape of the bedform. In general, the stress responsible for moving sediment is the stress at the bed. When bedforms are present, the stress at the bed is the skin friction shear stress, τ_F , which is equivalent to the total stress corrected for form drag. The interior flow region is defined as a flow region of strong wake influence, and the thickness is scaled by the extent of vertical wake influence. The height of the wake region is scaled by the height of the bedforms H , and as an approximation, the matching level between the interior and exterior layer is set to the bedform height, H above the bottom.

Smith and McLean (1977 [20]), obtained good results by assuming that the spatially averaged flow in the interior region could be described by a logarithmic velocity profile:

$$u = \frac{u_{*F}}{k} \ln \left(\frac{z}{z_{0F}} \right) \quad (3.11)$$

where u_{*F} is the shear velocity associated with the skin friction shear stress and z_{0F} is the bottom roughness parameter, related to the grain scale roughness of the boundary. Experiments have later indicated that the velocity structure even when spatially averaged deviates somewhat from logarithmic (*Wiberg and Nelson*, 1992 [23]).

In the case of flow over a plane bed and no bedload transport, the roughness parameter z_{0F} is specified according to the work of *Nikuradse*, 1933 [13]. When grains are in motion it is necessary to determine the z_{0F} related to the size of grains moving as bedload. As sediment rolls or saltates along the bed, collisions of moving grains with sediment particles on the bed, extract momentum from the moving material. Thus the sediment in the saltation layer is transported at a lower velocity than the surrounding fluid, a mechanism that is observed as a higher apparent roughness of the bed *Wiberg and Rubin*, 1989 [24]. The thickness of the saltation layer is here specified according to the results of *Wiberg and Rubin*, 1989 [24]. They found an

empirical relationship between hopping height of sediment grains, δ_b , a characteristic grain size D , and transport stage $T_* = \tau_F/\tau_{cr}$, where τ_{cr} is the threshold shear stress for sediment motion of a specific grain size, and it is specified according to *Shields*, 1936 [19];

$$\delta_b = \frac{A_1 T_*}{(1 + A_2 T_*)} D \quad (3.12)$$

The constant $A_1 = 0.68$, and A_2 is a function of grain size D moving in the bedload layer. In the *Wiberg and Rubin*, 1989 [24] formulation, the apparent roughness is a fraction of the thickness of the saltation layer which was empirically determined as:

$$z_{0F} = 0.056\delta_b \quad (3.13)$$

The thickness of the saltation layer is related to the skin friction shear stress, and to perform its calculation it is necessary to iterate. The calculation is generally stabilized after two or three iterations.

The ratio of total shear velocity, u_{*T} , to skin friction shear velocity u_{*F} may be obtained from equation 3.9 and by calculating the form drag according to equation 3.10:

$$\frac{u_{*T}}{u_{*F}} = \sqrt{1 + \frac{C_D H}{2\kappa^2 \lambda} \left(\ln \left(\frac{z_m}{z_{0F}} \right) - 1 \right)^2} \quad (3.14)$$

The mean velocity is found by integrating equation 3.11, from z_{0T} to z_m over the region of strong wake influence, where z_m is matching height between interior and exterior flow. For the purpose of these calculations, $z_m = H$.

In equation 3.14 the drag coefficient C_D and the ratio of bedform height H to wavelength λ , are critical parameters. In the case of flow over a plane bed, the region of wake influence goes to zero; because $H/\lambda \rightarrow 0$ and $C_D \rightarrow 0$, $u_{*F} \rightarrow u_{*T}$.

By matching the interior region and the exterior flow at the height z_m above the bed, the bedform roughness, z_{0T} , can be inferred from the ratio of total shear velocity to skin friction shear velocity.

$$z_{0T} = \frac{z_m}{\exp \left(\frac{u_{*F}}{u_{*T}} \ln \left(\frac{z_m}{z_{0F}} \right) \right)} \quad (3.15)$$

In Figure 3.22, the velocity profile in the interior and exterior flow is described schematically. In the exterior flow region, the two part velocity structure (equation

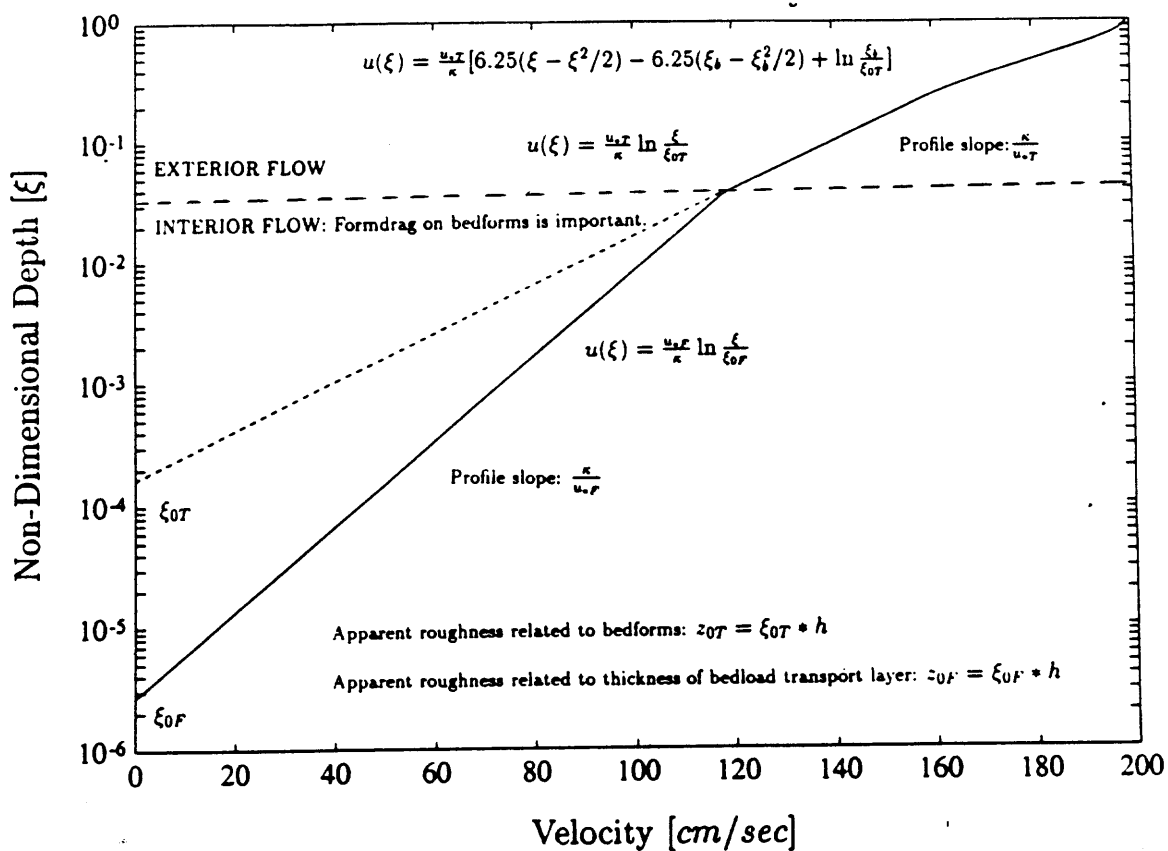


Figure 3.22: Schematic velocity profile. In the exterior flow region, the two part velocity structure (equation 3.6) is indicated, and in the interior flow region the flow is described as logarithmic (equation 3.11).

3.6) is indicated, and in the interior flow region the flow is described as logarithmic (equation 3.11).

In a river with unlimited supply of sediment and bedload dominated transport mode, bedforms are expected to develop fully to a height that corresponds to 20 % of the flow depth (*Middleton and Southard, 1984 [12]*). The bedforms observed at National Canyon were not of a height that corresponded to 20 % of the flow depth, but were much smaller. The small bedforms are related to a limited supply of sediment in the reach. The mixed sand and gravel system of the Colorado River does not allow for formation of fully developed bedforms.

3.5 *Determining the model parameters*

To estimate the magnitude of the form drag correction in the near boundary region, five parameters are needed. These are bedform height and wavelength, the drag coefficient C_D , skin friction roughness which requires a characteristic grain size, and the shear velocity of the exterior flow.

The ratio of height to wavelength for sand dunes is roughly 1/20. At lower boundary shear stresses, smaller and steeper ripples with a height to length ratio of roughly 1/10 may develop (*Middleton and Southard, 1984 [12]*).

The bedform height and wavelength were obtained from echo-sounding records collected at National Canyon during the study period. During the field study in July 1991, the flow fluctuated in diurnal cycles and suspended sediment transport was only significant within the highest part of the discharge range.

The bedforms were surveyed during the rising limb and during peak discharge, and it is likely that the surveyed bedforms represented characteristic bottom configurations during the high discharge velocity measurements. During lower discharges bedforms were not surveyed but it was initially chosen to assume that the measured dune geometry also was representative of the bottom configuration at low discharge although the boundary shear stress was significantly smaller.

The bedforms have different heights, lengths, and shapes, and the values used in the model calculation are average values of height and wave length. Significant peak and trough values were selected, and the bedform height was determined as the distance between peak and trough, and the corresponding length was determined as the distance between two peaks. A characteristic bedform height was obtained by

averaging all measured heights and a characteristic length was obtained by averaging all bedform lengths.

Bedform Height	Bedform Length
<i>cm</i>	<i>cm</i>
27	587

Table 3.6: Mean values of bedform height and wavelength.

The drag coefficient C_D is related the degree of flow separation that occurs over a bedform and thus scales the magnitude of the form drag. The value ranges around 0.2 for sharp crested bedforms and around 0.8 for well rounded features (*Smith and McLean*, 1977 [20]). The drag coefficient depends on the degree of flow separation around a bedform. Well rounded bedforms induce less separation of flow and hence the drag force acting on the bedform is greater which is reflected in the higher drag coefficient. The echo-sounding records indicated that the bedforms were typically sharp crested, and $C_D = 0.2$ was used in the calculations.

The skin friction roughness is a function of sediment sizes moving in the bedload layer. As the finer fraction of the total grain size distribution is suspended into the water column, the mean grain size of the bedload layer becomes coarser. Thus the characteristic grain size of the bedload layer is smaller at a discharge where the suspended sediment concentrations are minimal than at discharges where the suspended sediment concentrations are significant. It is required that bottom samples are made at flow stages that correspond to the discharge when velocity profiles were measured, to obtain an accurate sample of the bottom material. However, the difference in mean grain size is likely to be small, and since the calculations are not sensitive to this parameter, the mean grain size of sediment in the bedload layer is assumed to be the same during high and low discharge. Once again the nature of large rivers greatly complicates this task and it was not possible to obtain samples of the bottom material at a depth of 7 meters. Based on the size analysis of material caught in the suspended sediment sampler a characteristic size of the bedmaterial was estimated $D = 0.02cm$. This grain size is also in accordance with the median grain size found in sediment deposits in low gradient reaches by *Howard and Dolan*, 1981 [7].

The shear velocity of the exterior flow obtained from the velocity profile analysis was used to calculate the total shear stress, τ_T . Then the channel slope, which was

not surveyed, was calculated using this value of τ_T in conjunction with equation 3.1.

3.6 Summary of Results

From the analysis described previously, the following results are derived:

	High Discharge				
	z_{0T}	u_{*T}	Slope	z_{0F}	u_{*F}
	<i>cm</i>	<i>cm/sec</i>		<i>cm</i>	<i>cm/sec</i>
Measurement	0.18	9.1	0.000114	-	-
derived values					
Calculated	0.12	-	0.000114	0.0020	5.2

Table 3.7: Summary of results of velocity profile analysis of measurements made at high discharge, $h = 740$ *cm*.

	Low Discharge				
	z_{0T}	u_{*T}	Slope	z_{0F}	u_{*F}
	<i>cm</i>	<i>cm/sec</i>		<i>cm</i>	<i>cm/sec</i>
Measurement	0.37	7.3	0.00010	-	-
derived value					
Calculation I	0.12	-	0.000114	0.0019	4.5
Calculation II	0.12	-	0.000095	0.0018	4.1

Table 3.8: Summary of results of velocity profile analysis of measurements made at low discharge, $h = 570$ *cm*. Calculation I assumes the surface slope obtained from the high discharge measurements and Calculation II assumes the surface slope obtained from the low discharge measurements.

High Discharge				
Discharge at high flow	Unit discharge in center	Width of central segment	Discharge in central segment	Difference
m^3/sec	m^2/sec	m	m^3/sec	%
600	13.2	24.4	322	54
Low Discharge				
Discharge at high flow	Unit discharge in center	Width of central segment	Discharge in central segment	Difference
m^3/sec	m^2/sec	m	m^3/sec	%
325	6.7	28.7	192	59

Table 3.9: Channel discharge derived from the measured velocity profiles compared to the calculated discharge in the central portion of the river. At high discharge the surface width of the river is approximately 85 meters and at low discharge the surface width is approximately 80 meters.

3.7 Discussion of Results

One way to evaluate of the success of the statistical velocity profile analysis is by comparing surface slope obtained from the velocity measurements made at high discharge to the surface slope obtained from measurements made at low discharge. The slope calculated at low flow differs by 17 % from the slope obtained using the high discharge measurements (Tables 3.7 and 3.8). It is assumed that the surface slope of the reach remains constant at all discharges and therefore the analysis of the high and low profile should provide the same value of surface slope. The statistical uncertainty of the boundary shear stress was, in section 3.3, found to be approximately 12-14 %, which may explain the difference between the two calculated slopes. However, since the calculated slopes were different, it could also be speculated that there is a mechanism that changes the slope at different discharges. The National Canyon Rapid may produce an upstream backwater effect that increases surface slope at higher discharges. It would be very difficult to resolve whether such a mechanism exists. The obvious approach would be to make direct measurements of the surface slope, for instance using a pressure transducer, that would provide very precise recordings of

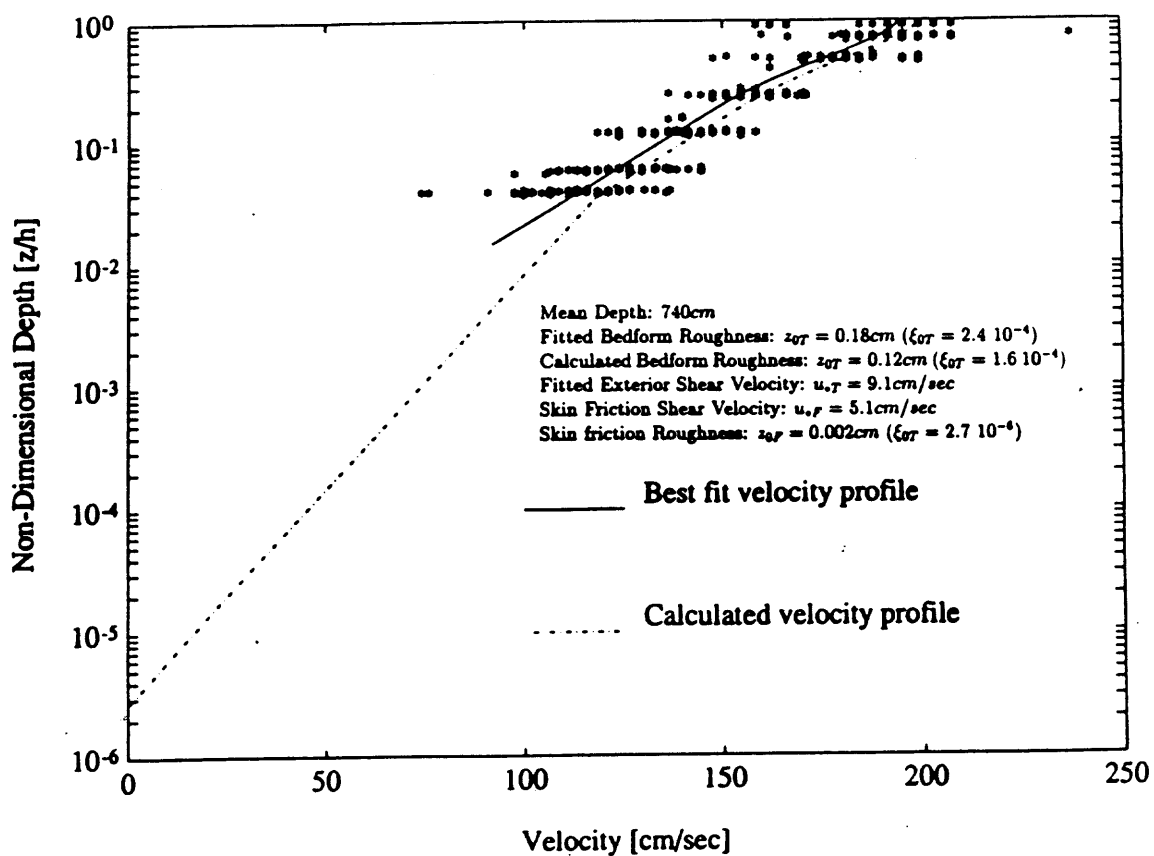


Figure 3.23: Comparison between best fit and calculated velocity profile at high discharge. The solid line describes the best fit profile to the combined measurements made at station 110, 130, 145, 160, 175 and 190, in the central segment of the river. The dash-dotted line is the velocity profile calculated, assuming the bedform dimensions of $h = 27\text{cm}$ and $\lambda = 587\text{cm}$ and taking the form drag in the near boundary region into account.

depth. However, since the slope is very small, the differences in depth between two gages would also be very small. If two pressure transducers are spaced 1000 meters apart, the elevation difference at low flow would be 10 centimeters and the elevation difference at high flow would be 11.7 centimeters, a difference of 1.7 centimeters between high and low discharge. Prior to making such measurements it would be necessary to consider whether the accuracy of the surveyed position of the two pressure transducers and the recordings of water surface elevation are of sufficient to resolve a difference in water surface elevation of 1 to 2 centimeters.

The bedform roughness calculated using the model for form drag correction, equation 3.15, produces very similar values of z_{0T} in the two cases. The bedform roughness is related to the bedform aspect ratio, H/λ , choice of drag coefficient, C_D , and choice of matching height, z_m . When the bed configuration is considered the same for profiles measured during high discharge and profiles measured during low discharge, the total roughness, z_{0T} , will be the same for the two cases. Contrary to this, the statistical velocity profile analysis produces values of z_{0T} that are very different from high to low flow. The measurement derived values of z_{0T} are higher than the calculated value of z_{0T} in both cases; approximately 30 % higher during high discharge and approximately 300 % higher during low discharge. Given the uncertainties inherent in determining the critical parameters, the deviation between calculated and empirically determined bedform roughness is acceptable in the case of high discharge, but the low discharge deviation is not.

The difference between z_{0T} calculated assuming dune geometry on the bed and z_{0T} derived from the low flow velocity profile is analyzed by considering the ratio of u_{*T}/u_{*F} and the non-dimensional form drag. The second part of the right hand side of equation 3.14, describes the ratio of form drag to skin friction shear stress, and is referred to as non-dimensional form drag.

The measurement derived value of z_{0T} is used to solve equation 3.15 for u_{*T}/u_{*F} and that result is used in equation 3.14, to derive a value of non-dimensional form drag. The non-dimensional form drag calculated using the measurement derived value of z_{0T} is 91 % greater than the form drag calculated using the surveyed bedform dimensions and the measurement derived value of u_{*T} in equation 3.14.

To determine the most likely explanation of the higher form drag at low discharge, the parameters, the drag coefficient, C_D , the bedform aspect ratio, H/λ , and the

Low Discharge		
Calculated Form Drag	Measurement derived Form Drag	Percent Difference
2.06	3.93	91

Table 3.10: Non-dimensional form drag calculated using equation 3.14 and assuming dunes on the bed, in comparison with non-dimensional form drag inferred from the measurement derived value of $z_{0T} = 0.37\text{cm}$.

matching height, z_m , that scale the magnitude of the form drag are evaluated. The three parameters are evaluated to determine likely deviations from the values chosen for the calculation of non-dimensional form drag in Table 3.10.

A drag coefficient that is 91 % greater than the chosen value of $C_D = 0.2$ is $C_D = 0.38$. Drag coefficients increase abruptly with increasing roundness and symmetry of the bedform geometry (*Smith and Mclean*, 1977 [20]). Moreover, the shapes of the bedforms that were recorded with the echo sounder do not indicate any reason to change the classification of bedforms from sharp crested and asymmetrical.

A re-evaluation of the drag coefficient $C_D = 0.21$ found by *Smith and McLean*, 1977 [20] for the Columbia River, indicated a slightly higher value of $C_D = 0.23$, (*Wiberg and Nelson*, 1992 [23]). In addition, experimental measurements of flow over asymmetric ripples provided $C_D = 0.17$ for $H/h = 0.17$ and $C_D = 0.3$ for $H/h = 0.09$ (*Wiberg and Nelson*, 1992 [23]). Thus, the choice of drag coefficient may be responsible for a portion of the difference between the two values of form drag, but at most 50 % and probably no more than 15 - 20 %.

The bedform aspect ratio, H/λ , is a more important parameter than the value of bedform height or wavelength. Generally the bedform aspect varies between 0.13 for ripples to 0.04 for dunes. It is possible that the bedforms become shorter and steeper during the lower discharge so that the aspect ratio becomes greater. A number of flume studies have examined the empirical relationship between mean velocity, mean sediment size, flow depth and bed configurations (*Middleton and Southard*, 1984 [12]). Since the flume experiments are one to two orders of magnitude smaller in scale than the flow in the Colorado River, these observations cannot be uncritically extrapolated to account for bedform configurations in the Colorado River. These empirical relationships do indicate that the combination of boundary shear stress

and mean sediment size found at National Canyon fall within a transitional regime between ripples and dunes (*Middleton and Southard*, 1984 [12], Figure 7.26). In order for the aspect ratio to explain the increased roughness during low flow, the bedforms have to adjust to a ripple bed, with an aspect ratio of approximately 0.09.

Since the flow fluctuated, it was not expected that the observed bedforms were in equilibrium with any specific discharge. The migration rate of a bedform is determined by relating the bedload transport rate, calculated using the modified Meyer-Peter Müller bedload equation, to bedform height and concentration of sediment within the bedform. The modified Meyer-Peter Müller bedload equation was selected because of its simple form, and for the grain sizes and transport rates considered here, other bedload equations as for instance the Einstein bedload equation or the Yalin bedload equation provide similar results. For moderate transport rates ($3 < T_* < 15$) ($T_* = \tau/\tau_{cr}$ is transport stage), the modified Meyer-Peter Müller bedload equation has the form:

$$\Phi_s = 8(\tau_* - \tau_{*cr})^{3/2} \quad (3.16)$$

The non-dimensional bedload transport rate $\Phi_s = q_s / (\frac{\rho_s - \rho}{\rho} g D^3)^{1/2}$, where q_s is sediment transport rate, ρ_s is sediment density and ρ is fluid density. The non-dimensional shear stress τ_* and the non-dimensional critical shear stress τ_{*cr} , are the shear stress and the critical shear stress non-dimensionalized by the parameter $(\rho_s - \rho)gD$.

The bedform migration rate U_B is calculated as:

$$U_B = \frac{q_s}{C_b H/2} \quad (3.17)$$

The calculation of the migration rate of a 30 cm high bedform during high and low discharge is demonstrated in Table 3.11. At high discharge the bedform migration rate was approximately 220 cm/hr and at low discharge the migration rate was approximately 40 cm/hr. These migration rates are of a time scale that indicate that the bed may adjust to changed flow conditions between high and low discharge.

Finally, the extent of strong wake influence over a dune is estimated as one bedform height. However, the wake formation may influence the flow to as much as $2H$ (*Wiberg and Nelson*, 1992 [23]). Assuming that the region of strong wake influence is $2H$ rather than H , and using this value in equation 3.14, the form drag increases by approximately 20 %.

Bedform Migration Rates									
	D	τ	τ_{cr}	T_*	τ_*	τ_{*cr}	Φ_s	q_s	U_b
	<i>cm</i>	<i>dy/cm²</i>	<i>dy/cm²</i>					<i>cm²/sec</i>	<i>cm/hr</i>
High Q	0.02	27.0	2.6	10.4	0.83	0.08	5.2	0.6	220
Low Q	0.02	10.8	2.6	4.1	0.33	0.08	1.0	0.0.117	40

Table 3.11: Bedform migration rates at high and low discharge (Q). The boundary shear stress used to calculate the migration rate at high discharge is obtained by using the relationship $\tau_F = \rho u_{*F}^2$, and u_{*F} from table 3.7. The boundary shear stress at low discharge is calculated using equation 3.15 and the measurement derived value of z_{0T} to calculate the ratio u_{*T}/u_{*F} , and relating the derived value of u_{*F} to a skin friction shear stress.

It is likely that the error between the calculated and the measurement derived bedform roughnesses are a combination of all of the above mentioned uncertainties in determining the appropriate magnitude of form drag. However, adjustment of the bed to a ripple bedform regime during low discharge is likely to occur, and in such a case this would account for a substantial portion of the deviation between the measurement derived and calculated value of roughness.

Since velocity was measured at several stations across the river, a region of uniform flow in the cross-stream direction could be identified. The region of uniform flow was evaluated to extend at least over the region that included the statistically similar velocity profiles. It was found that the region included the measurements made at stations 95-190 during low discharge which was equivalent to a width of 29 meters. During high discharge the uniform flow region included the measurements made at station 110-190, and was equivalent to a width of 24 meters (Table 3.9). The width of the uniform flow regions during both high and low discharge corresponded to approximately 30% of the total channel width at those discharges. In this same region 55-60 % of the total discharge occurred (Table 3.9).

The unit discharge in the wake region relative to the total unit discharge has been calculated for the purpose of demonstrating that since this is a small fraction of the total unit discharge the true structure of the flow in the wake region is primarily relevant when the problem of interest is related to sediment transport, and accurate values of boundary shear stress are important. The result of the calculation

is demonstrated in Table 3.12. The error incurred in neglecting flow in the interior region when calculating discharge of water is small.

High Discharge		
Unit discharge in center	Unit discharge in wake region	Fraction of total discharge
m^2/sec	m^2/sec	%
13.2	0.30	2
Low Discharge		
Unit discharge in center	Unit discharge in wake region	Fraction of total discharge
m^2/sec	m^2/sec	%
6.7	0.19	3

Table 3.12: Discharge in wake region relative to total discharge. The discharge in the wake region is calculated and compared to the total discharge. It is seen that the flow in the wake region is only a small percentage of the total flow.

Empirical relationships exist that relate channel roughness to mean velocity, such as for example the Manning equation (*Richards* 1982, [16]) or resistance equations (*Bathurst* 1985, [3]). Both the Mannings equation and the resistance equation provide convenient methods for determining mean flow velocity given relatively little information about the channel. However, since these relationships involve a generalization of the roughness parameter from a specific set of stream measurements, the derived relationship can only be applied with certainty to streams of similar nature. Furthermore, these types of relationships do not allow for describing the flow structure in the near boundary region where sediment transport processes occur. Due to the common and also straight forward application of these relationships, it is useful to compare the roughness parameter that may be derived by using the mean channel velocity and channel slope at National Canyon to values of the roughness parameter found in the literature.

In the Manning equation, the roughness parameter, n , depends on channel material, and whether the channel is straight or meandering (*Richards*, 1982 [16]). The relationship is strictly empirical. Values of n have been derived based on average

velocity in the channel during high and low discharge. These calculated values are compared to recommended values of n .

In SI units the Manning equation has the form:

$$\bar{u} = \frac{R^{2/3} S^{1/2}}{n} \quad (3.18)$$

In the Manning equation, mean velocity of channel flow \bar{u} , is related to channel slope S , hydraulic radius $R = A/P$, and n , a resistance coefficient, where P is the wetted perimeter of the channel and A is the cross-sectional area of the channel. The mean channel velocity is calculated the ratio of total discharge to the cross-sectional area, Q/A . Since the channel is wide relative to channel depth, the hydraulic radius is the mean channel depth.

	Slope	\bar{u}	R	n_{Calc}	n_{table}	Difference
		m/sec	m			%
High Discharge	0.0001	1.40	7.5	0.027	0.025	8
Low Discharge	0.0001	0.98	5.9	0.033	0.025	32

Table 3.13: Comparison between Mannings n derived from the measurements and the recommended Mannings n for a major stream more than 30 meters wide, that is clean and regular (*Richards*, 1982 [16]).

It may seem that the derived value of n is similar to the value of n recommended by *Richards*, 1982 [16]. However, since n is inversely proportional to mean velocity, any deviation in n will lead to the same percentage of error in the mean discharge. Since the difference in velocity between high and low discharge is 43 %, the value of n must be known to an accuracy that is greater than 43 %, preferably within 5 %, for the calculations to at least provide a good estimate of the mean channel velocity. However, n cannot be known to this degree of accuracy, because it is an empirical coefficient that does not have a physical meaning, but is related to a general experience of a certain type of channel behavior.

In resistance equations, the ratio of mean velocity to shear velocity is assumed to vary with the logarithm of the ratio of flow depth to bottom roughness. The roughness parameter k_s has been quantified using three different methods. A value of k_s was calculated from the mean velocity and u_{*T} of the best fit velocity profile.

This value was then compared to a value of k_s that corresponded to the measurement derived value of z_{0T} , and a value of k_s that was calculated according to an empirical relationship specified by *van Rijn* 1982, [22] to determine k_s for flow over sand dunes.

In a resistance equation, mean velocity is related to a characteristic roughness height, k_s , and it has the form:

$$\frac{\bar{u}}{u_{*T}} = \frac{1}{\kappa} \ln \left(\frac{h}{k_s/30} \right) + c_1 \quad (3.19)$$

Where c_1 is a constant. Because $z_{0T} = k_s/30$, the characteristic roughness height can easily be related to the measurement derived values of bedform roughness.

A method for determining the appropriate value of k_s in streams covered with bedforms is proposed by *van Rijn*, 1982 [22]. He found an empirical relationship where k_s is proportional to H^2/λ .

$$k_s = 1.1H(1 - e^{-25H/\lambda}) \quad (3.20)$$

The bedform roughnesses obtained using equation 3.20 are over-predicted in case (1), (2) and (3) relative to the measurement derived values (Table 3.14), and it is concluded that the *van Rijn* relationship is not appropriate for determining a roughness coefficient for the Colorado River. The roughness parameter determined using the measurement derived value of z_{0T} to determine k_s , indicates that this parameter is in reasonable agreement with the value expected of k_s (Table 3.14). However, if a value of z_{0T} is known, it is redundant to convert this value into k_s , because its definition is $k_s = z_{0T}/30$, and z_{0T} could be used instead.

	u_{*T}	\bar{u}	R	$k_{s(eq\ 3.19)}$	$k_{s(meas)}$	$k_{s(eq\ 3.20)}$	Difference
	<i>cm/sec</i>	<i>cm/sec</i>	<i>cm</i>	<i>cm</i>	<i>cm</i>	<i>cm</i>	%
(1) High Q	9.1	175	750	3.9	5.4	20.3	276
(2) Low Q	7.3	120	590	9.3	11.1	20.3	83
(3) Low Q	7.3	120	590	9.3	11.1	29.5	242

Table 3.14: Comparison between values of k_s derived from equation 3.19, measurement derived values, and the value calculated using equation 3.20. (1) and (2) are calculated using the bedform height and wavelength derived from the echo-sounding records. (3) is calculated assuming a bedform aspect ratio of 0.09, and a bedform height of 30 *cm*. The values compared are the measurement derived values and the values determined using the relationship by *van Rijn*, 1982 [22], equation 3.20.

Chapter 4

CONCENTRATION PROFILE ANALYSIS

4.1 The concentration Profile Model

Suspended sediment concentration, $C(z)$, at any given level in the flow, can be regarded as the balance between upward turbulent diffusion and downward settling of sand particles. When settling velocity, w , of a given grain size is small relative to the strength of the turbulent eddy viscosity, $K(z)$, sediment is diffused from the bed into the water column (Rouse, 1937 [17]).

In the one-dimensional, steady, and uniform case, the suspended sediment mass balance has the general form:

$$wC(z) + K(z)\frac{\partial C(z)}{\partial z} = 0 \quad (4.1)$$

In finding a solution for this equation, it is assumed that the horizontal velocity of sediment is equal to the horizontal velocity of water, i.e. sediment is not advected downstream at a velocity that differs from that of the surrounding flow. According to McLean, 1991 [11] the boundary condition necessary for solving equation 4.1 is a known reference concentration at a level in the vicinity of the boundary. In its general form, the solution to 4.1 is given as:

$$C_m(z) = C_m(z_a) \exp\left(-\int_{z_a}^z \frac{w_m}{K(z)} dz\right) \quad (4.2)$$

The subscript m refers to sediment of size component m , where $C(z) = \sum_{m=1}^M C_m(z)$; M is the number of size classes that represent the grain size distribution. The subscript a refers to a reference level, where concentration is known. The reference level is here taken as the top of the saltation layer, $z_a = \delta_b$ determined from equation 3.12. The solution to the integral in equation 4.2 yields a two-part structure of the concentration profile. McLean, 1991 [11] specifies that the concentration of a given size class at the level z_a is proportional to excess shear stress $S_m = (\tau_F - \tau_{crm})/\tau_{crm}$ and

may be expressed as:

$$C(z_a) = C_b \gamma S_m i_m \quad (4.3)$$

where C_b is the maximum possible concentration of packed sediment, and ranges between 0.6 - 0.65, and i_m is the fraction of the distribution represented by size m . The empirical constant γ is controlled by the upward suspension of sediment from the near bed region. The critical shear stress for a given grain size is specified according to *Shields*, 1936 [19]. Settling velocities of characteristic grain sizes were calculated according to *Dietrich*, 1982 [5] who devised an empirical method of determining settling velocity of natural grains, outside the Stokes range, that also corrects for sediment shape (Corey Shape Factor) and roundness (Powers roundness value).

Turbulent mixing is the mechanism by which sediment is maintained in suspension. In the interior flow region, where the flow is modified by bedforms, the eddy viscosity is scaled by u_{*F} and it is the skin friction shear stress that is responsible for lifting the grains off the bed. In the exterior flow the eddy viscosity is scaled by u_{*T} . Sediment is suspended at values of skin friction shear stress that are high relative to the settling velocity of a particular grain size. The grains in the finer end of the grain size distribution are the first to be put into suspension while coarser material continues to roll or saltate along the bed as bedload.

In Figure 4.1 the structure of the model profile is demonstrated. On a log-log scale the slope of a concentration profile is controlled by the Rouse number, $p_m = w_m/u_*\kappa$. To calculate the concentration profile over a bed of mixed grain sizes, the grain size distribution of the bottom material is divided into M size classes, each represented by its mean grain size. For a given flow condition, each size class will be represented by a characteristic reference concentration $C(z_a)$ and Rouse number p_m . The Rouse number is directly proportional to settling velocity, and the greater the grain diameter, the greater the settling velocity. The greater the Rouse number the more rapidly the concentration will decrease with distance above the bed. For each size class, a concentration profile is determined, and the bulk structure of the concentration profile is found by summing these profiles. The bulk profile will tend to be dominated by the finer size classes in suspension, particularly in the upper portion of the water column.

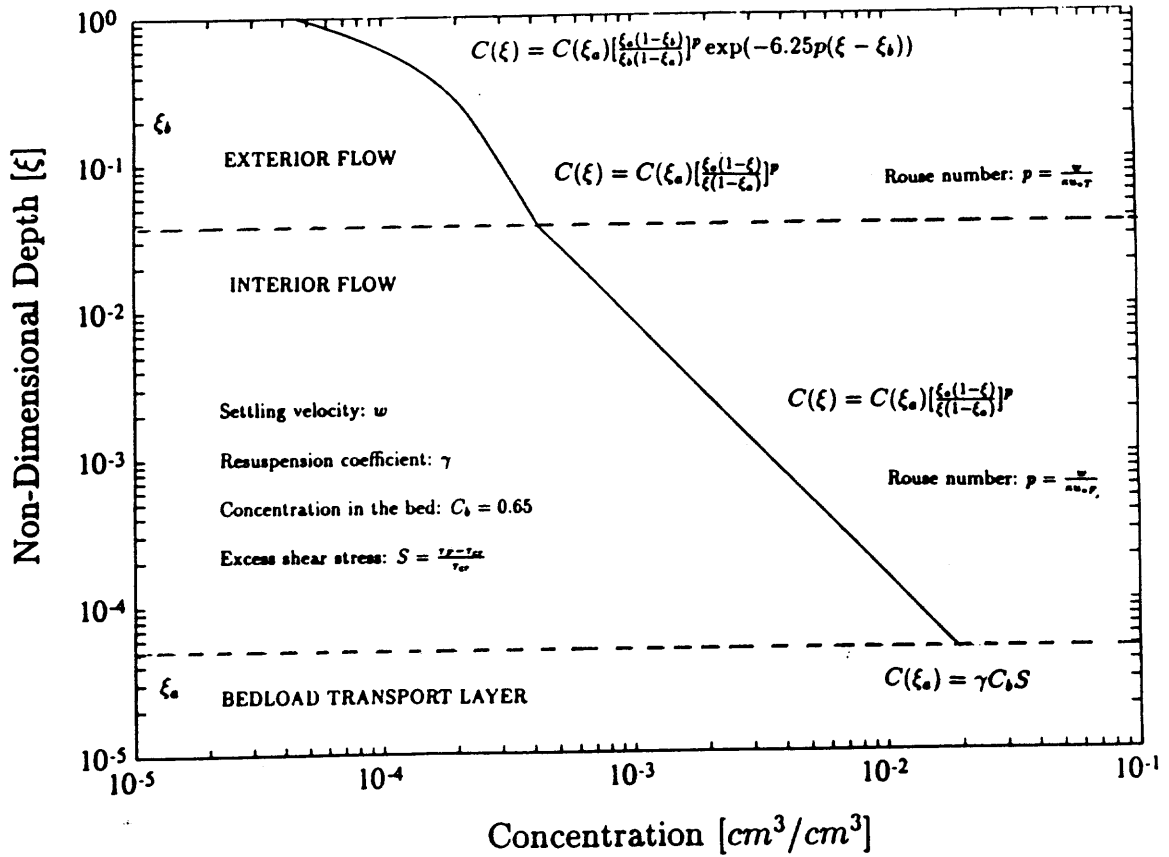


Figure 4.1: Schematic concentration profile. This Figure demonstrates the two part structure of the exterior flow in conjunction with the reduced concentration gradient of the interior flow.

4.2 Matching Concentration Profiles to Measurements

The measured concentration profiles were analyzed in a manner analogous to the method by which the velocity measurements were analyzed. However, rather than iterating to determine u_{*T} and z_{0T} , empirical values of the Rouse number, p_m , and bottom reference concentration, $C(z_a)$, were found, using values of u_{*T} and z_{0T} obtained from velocity profiles. In this calculation, the reference level, z_a , was specified as the value obtained from equation 3.12. The concentration at the level z_a was first calculated as the reference concentration that would exist if the bed was planar. When the best fit Rouse number had been found for the exterior flow, the Rouse number of the interior flow was found by scaling the empirically determined Rouse number by the ratio of u_{*T}/u_{*F} , obtained from the velocity profile analysis. The reference concentration at the level z_a , when considering the effect of bedforms was then found by matching the interior and exterior flow at height, H , above the bottom, and extrapolating to the concentration at the bed, $C(z_a)$. This calculation assumes that the concentration profile can be described by a single Rouse number, which is the same as assuming that one grain size exists that is characteristic of the suspended load throughout the depth of flow.

The structure of concentration profiles is expected to vary from station to station across the river in accordance with variations in the velocity field. In the center of the river where velocities are higher, the shear stress is also higher, and the concentration of suspended sediment is expected to be higher.

To visualize the structure of the measured concentration profiles, the mean concentration profile at each station, was initially found by calculating the average concentration of sediment at each of the seven levels in the flow. The mean profiles are indicated as the dash-dotted line on Figures 4.2 to 4.11, which is the same curve indicated as a solid line on Figures 2.22 to 2.31.

A best fit profile was determined for the measurements made at each station by specifying a bottom reference concentration and varying the Rouse number until the profile that produced the smallest possible variance had been found. This process was repeated for a number of values of $C(z_a)$ until the best fit profile had been obtained. The results of this analysis are listed in Table 4.1 and the best fit profiles are indicated as the dotted lines on Figures 4.2 to 4.11.

From Figures 4.2 to 4.11, it is seen that the matched concentration profiles all are

High Discharge			
Station	C_a	p_m	σ_a^2
	cm^3/cm^3		
75	0.0008	0.14	0.036
95	0.0027	0.21	0.044
110	0.0112	0.28	0.084
130	0.0132	0.29	0.16
145	0.0165	0.31	0.042
160	0.0338	0.35	0.065
175	0.0263	0.33	0.039
190	0.0244	0.35	0.049
210	0.0075	0.27	0.068
225	0.0036	0.21	0.042
Lumped Data Set	0.019	0.32	0.085

Table 4.1: Characteristics of the imposed concentration profiles that produce the smallest variance, σ_a^2 . Mean depth during high flow is 740 cm.

in close agreement with the measurement averaged concentration profiles, indicating that the structure of the measured concentration profiles are in good agreement with the expected structure of the selected model profile.

The profiles that produced similar values of Rouse number and bottom reference concentration were lumped into one single data set that characterized the measured concentration profile in the central portion of the river. The best fit profile to this lumped data set was found in the iterative manner described above. The lumped measurements were made at six stations, 110, 130, 145, 160, 175, and 190, the same stations which correspond to the lumped velocity profile data. The best fit profile to the lumped data set is indicated as the solid line on Figures 4.2 to 4.11. An F-test was performed to determine whether the best fit profile to the lumped data set matches the best fit to the individual profiles in a statistical sense. Using an F-test, the null-hypothesis, $\sigma_a^2 = \sigma_b^2$ is rejected if the comparison is false within a 98 % confidence interval. The lower limit for rejection is $\frac{\sigma_a^2}{\sigma_b^2} = 0.54$ (Devore 1987 [4]). The result of the test is listed in Table 4.2.

High Discharge				
Station	σ_a^2	σ_b^2	$\frac{\sigma_a^2}{\sigma_b^2}$	null-hypothesis
75	0.036	0.746	0.05	False
95	0.044	0.293	0.15	False
110	0.084	0.093	0.91	True
130	0.160	0.167	0.98	True
145	0.042	0.044	0.96	True
160	0.065	0.087	0.74	True
175	0.039	0.044	0.88	True
190	0.049	0.082	0.59	True
210	0.068	0.137	0.50	False
225	0.042	0.146	0.29	False

Table 4.2: Comparison of standard deviations around best fits to measurements made at individual stations, represented by σ_a to standard deviations of the same measurements around the best fit to the lumped data set, σ_b .

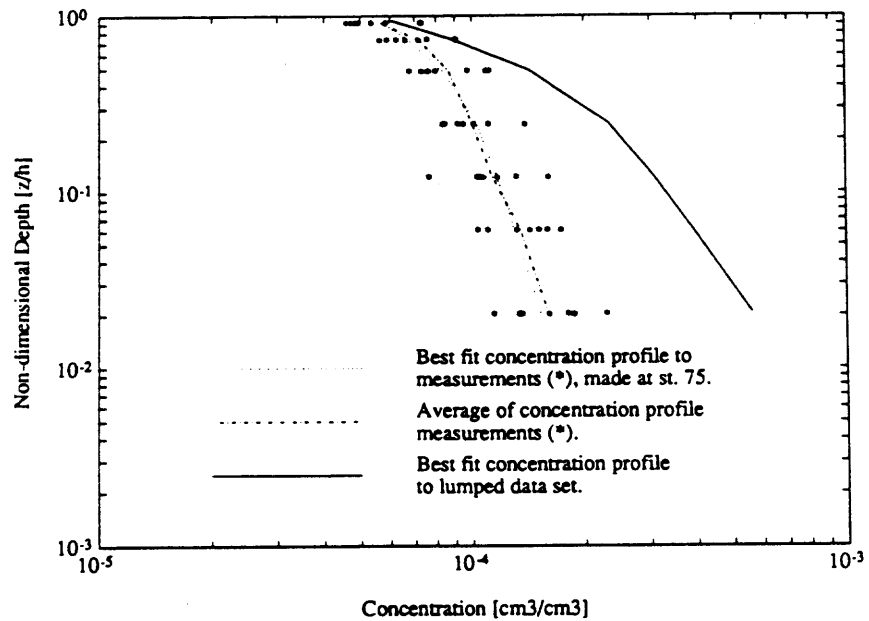


Figure 4.2: Fits to concentration measurements made at station 75. The three fits are the measurement averaged profile, the best fit in a least squares sense, and the best fit to the lumped data set.

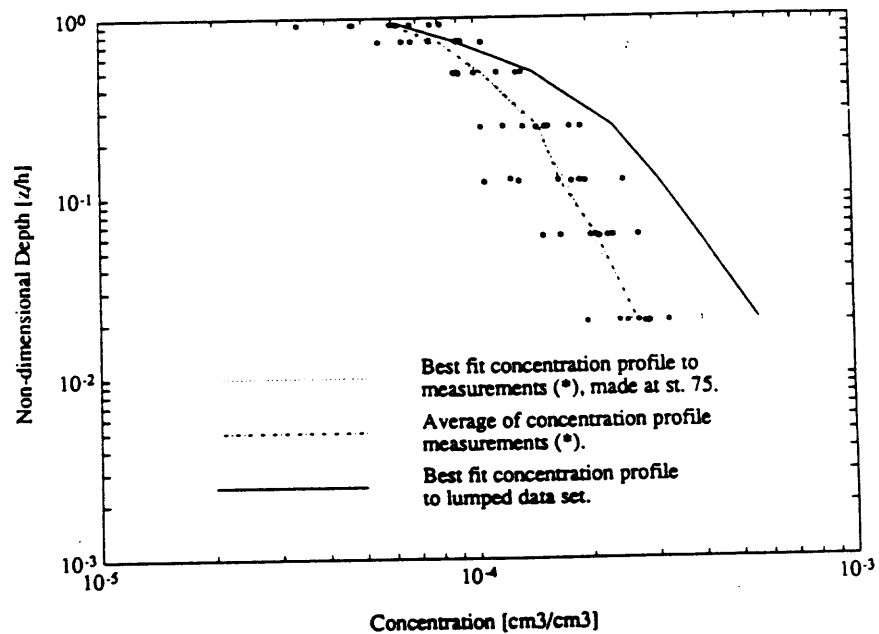


Figure 4.3: Fits to concentration measurements made at station 95. The three fits are the measurement averaged profile, the best fit in a least squares sense, and the best fit to the lumped data set.

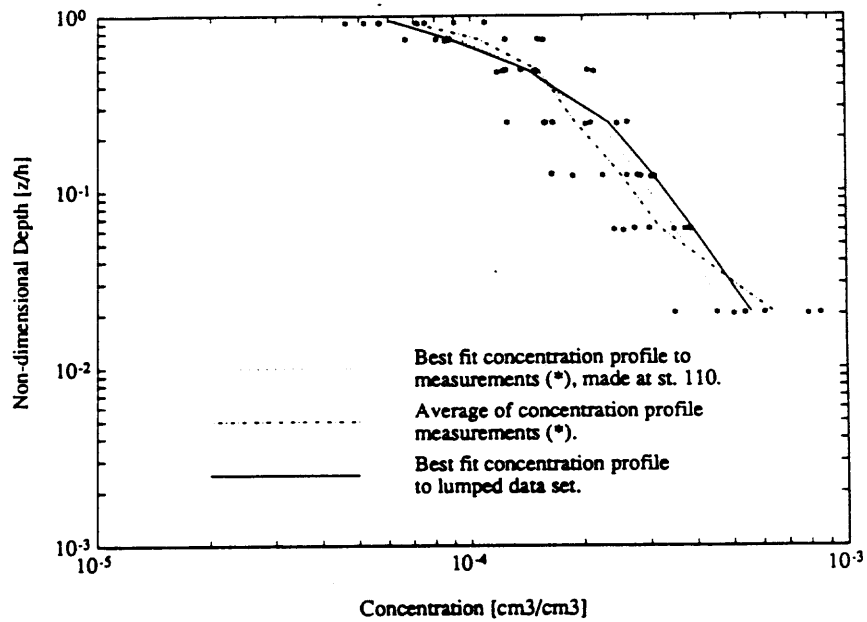


Figure 4.4: Fits to concentration measurements made at station 110. The three fits are the measurement averaged profile, the best fit in a least squares sense, and the best fit to the lumped data set.

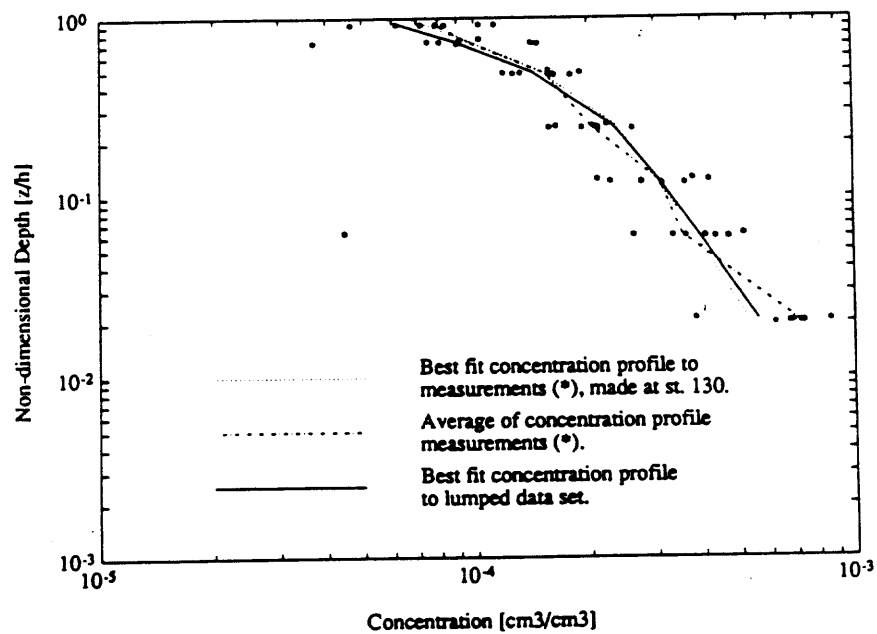


Figure 4.5: Fits to concentration measurements made at station 130. The three fits are the measurement averaged profile, the best fit in a least squares sense, and the best fit to the lumped data set.

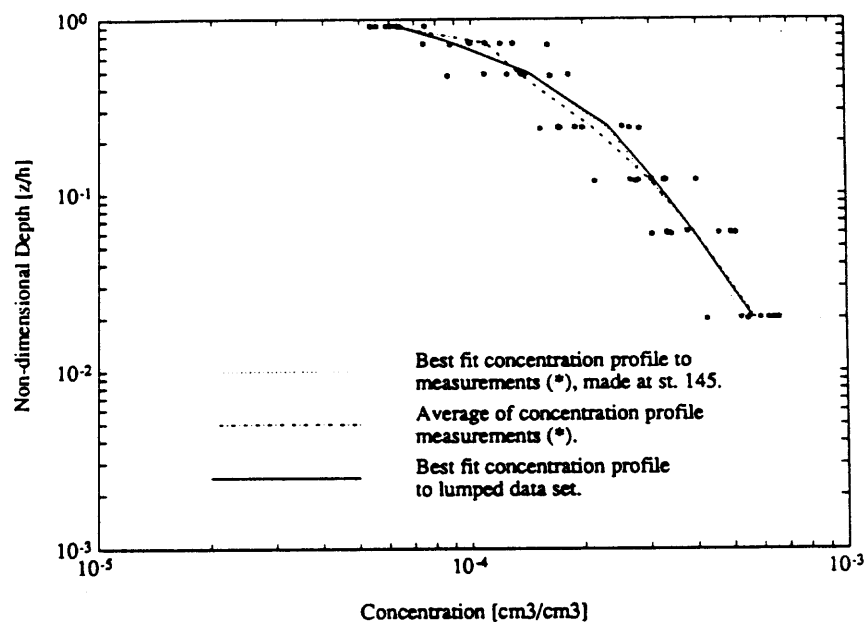


Figure 4.6: Fits to concentration measurements made at station 145. The three fits are the measurement averaged profile, the best fit in a least squares sense, and the best fit to the lumped data set.

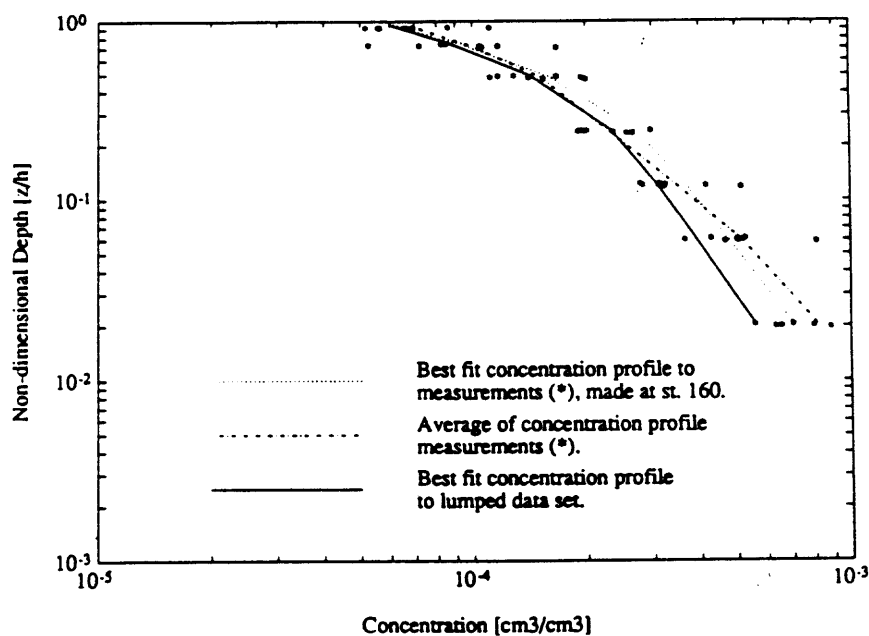


Figure 4.7: Fits to concentration measurements made at station 160. The three fits are the measurement averaged profile, the best fit in a least squares sense, and the best fit to the lumped data set.

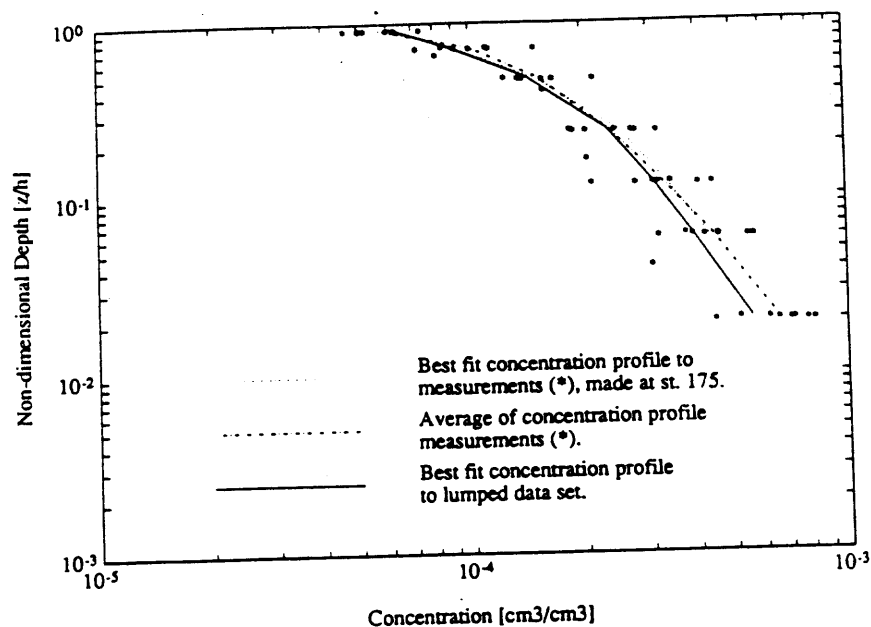


Figure 4.8: Fits to concentration measurements made at station 175. The three fits are the measurement averaged profile, the best fit in a least squares sense, and the best fit to the lumped data set.

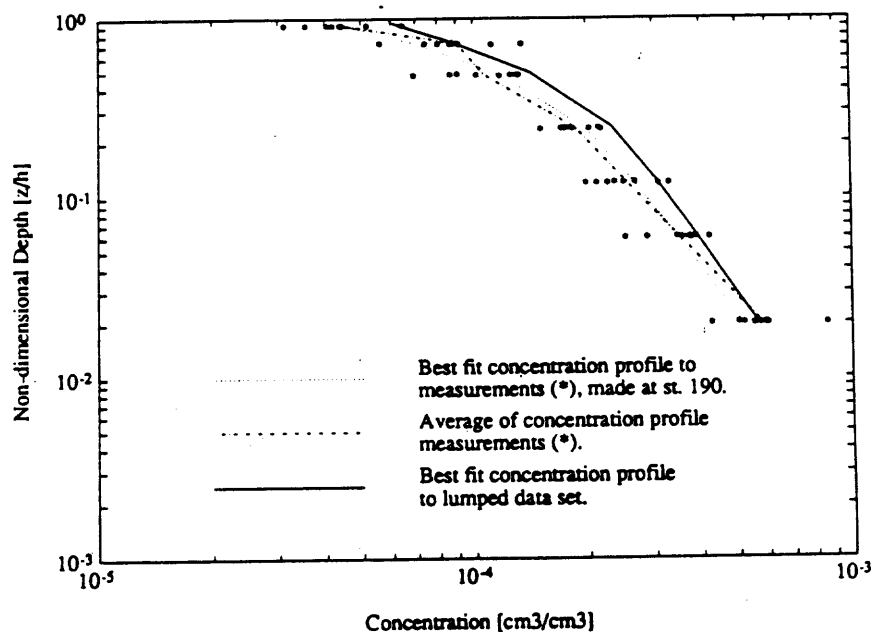


Figure 4.9: Fits to concentration measurements made at station 190. The three fits are the measurement averaged profile, the best fit in a least squares sense, and the best fit to the lumped data set.

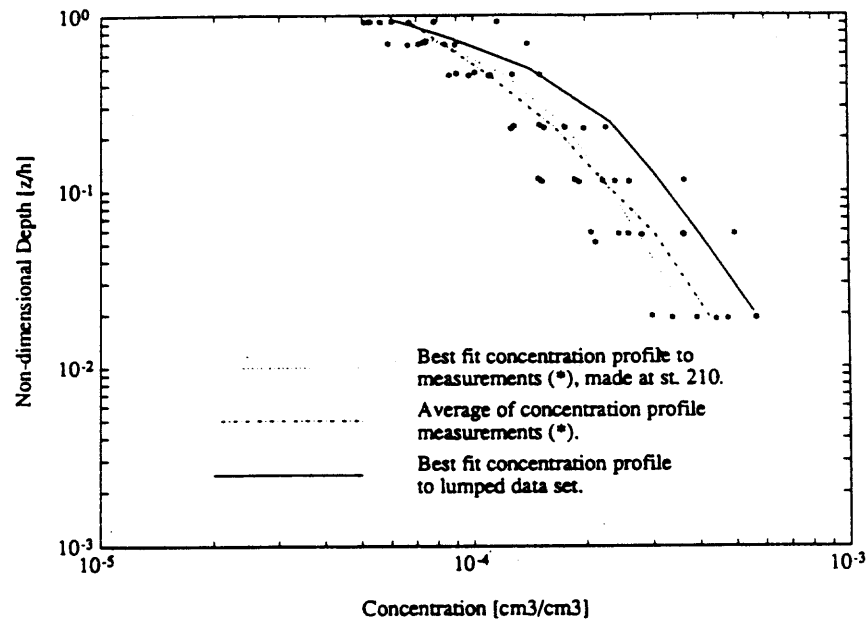


Figure 4.10: Fits to concentration measurements made at station 210. The three fits are the measurement averaged profile, the best fit in a least squares sense, and the best fit to the lumped data set.

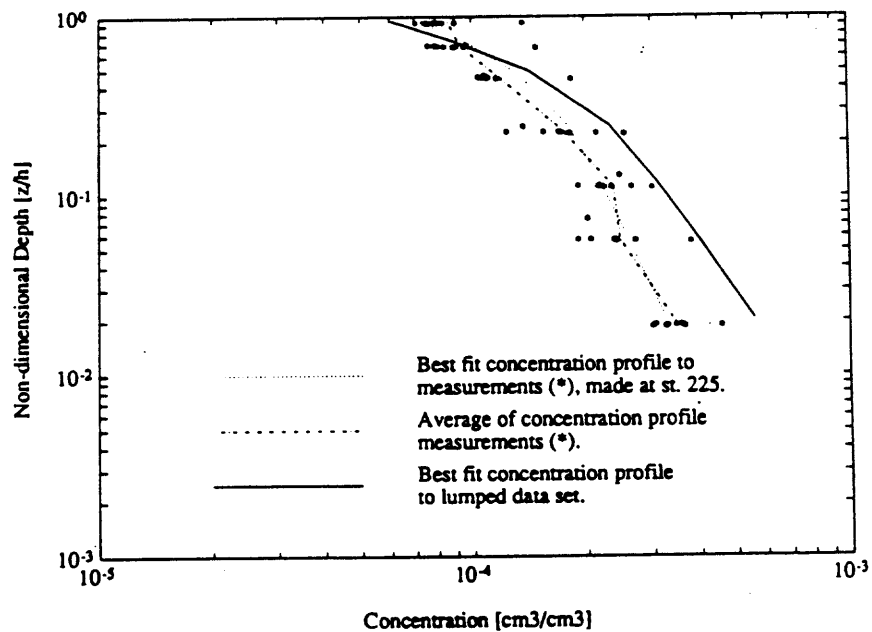


Figure 4.11: Fits to concentration measurements made at station 225. The three fits are the measurement averaged profile, the best fit in a least squares sense, and the best fit to the lumped data set.

4.3 Application of Concentration profile Analysis.

Inferences are made of characteristic settling velocity, w , and the coefficient γ , from the Rouse number and bottom reference concentration of the bulk concentration profile, and the total shear velocity of the lumped velocity profile. The settling velocity is calculated from the measurement derived Rouse number and shear velocity, and the corresponding grain size is determined according to *Dietrich*, 1982 [5].

The coefficient, γ , is calculated from equation 4.3. The excess shear stress, S necessary to determine this parameter is calculated using the skin friction shear stress in the near boundary region and the critical shear stress of the characteristic sediment size. The unit $\phi = \log(D)/\log(2)$, where D is a characteristic grain diameter in millimeters, is used to characterize grains on a logarithmic scale rather than on a linear scale.

Settling Velocity				
u_{*T}	p_m	w	D	D
cm/sec		cm/sec	cm	ϕ
9.1	0.32	1.16	0.0150	-2.74

Table 4.3: The characteristic settling velocity and grain size of the best fit to the lumped concentration profile. The corresponding grain size is found assuming a Powers Roundness value, $P = 0.7$, and a Correy Shape Factor, $CSF = 3.5$.

The Coefficient γ					
$C(z_a)$	C_b	τ_F	τ_{cr}	S	γ
cm ³ /cm ³	cm ³ /cm ³	dy/cm ²	dy/cm ²		
0.019	0.65	26.6	1.8	13.8	0.0021

Table 4.4: The coefficient, γ , characteristic of the best fit to the lumped concentration profile.

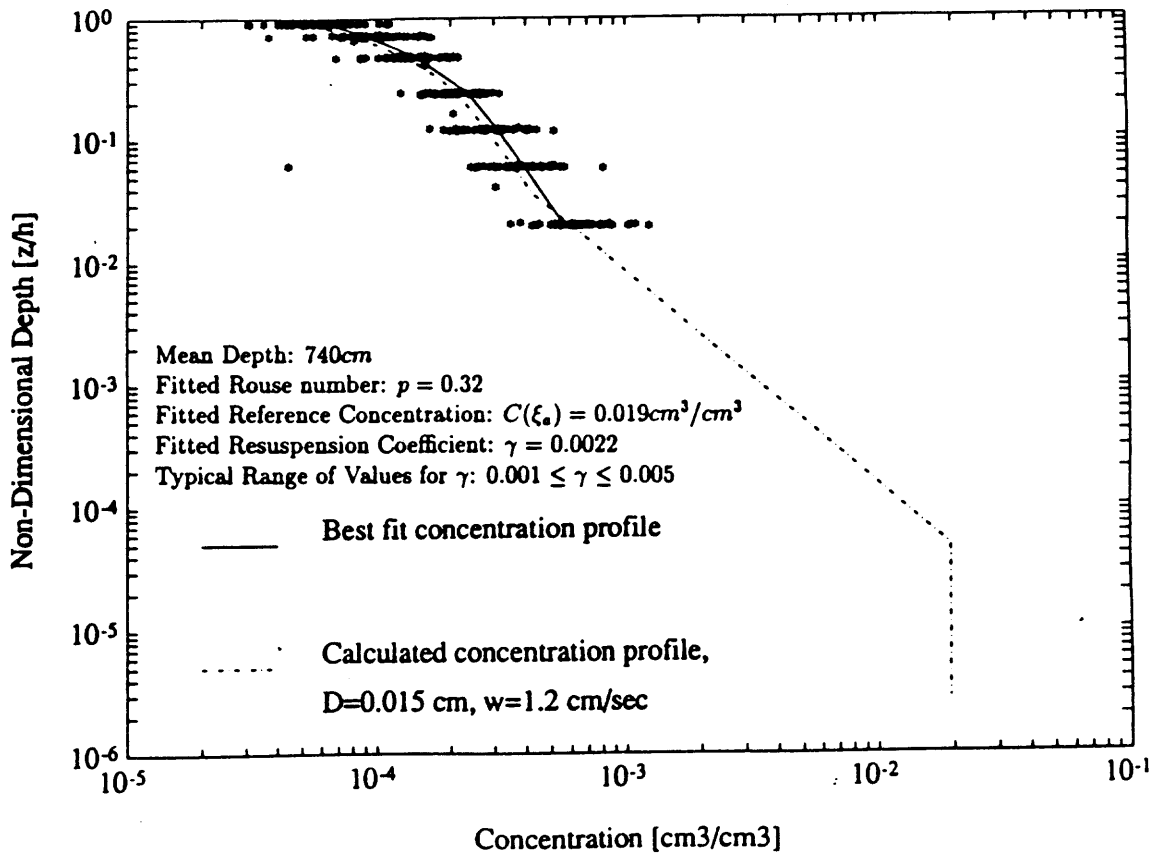


Figure 4.12: Comparison between best fit and calculated concentration profile at high discharge. The solid line describes the best fit profile to the combined measurements made at station 110, 130, 145, 160, 175 and 190, in the central segment of the river. The dash-dotted line is the concentration profile calculated, assuming the bedform dimensions of $h = 27 \text{ cm}$ and $\lambda = 587 \text{ cm}$ and taking the form drag in the near boundary region into account.

The coefficient, γ , is an empirical coefficient of the order of magnitude 10^{-3} , and it has been calculated in a manner similar to that demonstrated in Table 4.4 for other data sets. The value of γ calculated for the National Canyon measurements is found in agreement with values found in other studies. *Smith and McLean, 1977* [20] found $\gamma = 0.0022$ in the Columbia River and *Wiberg (Pers. Comm.)* re-calculated their value to be $\gamma = 0.004$.

The grain size $D=0.0150$ cm (-2.74ϕ), characteristic of the best fit model profile, corresponds well to the size analysis performed of the suspended sediment samples. The size analysis indicated that the mean grain sizes ranged from 0.0165 cm (-2.6ϕ) near the bottom to 0.0088 cm (-3.5ϕ) in the vicinity of the surface which is demonstrated by the distribution functions shown in Figures 2.19 to 2.21.

Settling Velocities				
D_m	D_m	w_m	Difference from D_{mean}	Difference from w_m of D_m
ϕ	cm	cm/sec	%	%
-2.6	0.0165	1.34	10	16
-2.7	0.0154	1.21	2	4
-2.8	0.0144	1.08	4	7
-2.9	0.0134	0.97	11	16

Table 4.5: Settling velocities for grain sizes in vicinity of the empirically determined mean grain size. The settling velocities are calculated assuming the shape factor $CSF = 0.7$, and a Powers Roundness value $P = 3.5$.

It could be argued that $D=0.0150$ cm (-2.74ϕ) is a high value of mean grain size. The value is certainly more representative of the bottom material than the material suspended near the surface (Figures 2.19 through 2.21). However, since the grain size is inferred from settling velocity, and two different techniques were used to determine the relationship between settling velocity and grain size in the sample analysis and in the calculation, the different methods may yield slightly different grain sizes for the same settling velocity, and direct comparison of measured and calculated grain size may not be possible. In Table 4.5 it is seen that settling velocity calculated according to *Dietrich, 1982* [5] changes significantly with change in grain size. Since settling velocity is very sensitive to grain size, there is a potential for the same settling velocity

producing a different grain size, if the two methods used to relate settling velocity to grain size are not consistent.

The structure of the calculated best fit concentration profile corresponds well to the structure of the measured concentration profile although the calculation is based on the assumption of only one grain size in suspension. However, the grain size analysis of the suspended sediment samples indicated that the sediment is comprised of a range of grain sizes, rather than by a single grain size, and that mean size and standard deviation decreases towards the surface, see Figures 2.19, 2.20 and 2.21.

There are two possible sources of error associated with the method of analysis used to determine the grain size distribution, one is associated with the small sample size and the other is associated with grains of the same size settling at different velocities in the VA-tube, and both of these errors tend to distort the grain size distribution towards a broader distribution than present in the sample. If the effect of the errors in the grain size analysis is strong, the observed profile structure may be explained by assuming that the bottom material consists of well sorted sediment with a standard deviation less than 0.5ϕ and a mean size of -2.74ϕ , which is the grain size estimated from the best fit profile.

If the effect of errors in the grain size analysis on the other hand is weak, it is reasonable to consider bed material of a range of sediment sizes and evaluate the calculated profile shape and slope relative to the measured profile. The discrepancy between measured and expected profile structure may also be related to the sampling technique, and it may not be possible to resolve the precise structure of the suspended sediment concentration profile using a milk bottle suspended sediment sampler.

Though there is a large scatter in the data used to determine the sediment distribution functions, the scatter is less towards the bottom. At the lowest level of sediment measurements, which was 15 cm above the bed, a sediment distribution function was estimated with a mean of -2.6ϕ and a standard deviation of 0.9ϕ , indicating moderately sorted sediment at this level.

It was chosen to represent sediment in the bed by three different log-normal distributions. Each distribution had a different mean, but the standard deviation was held constant for the three cases. The total sediment concentration profile was calculated for each distribution, and the profile is seen as the solid line on Figures 4.13, 4.15 and 4.17.

The structure of the sediment profile calculated using a distribution of grain sizes, was different from the profile structure obtained when considering a single grain size. The concentration of suspended sediment is higher near the surface, than the concentration calculated using a single grain size, see Figures 4.13, 4.15 and 4.17. The coarser grains have a higher settling velocity, and are therefore not carried as high into the water column as the fine material. The profile slope becomes steeper with decrease in sediment size, which leads to a higher calculated concentration of suspended sediment near the surface. The calculated increase in concentration towards the surface is not observed in the measured concentration profiles.

For each of the three selected sediment distribution functions, the volume of sediment in suspension was calculated along with mean erosion depth. The mean erosion depth is the the total volume of sediment in suspension, V , relative to the maximum bed concentration, C_b . The thickness of the turnover layer required to obtain the determined volume of the finest size fraction is also calculated ($= V/(C_b i_m)$). These values are listed in Table 4.6.

Characteristics of four sediment distributions					
D_{50}	σ	V	C_b	Required thickness of reworked layer	Mean erosion depth
ϕ	ϕ	cm^3/cm^2	cm^3/cm^3	cm	cm
-2.74	0	0.147	0.65	0.2	0.2
-2.5	0.6	0.264	0.65	3.2	0.4
-2.7	0.6	0.508	0.65	5.2	0.8
-2.9	0.6	0.912	0.65	7.8	1.4

Table 4.6: Calculation of the mean bed thickness that corresponds to the amount of material in suspension, assuming that the maximum concentration of material in the bed is $0.65 cm^3/cm^3$. The required erosion depth corresponds to the thickness of the reworked sediment layer necessary to obtain the calculated volume of the finest size fraction of sediment in suspension.

The volume of sediment in suspension can be related to a corresponding bed thickness by considering the volume of sediment in suspension per unit area, V , calculated as the area of concentration profile, relative to the concentration of sediment in the bed. In the simplified case of only one grain size in suspension, the bed thickness is

obtained by integrating the calculated concentration profile to obtain the volume of sediment in suspension, V , and relating V to the concentration of sediment in the bed. The result of the calculation is seen in Table 4.6. In the case where a distribution of sediment is considered, the distribution is divided into an appropriate number of size classes, and the volume of suspended sediment for each size class is calculated. The mean erosion depth in Table 4.6 is calculated as the total volume of suspended sediment relative to the maximum concentration of sediment in the bed. In this calculation, seven size classes were used. In Figures 4.14(a), 4.16(a) and 4.18(a), the volume of each size class, relative to the total volume of sediment in suspension is demonstrated, and the corresponding distribution function of bottom sediment is also shown.

The finest size class in the bed material is represented by the smallest fraction in the grain size distribution, but the largest volume of suspended sediment. In addition, the calculated transport capacity of the finer size classes is much greater than the transport capacity of the coarser fractions, although the sediment is symmetrically distributed around the mean. To obtain the calculated volume of the finest size class, the layer of reworked sediment must be of a thickness that is large enough to supply sufficient sediment. Sediment moving as bedload can be thought of as a conveyor belt that is constantly bringing new material to the surface. The thickness of the bed layer being reworked must be sufficient to allow for the volume of suspended sediment, that corresponds to the transport capacity of the finest sediment in order for the measured profile to correspond to the unlimited transport capacity of the bed.

In Figures 4.13, 4.15 and 4.17, and in Table 4.6, it is seen that, regardless of which of the three sediment distributions is considered, the concentration of sediment is greatly over predicted as are the calculated volumes of sediment in suspension. Furthermore, the thickness required of the reworked sediment layer is five to eight times greater than the calculated mean thickness of the eroded bed material.

The volume of suspended sediment may be limited by availability of material in the bedload. To obtain the calculated concentration profiles, the reworked sediment layer must be at least the calculated required thickness, so that the amount of sediment of the finest size class brought to the surface of the bedload corresponds to the transport capacity of that size. If the thickness of the reworked sediment layer is less, the calculated profile will be starved of the the finest size fractions, and better

estimates of the sediment concentration profile may be obtained by considering a limited thickness of the reworked layer of sediment.

Effect of limiting thickness of the reworked layer					
D_{50}	σ	V	C_b	Thickness of reworked layer	Mean erosion depth
ϕ	ϕ	cm^3/cm^2	cm^3/cm^3	cm	cm
-2.74	0	0.147	0.65	0.2	0.2
-2.5	0.6	0.167	0.65	1.0	0.3
-2.7	0.6	0.152	0.65	0.5	0.2
-2.9	0.6	0.112	0.65	0.25	0.2

Table 4.7: Effect of limiting the thickness of reworked sediment. The volume of sediment in suspension is calculated for three different size distributions and by limiting the erosion depth. The thickness that corresponds to the volume of sediment in suspension is also calculated (mean erosion depth).

The sediment profiles corresponding to the profiles starved of the finest size fractions are shown as the dotted line in Figures 4.13, 4.15 and 4.17. In addition, the volume of sediment of each size class, relative to the total volume of sediment is plotted in Figures 4.14 (b), 4.16 (b) and 4.18 (b). Figures 4.14 (b), 4.16 (b) and 4.18 (b) indicate that the relative volumes of sediment of each size class correspond better to the distribution of bed sediment. To obtain a volume of sediment in suspension that approximately matches the volume of sediment found when considering a single grain size in suspension, it is necessary to consider different thicknesses of the reworked sediment layer for the different sediment distributions. The result of the calculations are listed in Table 4.7. It is seen that the smaller the mean grain size, the more it is necessary to limit the erosion depth. The smaller the mean grain size is, the greater the transport capacity of that size is, and the more it is necessary to limit the thickness of the reworked sediment layer.

The calculated concentration profiles are compared to the best fit profile, obtained assuming a single grain size in suspension, by two measures, the variance of the measured concentration around the calculated profile and the calculated versus the measured volume of sediment in suspension.

It is seen that the sediment distribution with mean grain size of -2.7ϕ , which

D_{50}	σ	V_{single}	V_{dist}	Difference	σ_{single}^2	σ_{dist}^2	Difference
ϕ	ϕ	cm^3/cm^2	cm^3/cm^2	%	cm^3/cm^3	cm^3/cm^3	%
-2.5	0.6	0.147	0.167	14	0.085	0.16	88
-2.7	0.6	0.147	0.152	3	0.085	0.14	65
-2.9	0.6	0.147	0.112	24	0.085	0.17	100

Table 4.8: Comparison of volume of suspended sediment calculated assuming a single grain size of diameter -2.74ϕ (0.015 cm) versus a distribution of sediment in suspension. The goodness of fit to the measured profile is also calculated. σ_{dist}^2 denotes the variance of the measurements around the profile structure calculated using a distribution of sediment.

is in vicinity of the grain size calculated from the best fit profile provides the best fit both in terms of calculated transported volume and structure of the calculated concentration profile.

As a final calculation, it is relevant to calculate the suspended sediment transport parameters in terms of the total unit suspended sediment discharge q_s . Also, since the conditions in the near boundary region are extrapolated from a model, and not from measurements, the portion of sediment unit discharge in the near boundary region is calculated relative to the total unit discharge.

Suspended sediment transport parameters				
D_{50}	σ	q_s	$q_{s(wake)}$	fraction of total
ϕ	ϕ	cm^2/sec	cm^2/sec	%
-2.74	0	22.8	2.7	12
-2.5	0.6	27.3	2.1	8
-2.7	0.6	24.8	2.0	8
-2.9	0.6	18.2	1.4	8

Table 4.9: Suspended sediment transport parameters at a river discharge of $600\text{ m}^3/sec$.

The calculations indicated in Table 4.9, demonstrate that approximately 10 % of the sediment discharge is transported in the wake region, which indicates that it is important to include the sediment transport in the interior flow region.

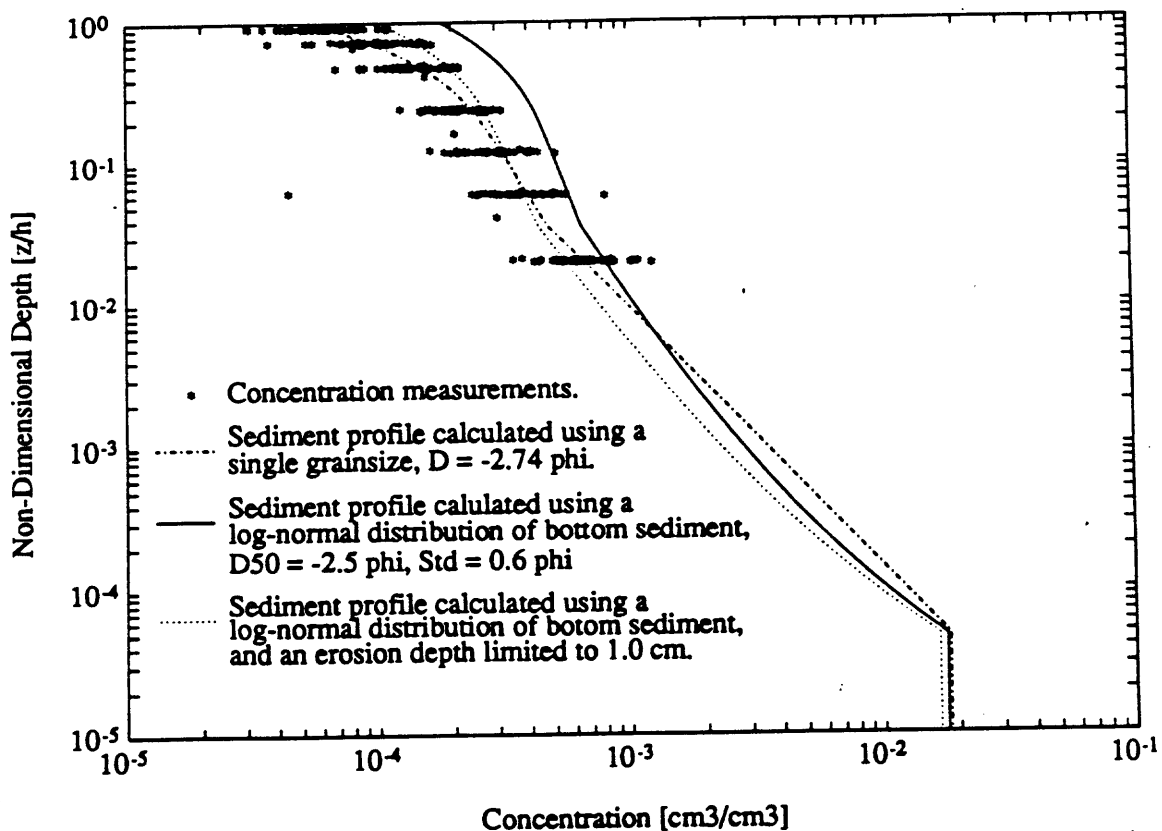


Figure 4.13: Concentration profile calculated using a log-normal sediment distribution with $D_{50} = -2.5\phi$, $\sigma = 0.6\phi$. The Figure indicates the best fit profile calculated assuming a single grain size, the sediment profile calculated assuming all grain sizes are available in proportion to the transport capacity of the flow and the profile calculated assuming that the availability of the finest size fractions are limited.

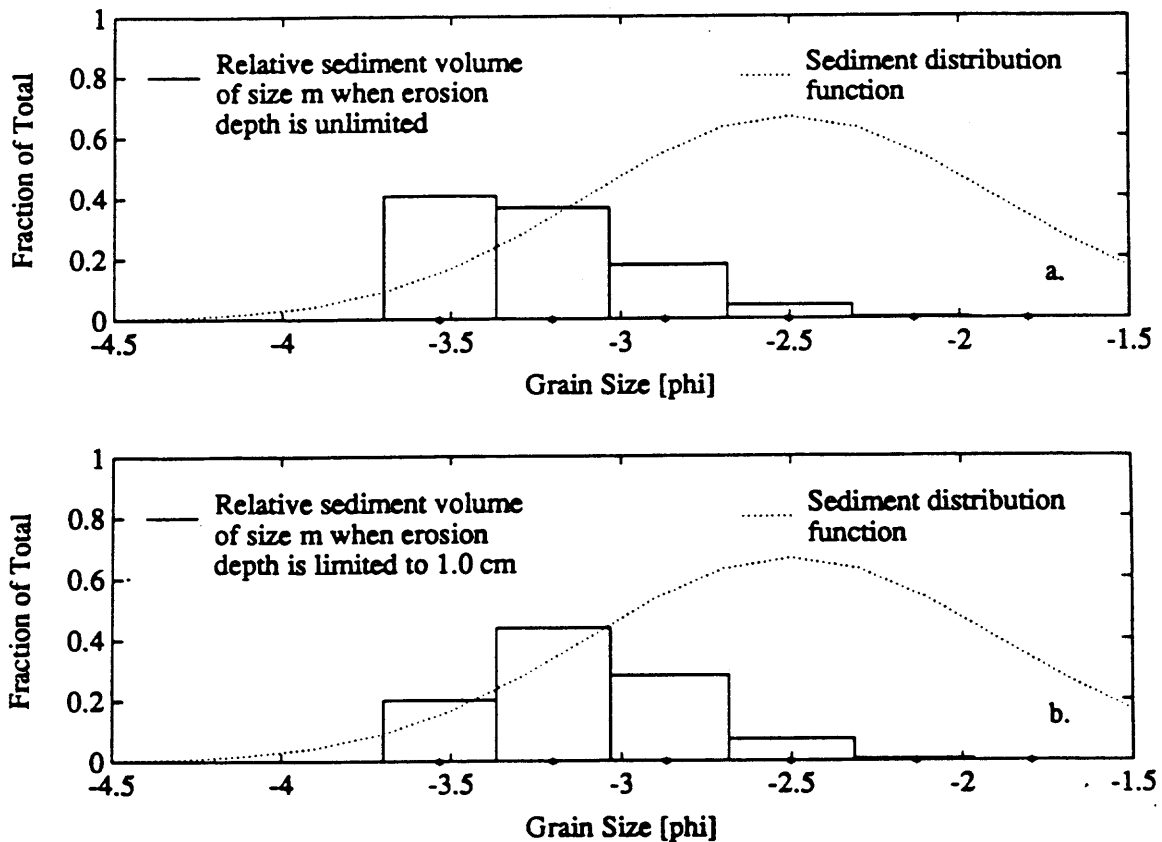


Figure 4.14: (a.) Relative volume of suspended sediment distributed over seven size classes, when unlimited availability of sediment is assumed. The calculated total volume of sediment in suspension is $0.264 \text{ cm}^3/\text{cm}^2$. The volumetric distribution of sediment is compared to a log-normal sediment distribution with $D_{50} = -2.5\phi$, $\sigma = 0.6\phi$.

(b.) Relative volume of suspended sediment distributed over seven size classes, when limited availability of sediment is assumed. The calculated total volume of sediment in suspension is $0.167 \text{ cm}^3/\text{cm}^2$. The volumetric distribution of sediment is compared to a log-normal sediment distribution with $D_{50} = -2.5\phi$, $\sigma = 0.6\phi$.

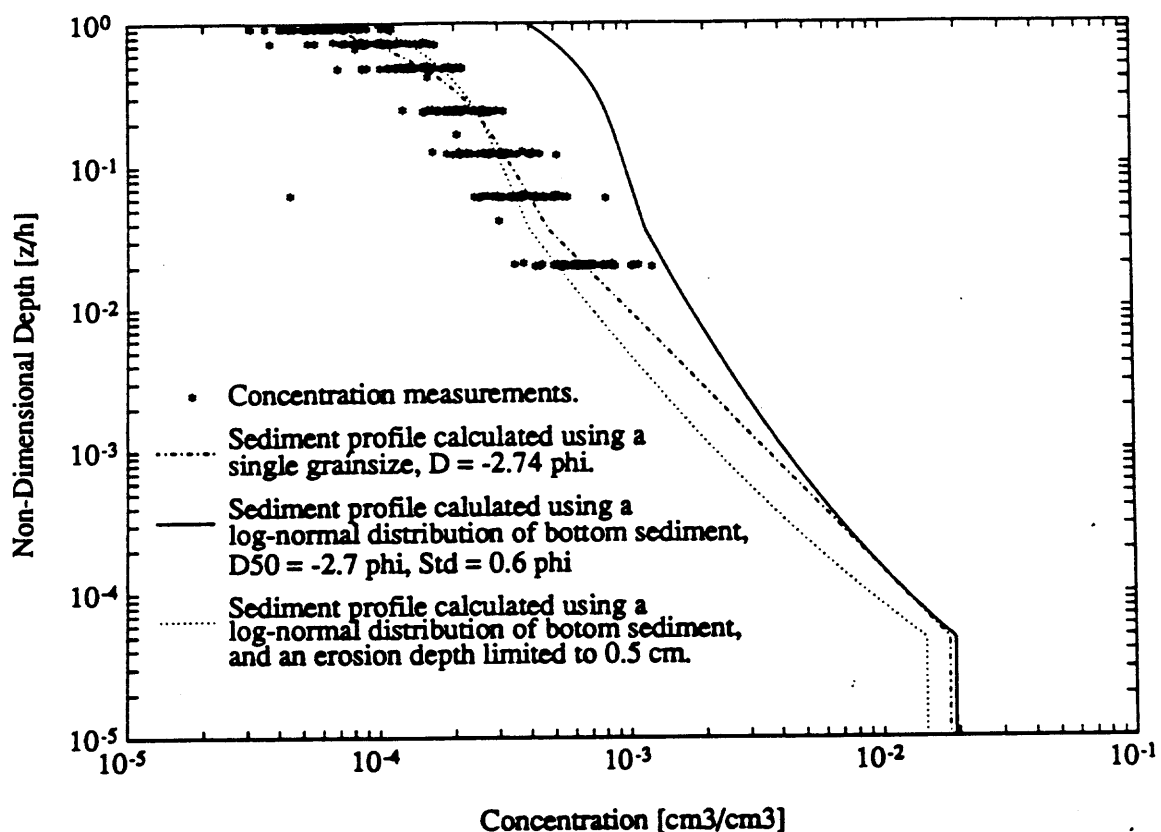


Figure 4.15: Concentration profile calculated using a log-normal sediment distribution with $D_{50} = -2.7\phi$, $\sigma = 0.6\phi$. The Figure indicates the best fit profile calculated assuming a single grain size, the sediment profile calculated assuming all grain sizes are available in proportion to the transport capacity of the flow and the profile calculated assuming that the availability of the finest size fractions are limited.

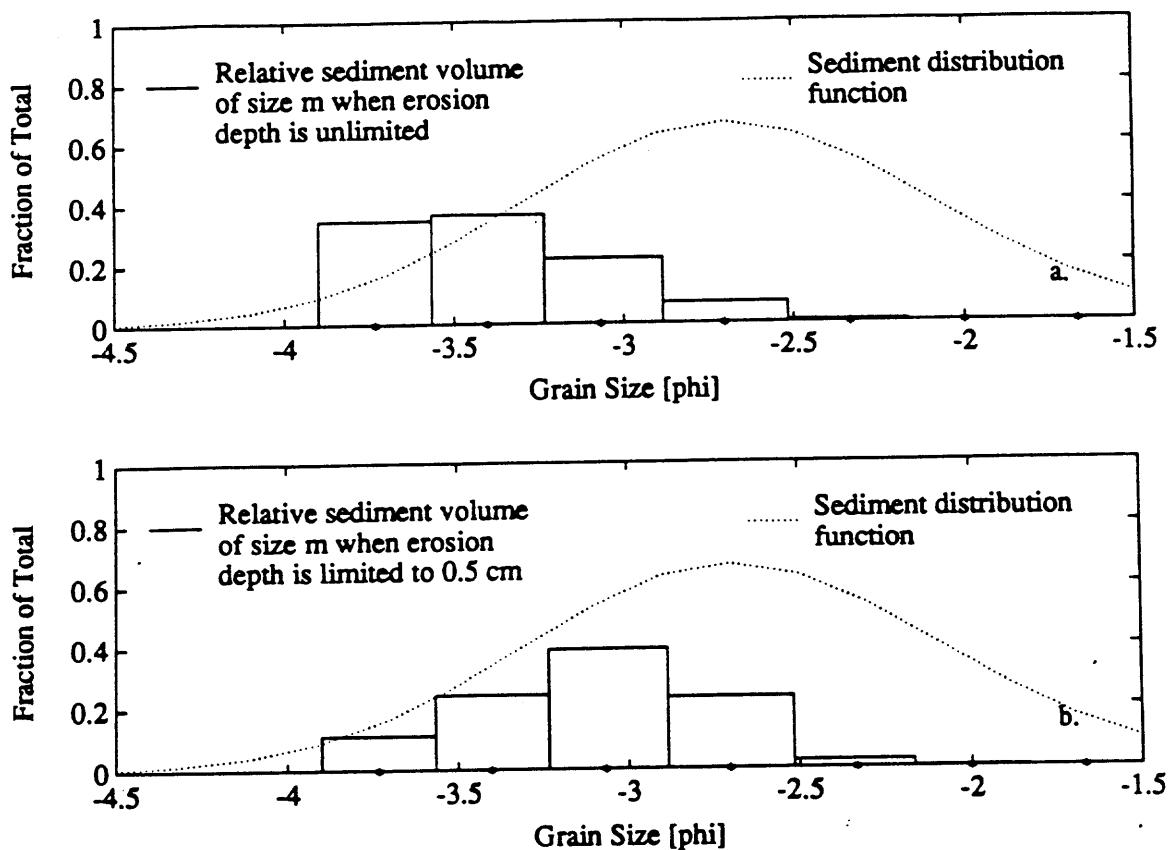


Figure 4.16: (a.) Relative volume of suspended sediment distributed over seven size classes, when unlimited availability of sediment is assumed. The calculated total volume of sediment in suspension is $0.508 \text{ cm}^3/\text{cm}^2$. The volumetric distribution of sediment is compared to a log-normal sediment distribution with $D_{50} = -2.7\phi$, $\sigma = 0.6\phi$.

(b.) Relative volume of suspended sediment distributed over seven size classes, when limited availability of sediment is assumed. The calculated total volume of sediment in suspension is $0.152 \text{ cm}^3/\text{cm}^2$. The volumetric distribution of sediment is compared to a log-normal sediment distribution with $D_{50} = -2.7\phi$, $\sigma = 0.6\phi$.

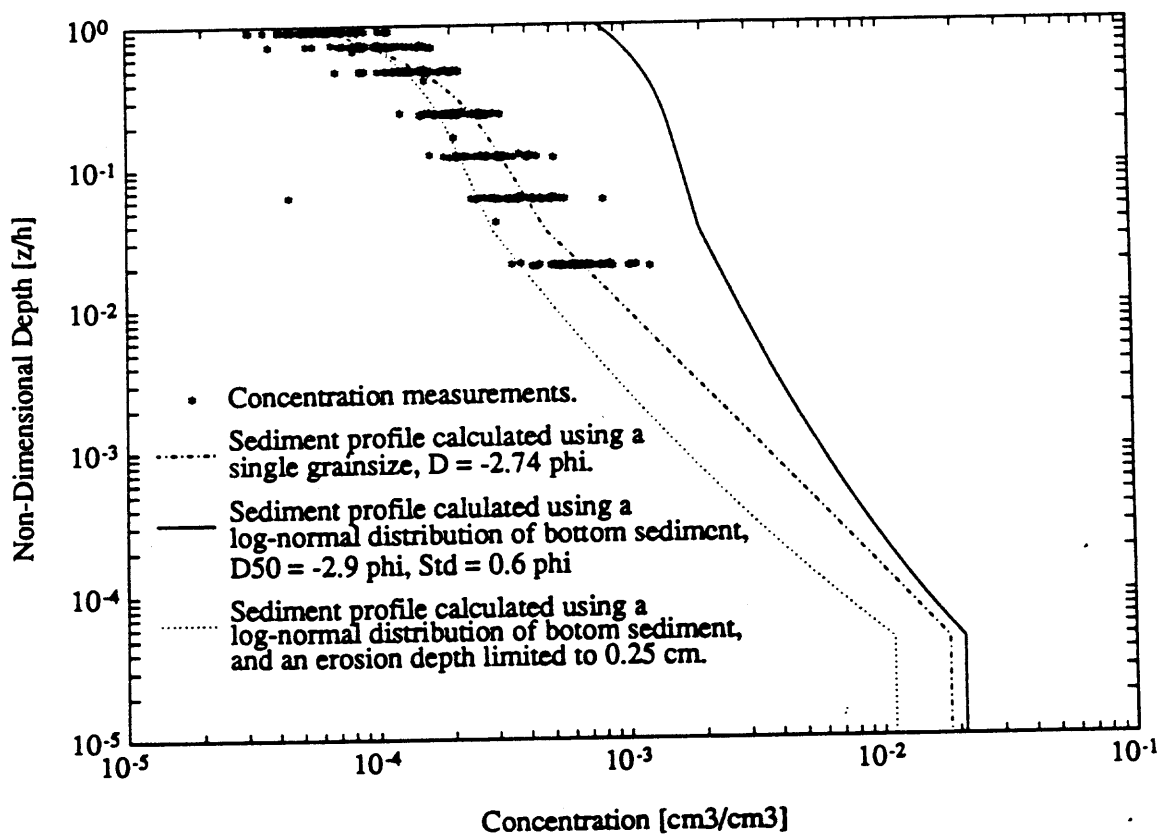


Figure 4.17: Concentration profile calculated using a log-normal sediment distribution with $D_{50} = -2.9\phi$, $\sigma = 0.6\phi$. The Figure indicates the best fit profile calculated assuming a single grain size, the sediment profile calculated assuming all grain sizes are available in proportion to the transport capacity of the flow and the profile calculated assuming that the availability of the finest size fractions are limited.

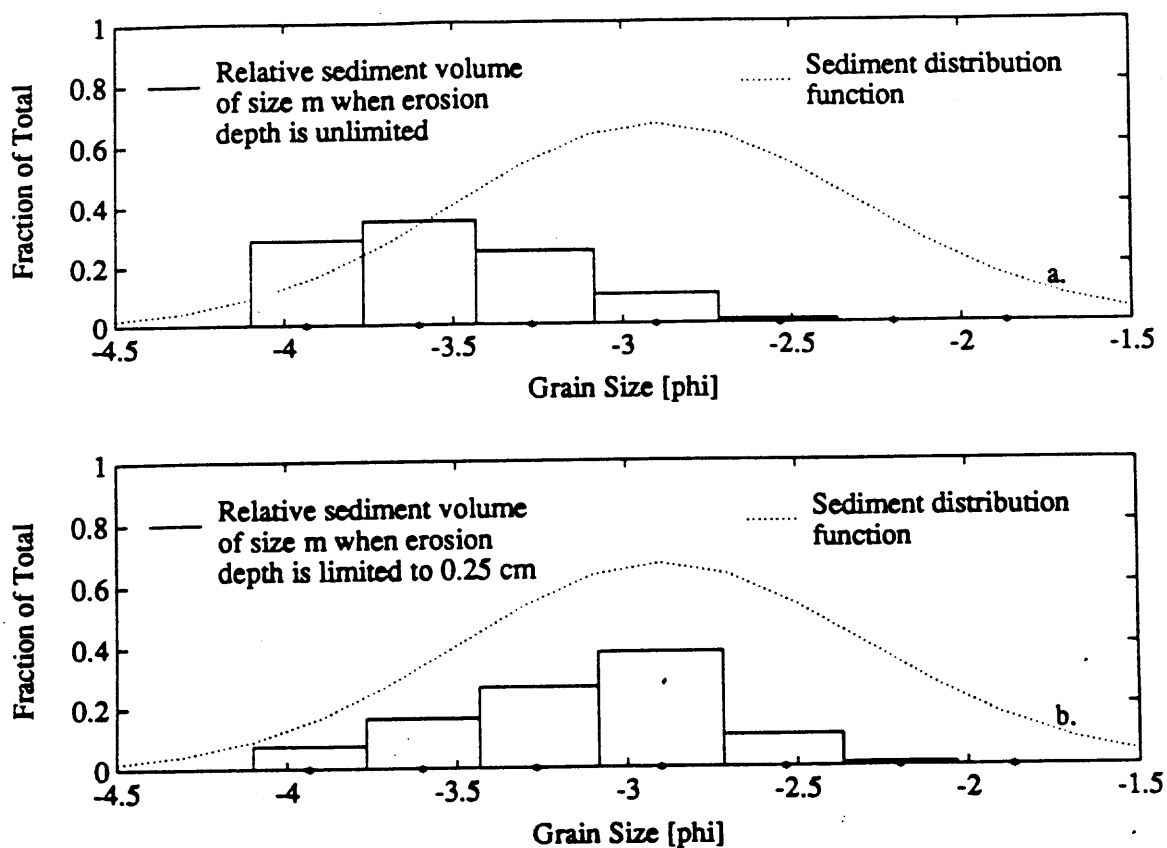


Figure 4.18: (a.) Relative volume of suspended sediment distributed over seven size classes, when unlimited availability of sediment is assumed. The calculated total volume of sediment in suspension is $0.912 \text{ cm}^3/\text{cm}^2$. The volumetric distribution of sediment is compared to a log-normal sediment distribution with $D_{50} = -2.9\phi$, $\sigma = 0.6\phi$.

(b.) Relative volume of suspended sediment distributed over seven size classes, when limited availability of sediment is assumed. The calculated total volume of sediment in suspension is $0.112 \text{ cm}^3/\text{cm}^2$. The volumetric distribution of sediment is compared to a log-normal sediment distribution with $D_{50} = -2.9\phi$, $\sigma = 0.6\phi$.

Chapter 5

CONCLUSIONS

The selected model profiles for velocity and suspended sediment in the exterior flow were in good agreement with the structure of the observed and the measured profiles in central 30% of the reach of the Colorado River, located in vicinity of National Canyon.

The high discharge velocity measurements indicated that the measurement derived bedform roughness, z_{0T} , approximated the value of roughness expected from the height and length of bedforms surveyed in the reach. The surveyed bedforms were found to have a characteristic dune geometry, with a height to length ratio of approximately 1/20.

The low discharge velocity measurements indicated that bedform roughness, z_{0T} , greatly increased during low discharge, and did not correspond to the roughness expected from the geometry of the surveyed bedforms. The greater roughness may be due to bedforms changing from characteristic dune geometry during high discharge to smaller and steeper ripple geometry during low discharge.

The shear velocity, u_{*T} , derived from the low and high discharge velocity profiles were related to boundary shear stress, and water surface slope was calculated using the depth-slope product. The water surface slopes calculated in this manner were in reasonable agreement with each other. The surface slope was found 17 % greater at high discharge than low discharge surface slope. The difference may be explained by uncertainty in the estimate of u_{*T} . An error analysis indicated that the statistical uncertainty of u_{*T} was of the order of magnitude 7-9 % which converts into an uncertainty of 14-17 % of the boundary shear stress. However, it is also possible that the difference is related to a physical mechanism that differs between high and low discharge, for example a backwater effect at low discharge perhaps due to the increased roughness.

A characteristic grain size and a value of the resuspension coefficient were derived from the best fit concentration profile. The characteristic grain size was compared

to sediment sizes found in the suspended sediment samples and the coefficient γ was compared to values of this parameter found in the literature. The comparison showed that the derived values of both grain size and coefficient γ were in good agreement with the values expected, which supports that a reasonable value of total boundary shear stress was derived from the velocity measurements at high discharge.

Suspended sediment concentration profiles were calculated using three likely distributions of sediment. It was found likely that the availability of the finest size fractions of the sediment distribution was limited by the thickness of the reworked layer of sediment.

A region of uniform flow and sediment discharge was identified in the central portion of the channel. At high discharge this region is approximately 25 meters wide, or approximately 30 % of the total channel width, and approximately 54 % of the total discharge is in this portion of the river. During low discharge, the region of uniform flow is wider, approximately 29 meters, which is approximately 36 % of the channel width at low discharge. The discharge in the region of uniform flow is approximately 59 % of the total low discharge.

The ability of the Manning equation and the resistance equation to predict mean channel velocity was evaluated. It was found that the Manning equation, at best would produce a mean channel velocity of the correct order of magnitude, but it was not possible to make sufficiently precise distinction between mean velocity at high and low discharge. The resistance equation provided reasonable estimates of mean velocity, if the measurement derived values of bedform roughness were used to calculate the roughness parameter. An empirical relationship proposed by *van Rijn*, 1982 [22] for calculating roughness of sand bedded streams covered with bedforms was used, but this relationship greatly over-estimated the bedform roughness parameter, and was not considered appropriate for evaluating bedform roughness at National Canyon.

The conclusions drawn in this study would obviously be strengthened by an independent measurement of water surface slope. Since the slope of the reach is low, it is necessary to use pressure transducers in order to obtain sufficiently accurate measurements of water surface elevations. In addition, one would have better confidence in the final result if the grain size distribution of the bottom material was known more accurately.

Because it is of interest to characterize flow and sediment transport at a range of discharges, more information regarding the hypothesized variation of bedform geometry at different discharges is desirable.

Bibliography

- [1] E. D. Andrews. Sediment transport in the Colorado River basin. In *Colorado River Ecology and Dam Management*, pages 54–73, Santa Fe, New Mexico, May 24–25 1990. National Academy Press.
- [2] S. P. S. Arya. A drag partitioning theory for determining the large-scale roughness parameter and wind stress on the arctic pack ice. *Journal of Geophysical Research*, 80(24):3447–3454, August 1975.
- [3] J. C. Bathurst. Flow resistance in steep mountain streams. *Journal of Hydraulic Engineering*, 111(4):625–643, April 1985.
- [4] J. L. Devore. *Probability and Statistics for Engineering and the Sciences*. Brooks/Cole Publishing Company, 2nd edition, 1987.
- [5] W. E. Dietrich. Settling velocity of natural particles. *Water Resources Research*, 18(6):1615–1626, 1982.
- [6] J. Fredsøe. *Hydrodynamik*. Den Private Ingeniørfond, Danmarks Tekniske Højskole, Denmark, 1990.
- [7] A. Howard and R. Dolan. Geomorphology of the Colorado River in the Grand Canyon. *Journal of Geology*, 89(3):269–298, May 1981.
- [8] L. B. Leopold. The rapids and the pools—Grand Canyon. U.S. Geological Survey Professional Paper 669, U.S. Geological Survey, 1969.
- [9] R. D. Jarret Marchand, J. P. and L. L. Jones. Velocity profile, water-surface slope, and bed-material size for selected streams in Colorado. Open-file Report 84-733, U.S. Geological Survey, 1984.
- [10] S. R. McLean. The stability of ripples and dunes. *Earth Science Review*, 29:131–144, 1990.

- [11] S. R. McLean. Depth-integrated suspended load. *Journal of Hydraulic Engineering*, 117(11):1440-1458, January 1991.
- [12] G. V. Middleton and J. B. Southard. *Mechanics of Sediment Transport*. Society of Economic Paleontologists and Mineralogists, 2nd edition, 1984.
- [13] J. Nikuradse. Laws of flows in rough pipes. NACA Technical Memorandum 1292, 1933. English Translation.
- [14] Interagency Committee on Water Resources. A study of methods used in measurement and analysis of sediment loads in streams. report 14, Interagency Committee on Water Resources, Minneapolis, Minnesota, 1963.
- [15] M. Rattray, Jr. and E. Mitsuda. Theoretical analysis of conditions in a salt wedge. *Estuarine and Coastal Marine Science*, 2:375-394, 1974.
- [16] K. Richards. *Rivers, form and process in alluvial channels*. Methuen and Co., 1982.
- [17] H. Rouse. Modern conceptions of the mechanics of turbulence. *Transactions of American Society of Civil Engineers*, 102:436-505, 1937.
- [18] J. C. Schmidt and J. B. Graf. Aggradation and degradation of alluvial sand deposits, 1965 to 1986, Colorado River, Grand Canyon, Arizona. U.S. Geological Survey Professional Paper 1493, U.S. Geological Survey, 1990.
- [19] A. Shields. Application of the theory of similarity and turbulence research to the bedload movement. *Mitteilung Preuss. Vers. Wasser Schiff*, 26:5-24, 1936.
- [20] J. D. Smith and S. R. McLean. Spatially averaged flow over a wavy surface. *Journal of Geophysical Research*, 82(12):1735-1746, April 1977.
- [21] J. D. Smith and S. Wiele. Flow and sediment transport in the Colorado river between Lake Powell and Lake Mead. Report to the US Bureau of Reclamation, 1992.

- [22] L. C. van Rijn. Equivalent roughness alluvial bed. *Journal of Hydraulic Division, American Society of Civil Engineers*, 108:1215-1218, October 1982.
- [23] P. L. Wiberg and J. M. Nelson. Unidirectional flow over asymmetric ripples. *Journal of Geophysical Research*, 97(C8):12745-12761, August 1992.
- [24] P. L. Wiberg and D. M. Rubin. Bed roughness produced by saltating sediment. *Journal of Geophysical research*, 94(C4):5011-5016, April 1989.
- [25] P. L. Wiberg and J. D. Smith. Velocity distribution and bed-roughness in high-gradient streams. *Water Resources Research*, 27(5):825-838, May 1991.
- [26] R. H. Wilkinson. A method for evaluating statistical errors associated with logarithmic velocity profiles. *Geo-Marine Letters*, 3:49-52, 1984.